Ludwig-Maximilians-Universität

# Evolution of Radio Galaxies Across Cosmic Time

**Dissertation der Fakultät für Physik**

Dissertation of the Faculty of Physics

**der Ludwig-Maximilians-UniversitätMünchen**

at the Ludwig Maximilian University of Munich

**für den Grad des**

for the degree of

**Doctor rerum naturalium**

**vorgelegt von Emilio Donoso**

presented by

**aus San Juan, Argentinien**

from

**München,2010**


**1. Gutachter: Prof. Dr. Simon D. M. White**

**2. Gutachter: Priv.-Doz. Dr. Hans Böhringer**

**Tag der mündlichen Prüfung: 10.03.2010**

To my beloved wife and star, Silvana

Yo digo que las estrellas le dan gracias a la noche,
pues encima de otro coche no pueden lucir más bellas,
y digo que es culpa de ellas, la noche, el universo,
cual son culpables estos versos,
de que haya noche y estrellas.

*Silvio Rodriguez – La Habana, Cuba, 1975*

# Contents

# List of Figures

# List of Tables

# Zusammenfassung

Obwohl Radiogalaxien eine Minderheit unter der Galaxienpopulation darstellen, finden sie immer mehr Beachtung aufgrund der energetischen Rückkopplung, die sie auf ihre Umgebung ausüben. Radiogalaxien beheimaten einen aktiven galaktischen Kern, der große Mengen an Energie in Form von Radio und Röntgenstrahlung-Jets abgibt, was in einigen Fällen Strahlungskühlprozesse des in dunklen Materie Halos kondensierenden Gases kompensieren kann. Zum Verständnis der Galaxienentstehung und Entwicklung, ist es daher notwendig die Rolle von aktiven galaktischen Kernen (AGNs) in diesem Zusammenhang zu verstehen.

Der erste Teil dieser Arbeit konzentriert sich auf die Zusammenstellung eines Auswahl von Radiogalaxien. Dies ist allerdings kein einfaches Unternehmen, da diese Galaxien sehr verschiedene Morphologien in verschiedenen Surveys zeigen, und oft in mehrere Komponenten aufgebrochen sind. Diese diversen Komponenten müssen mit einer eindeutig optisch sichtbaren Galaxie identifiziert werden. Hierzu haben wir zwei verschiedene Radio Surveys (NVSS und FIRST) mit einem Sample von leuchtkräftigen roten Galaxien des Sloan Digital Sky Survey (SDSS) korreliert. NVSS ermöglicht eine sehr genaue Bestimmung des Flusses ausgedehnter Quellen, wohingegen die Winkelauflösung von FIRST eine sehr genaue Identifikation der Heimat-Galaxie erlaubt. Weiter haben wir den Abgleich von Quellen unter dem nominalen 1 mJy Detektionslimit von FIRST verbessert, um die Verlässlichkeit und die Vollständigkeit des endgültigen Katalogs zu erhöhen. Diese Techniken erlaubten es uns den derzeit größten Radiogalaxien-Katalog zusammenzustellen. Er besteht aus circa 14,000 radiolauten AGNs bei mittleren Rotverschiebungen ($0.4 < z < 0.8$) und 1.4 GHz Flußstärken über 3.5 mJy. Die Abgleichkriterien wurden mit Monte-Carlo Simulationen getestet und verbessert, was zu einer geschätzen Verläßlichkeit von ∼98.3% und einer Vollständigkeit von circa 95% für den Katalog führte.

Mit Hilfe dieses Katalogs waren wir in der Lage Radiogalaxien bei $z \sim 0.55$ mit einer ähnlichen Auswahl im lokalen Universum zu vergleichen. Wir haben dann ihre Entwicklung studiert, wie ihre Raumdichte sich mit der Zeit ändern und wie der Anteil radioemittierender Quellen sich mit den Galaxieneigenschaften wie stellare Masse, Radioleuchtkraft und Rotverschiebung ändert. Weiter präsentieren wir eine neue Bestimmung der Leuchtkraftfunktion von Radio-AGNs bei $z \sim 0.55$ und vergleichen diese mit der Leuchtkraftfunktion naher ($z \sim 0.1$) Radioquellen des SDSS Surveys. Die mitbewegte Anzahldichte von Radio-AGNs mit Leuchtkraft weniger als $10^{25}$ W Hz$^{-1}$ steigt um einen Faktor $\sim 1.5$ zwischen $z = 0.1$ und $z = 0.55$ an. Zu höheren Leuchtkräften hin, steigt dieser Faktor stark an, und erreicht Werte von mehr als 10 bei Radio-Leuchtstärken größer als $10^{26}$ W Hz$^{-1}$.

Anschließend haben wir untersucht wie sich die Relation zwischen Radio-AGNs und ihren Heimat-Galaxien mit der Rotverschiebung entwickelt. Unsere Hauptschlußfolgerung ist, dass der Anteil radiolauter AGNs in allen massiven Galaxien zu höheren Rotverschiebungen hin ansteigt. Diese Entwicklung ist für weniger massive Galaxien in unserer Auswahl besonders ausgeprägt. Diese Trends können verstanden werden, wenn zwei Klassen von Radiogalaxien angenommen werden (wahrscheinlich assoziiert mit der "radio" und "quasar mode" Dichotomie), die unterschiedliche Fuelling und Triggering Mechanismen haben, und sich deshalb verschieden entwickeln. Wir schließen daraus, dass die stellare Masse ein wichtiger Einflußdarauf hat, ob die Galaxie helle und mächtige Jets entwickelt.

Es gibt auch die Vermutung, dass die Umgebung einer Galaxie beeinflußt, ob die Galaxie radialaut ist. Um dieser Fragestellung nachzugehen, haben wir untersucht wie Radiogalaxien im Universum verteilt und gehäuft sind. Die Häufung haben wir dabei abhängig von der stellaren Masse und Radioleuchtkraft betrachtet. Hierzu haben wir die Kreuzkorrelationsfunktion zwischen Radiogalaxien und der Eltern-LRG-Population berechnet. Um die eigentliche RLAGN-Häufung zu quantifizieren, haben wir unsere Auswahl mit einem Kontroll-Sample radioleiser Galaxien verglichen, die mit den selben Eigenschaften wie die AGNs selektiert wurden. Das Hauptresultat dieser Analyse ist, dass RLAGN signifikant stärker gehäuft sind als radioleise Objekte, insbesondere unterhalb von $\sim$1 Mpc $h^{-1}$. Dies deutet darauf hin, dass die Gasumgebung von Radioquellen auf den Skalen ihres dunkle Materie Halos einen wichtigen Einflußauf die beobachtete Radiolautstärke hat.

Vereinheitliche Modelle sagen vorher, dass die Umgebungen von radiolauten Galaxien und radiolauten Quasaren äquivalent sein sollten, da sie die gleichen Objekte nur von unterschiedlichen Orientierungen aus beobachtet darstellen. Wir haben die Häufungsmessungen für diese beiden Typen von Objekten verglichen, und konnte wichtige Einschränkungen an die Bedingungen stellen, die für die Gültigkeit der Modelle notwendig sind. Wir finden Hinweise dafür, dass die Idee der Vereinheitlichung nur gültig sein kann für die hellsten Radiogalaxien unser Auswahl.

Im letzten Teil der Arbeit haben wir die radiolaute Population von AGNs bei $z = 0.5$ mit Hilfe einer einfache Beschreibung der Verteilung von Radiogalaxien in dunklen Materie Halos aus N-Body Simulationen modelliert. Durch Kombination eines Vergleichs für die mechanische Energie von Radioquellen mit unsere Bestimmung der Leuchtkraftfunktion ist es uns dadurch gelungen den Heizeffekt von RLAGNs in Halos verschiedener Masse abzuschätzen. Die Heizstärke in Halos von $\sim 10^{15}$ $M_\odot$ $h^{-1}$, den massereichsten in unserem Sample, ist einen Faktor 6-7 größer als in den masseärmsten Systemen mit $\sim 10^{13}$ $M_\odot$ $h^{-1}$. Dieses Resultat kann verwendet werden, um die Implementierung von Rückkopplungs-Modellen zur Untersuchung von Galaxienentstehung zu verbessern.

# Abstract

Despite being a minority among the total population of galaxies, radio galaxies have gained increasing attention, because of the energetic feedback they can provide to the surrounding environment. These systems host an active nucleus that produces large amounts of energy in the form of radio/X-ray emitting jets, injecting energy that in some cases can balance the radiative loses of the gas that cools and condenses within massive halos of dark matter. Therefore, if we want to understand galaxy formation and evolution, we have to understand the role of active galactic nuclei (AGN) in the galaxy assembly process.

My work concentrated, first, on constructing a complete sample of radio galaxies. This is not an easy task as they have very different morphologies in different surveys, and ofter break up into separate componentes. These components must be correctly associated with a unique optical galaxy. We cross-correlated two different radio surveys (NVSS and FIRST) with a sample of luminous red galaxies derived from the Sloan Digital Sky Survey (SDSS). The NVSS provides accurate flux measurements for extended sources, while the angular resolution of FIRST allows the host galaxy to be identified accurately. We also improved the matching of sources below the nominal 1 mJy detection limit of FIRST, to increase the reliabiliy and completeness of the final catalogue. These techniques allowed us to assemble the largest radio galaxy catalogue to date, consisting of around 14,000 radio–loud AGN at intermediate redshifts ($0.4 < z < 0.8$), with 1.4 GHz fluxes above 3.5 mJy. The matching criteria were tested and refined using Monte–Carlo simulations, leading to an estimated reliability of ∼98.3% and completeness level of about 95% for our catalogue.

With this catalog in hand, we were able to compare radio galaxies at $z \sim 0.55$ with similar samples in the local universe. We studied the evolutionary properties of radio galaxies, how their spatial density changes as function of time and how the fraction of radio emitting sources varies with galaxies properties such as stellar mass, radio luminosity and redshift. We present a new determination of the luminosity function of radio AGN at $z \sim 0.55$ and compare this to the luminosity function of nearby ($z \sim 0.1$) radio sources from the SDSS main survey. The comoving number density of radio AGN with luminosities less than $10^{25}$ W Hz$^{-1}$ increases by a factor $\sim 1.5$ between $z = 0.1$ and $z = 0.55$. At higher lumiosities, this factor increases sharply, reaching values of more than 10 at radio luminosities larger than $10^{26}$ W Hz$^{-1}$. We then study how the relation between radio AGN and their host galaxies evolves with redshift. Our main conclusion is that the fraction of radio–loud AGN increases towards higher redshift in all massive galaxies,

but the evolution is particularly strong for the lower mass galaxies in our sample. These trends may be understood if there are two classes of radio galaxies (likely associated with the "radio" and "quasar mode" dichotomy) that have different fuelling/triggering mechanisms and hence evolve in different ways. We conclude that stellar mass seems to be the a very important factor in deciding whether a galaxy develops bright, powerful radio jets.

There is also the suggestion that the environment of a galaxy is also crucial in deciding whether it becomes radio-loud. To address this question, we studied how radio galaxies are clustered in the universe and quantified the clustering dependence on stellar mass and radio power. We do this by computing the cross-correlation function between radio galaxies and the parent LRG population. In order to isolate the true clustering of RLAGN, we compare respect to control radio-quiet galaxies selected with the same properties as radio AGN. The main result is that RLAGN are significantly more clustered than radio-quiet objects, particularly below $\sim$1 Mpc $h^{-1}$, indicating that the gaseous environment of a radio sources at the scale of its dark matter halo is important in modulating the observed output power and determining its radio loudness.

Unification models predict that the environments of radio-loud galaxies and radio-loud quasars should be equivalent, as they represent the same object that is observed at different orientations with respect to the line of sight. We have compared our clustering measurements for these two types of objects, setting important restrictions on the conditions that must be met if the models are valid. We find evidence that the idea of unification can hold only for the most luminous radio galaxies in our sample, with radio power above $\sim 10^{26}$ W $Hz^{-1}$.

Finally, we have also modeled the radio-loud population of AGN at $z = 0.5$ by applying a simple prescription for the distribution of radio galaxies in dark matter haloes extracted from N-body simulations. This proves the applicability at high redshift of models that have been shown to work well in the local universe and test directly the radio-mode heating recipe implemented in semianalyitcal models of galaxy formation. By combining an estimate for the mechanical power of radio sources with our determination of the luminosity function we have been able to estimate the heating effect that RLAGN produce in haloes of different mass. The heating power in haloes of $\sim 10^{15}$ $M_\odot$ $h^{-1}$, the most massive in our sample, is a factor of 6-7 larger than in less massive systems of $\sim 10^{13}$ $M_\odot$ $h^{-1}$, and a factor of $\sim$ 2.5 larger at $z = 0.5$ than at in the local universe. This result can be used to improve the implementation of radio feedback in models of galaxy formation.

# 1

# General Context and Motivation

I will discuss the development of radio astronomy, paying particular attention to the advance of wide-area radio and optical surveys during the last 60 years. Then, I will briefly review basic properties of the different AGN types that make up the diversity of the AGN zoo, focusing on radio AGN and quasars, their morphology and classification.

Radio galaxies are also important cosmological tools to study galaxy evolution. I briefly address the cosmological context and the formation of structure in the universe. Finally, I will highlight the important role that radio AGN play in galaxy evolution. Galaxy formation models successfully incorporate the heating effect of radio sources to reproduce observations. The ideas presented in this chapter will provide the framework, main concepts and motivation for this work, as well as serve as an introduction to the more in-depth discussions in the following chapters.

## 1.1 An Exciting Time For Radio Astronomy

The first systematic survey of the radio universe was carried out in 1943 by Grote Reber, a pioneering radio engineer who followed the footsteps of Karl Jansky, the discoverer of the first radio signals from outer space. Using a backyard telescope with a beamwidth of 16 deg operating at a frequency of 150 MHz, it took Reber more than a year to map the northern sky down to a flux density limit of a few thousand janskys. The resulting survey revealed various regions emitting at radio wavelengths along the Milky Way plane, whose centroid was offset more than 30 deg from the zero point of Galactic longitude known at that time. He provided the astronomical community with the first picture of our Galaxy at wavelengths beyond the optical, and showed that in some cases this radiation had to be of non-thermal origin. Over 60 years later, modern surveys like the Faint Images of the Radio Sky at 20-cm (FIRST) are 5 million times more sensitive and map dozens of millions of sources.

Most fields of science are considered as experimental in nature: scientists design experiments to test hypotheses. Astronomy is no exception to this rule: astronomers

carry out the equivalent of experiments by discovering, studying and uncovering relationships between astrophysical systems with a variety of properties that exist in many different physical conditions. Observation is a key task in astronomy, and surveys are central to progress in the discipline as they generate the set of "laboratories" to conduct studies. Deep surveys, which provide a representative population of objects, are the best tool to discover new and unexpected phenomena, constrain the actual links between different source classes, and deduce their underlying physics. Moreover, in many cases the same astrophysical process leads to significant emission of radiation across the electromagnetic spectrum, so surveys in widely separated wavelength bands are essential in constructing a complete picture of a population of sources.

Both, optical and radio astronomers have always been aware of this particular need. The first large modern effort to build a census of the sky at optical wavelengths was the National Geographic-Palomar Observatory Sky Survey (POSS-I). It has been a fundamental resource for almost 50 years of research, providing images, positions and catalogs of optical emitting sources over the entire northern sky. In the last decade, new ground-based surveys like the Sloan Digital Sky Survey (SDSS) have surveyed large regions of the sky more than four magnitudes deeper than in the POSS-I plates.

In the meantime, radio astronomers have produced a large number of surveys since the discipline begun to gain attention after World War II. Over the last three decades, they have conceived and built special telescopes and instruments, sometimes dedicated solely to conducting a specific survey. The series of Cambridge surveys (3C,4C,5C,6C,7C,8C,9C) are examples of such an approach and even today, they remain as the most well studied samples of bright radio sources at frequencies between 80 MHz and 15 GHz. The first quasars where discovered among the 3C objects. Interferometric arrays that combine the signals from multiple receivers separated over long baselines, like the Westerbork Synthesis Radio Telescope (WSRT) and the Very Large Array (VLA), have allowed to reach very low flux densities, revealing the properties of mJy-level radio sources. The great majority of optical counterparts of $\sim 3$ mJy [1] sources are fainter than $m_V = 20$, so precise coordinates are needed to correctly cross-match with radio sources, determine distances and study their evolution.

The list of prospective new instruments and surveys that are planned or entering operations in the near future indicate that radio astronomy will play an important role for the advance of astrophysics. We will briefly discuss these projects at the end of this thesis. Another aspect that enables astrophysics to develop in large leaps is the ever growing computing capability. Until a few years ago, computing capacity was insufficient or too expensive to carry out the digital signal processing of a large sky survey. This is no longer the case. And no less important, fully digital surveys,

[1] 1 Jy = $10^{-26}$ W Hz$^{-1}$

maps and catalogs are instantly accessible to the astronomical community.

## 1.2 The Zoo of Active Galactic Nuclei (AGN)

A few percent of the known galaxies in the Universe contain active central regions. This activity originates in an extremely compact region, order of magnitudes smaller than the typical (few kpc) size of galaxies. However, in some cases the power output of AGN can exceed the luminosity of $> 10^3$ normal galaxies. In the most broad sense, an active galactic nucleus (AGN) can be defined a region in the center of a galaxy whose energy content or spectral energy distribution cannot be explained by starlight alone.

The study of AGN has made significant advances in the last 60 years. The first radio sources detected in the 1950s, were successfully associated with point-like optical sources or optical galaxies located outside the Milky Way. As some radio sources displayed significant variability on very short time scales, the energy had to be produced within a tiny region (1-10 pc) compared to the total size of a galaxy. Lynden-Bell [1969] suggested the accretion of matter onto super-massive black holes as the energy production mechanism. However, black holes were only hypothetical objects at that time. Today, there is mounting evidence that black holes reside at the center of most, if not all, massive galaxies. Two examples are provided by the detection of high excitation iron lines with strong relativistic effects (Nandra et al. 1997), and the direct observation of stars orbiting around an object of several $10^6$ $M_\odot$ at the center the Galaxy (Genzel et al. 1997).

AGNs are observed over most of the electromagnetic spectrum, from 100 MHz radio waves to 100 MeV gamma rays. This, toegether with the difficulties in combining multi-wavelength datasets, has lead to a confusing AGN terminology where the classification of various types of sources has been a reflection of the initial methodologies by which the objects where discovered, rather than physical properties of the different classes.

Historically, the majority of AGN were classified into quasars or Seyfert galaxies according to the amount of radiation emitted by the central source. For the case of Seyfert galaxies, the total energy at optical wavelengths emitted by the nuclear source is comparable to the total luminosity of the galaxy. In quasars, the central AGN can be so bright that it outshines the host galaxy luminosity by factors of $10^{2-3}$. Today, the definition of the different classes has evolved to try to reflect the underlying physics rather than the way we observe them. For example, Seyfert galaxies are identified by the presence of high-ionization emission lines in the spectra.

AGN are often classified according to: (1) *radio luminosity* into radio-loud or radio-quiet classes; and (2) *spectral features* into Type 0, 1 or 2. The classification as radio-loud or radio-quiet is often made according to the ratio between radio and

optical luminosity. Type 1 AGN have broad emission lines and a bright continuum in the spectra, while Type 2 AGN have narrow emission lines and a weak continuum.

Here, we will summarize the basic characteristics of the different classes of AGN that are generally recognized, and reserve for the following section a more detailed discussion about the properties of radio AGN.

- **Seyfert Galaxies**: these are low luminosity AGNs identified spectroscopically by the presence of high-ionization emission lines in the spectra. Most Seyferts are hosted by spiral galaxies with quasar-like nuclei. Type 1 Seyferts show both broad ($10^4$ km s$^{-1}$) lines and narrow ($\sim$400 km s$^{-1}$) lines. In Type 2 Seyferts only the narrow lines are present.

- **Quasars**: these are the most luminous class of AGNs. Historically, quasars were identified as star-like objects associated with strong radio sources and emission spectra, while the term QSO was reserved for sources with the same emission-line optical spectra but no detected radio emission. Quasars often appear as spatially unresolved objects, and they have spectra very similar as of Seyfert galaxies.

- **Radio Galaxies**: these are spatially resolved galaxies associated with bright radio sources (although powerful radio sources are also identified with radio-loud quasars). In analogy with Seyferts, radio galaxies can be divided into broad-line and narrow-line radio galaxies, according to the optical spectra. Typically, radio galaxies are associated with elliptical galaxies.

- **LINERs**: these are the low-ionization emission-line regions that are found in a substantial fraction of galaxies when sensitive observations are made. About half of spiral galaxies host LINERs. They have similar spectra as of Seyferts, but with relatively strong low-ionization lines (e.g. OI $\lambda$6300, NII $\lambda$6583). They are more easily recognized using the intensity ratio of two pairs of spectral lines (i.e. the BPT diagram, see Section 2.6).

- **BL Lac**: these objects show a strong nuclear continuum, high levels of polarization and rapid variability. In the optical spectra, emission lines are absent or very weak. They are commonly associated with X-ray or strong radio sources.

The diversity in the observational properties of the different types of AGNs outlined above is enormous. However, most AGN classes can be described in a simple manner by the so called unified model of AGN. In this model, the energy is produced by a hot accretion disk of matter infalling onto a super-massive $10^6$-$10^9$ $M_\odot$ black hole that is surrounded by an obscuring dusty torus. The accretion produces photo-ionising UV radiation, and gives rise synchrotron radio emission and X-ray emission via Compton scattering. The high velocity dispersion of the gas clouds located within $\sim$1 pc of the obscuring torus gives rise to the broad emission

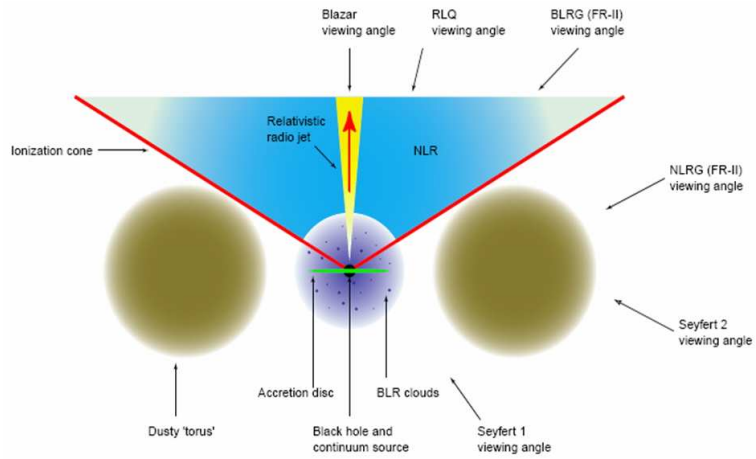


**Figure 1.1** • Sketch of the basic elements of the AGN model, and the different classes of sources that are visible at varying orientation respect to the line of sight according to unification schemes.

lines observed in optical quasars and Seyfert-1 galaxies. Gas clouds situated further away at ∼10-100 pc have lower velocity dispersions and are responsable for narrow emission lines. The distinguishing feature of radio-loud AGN is a pair of relativistic jets, originating within a few tens of Schwarzschild radii of the accreting black hole.

Unification model states that, depending on viewing angle, the observer either sees the accretion disk and the broad emission lines, or due to obscuration by the optically thick torus, sees only the narrow emission lines (first suggestion was made by Osterbrock 1978). This anisotropic radiation is the basis of optical unification schemes, and explains why there are AGNs (i.e. Seyfert 2) without broad emission lines. The same concept applies for radio-loud AGN due to the anisotropy of the radio jet emission, suggesting that objects like BL Lac and quasars are more "aligned" versions of radio galaxies, i.e. when the line of sight is close to the jet direction (e.g. Blandford and Rees 1978; Browne 1983; Barthel 1989). Figure 1.1 sketches the basic elements of AGN unification.

## 1.3 Properties of Radio Galaxies and Quasars

### 1.3.1 Radio Galaxies

The population of radio-emitting galaxies is composed of two main classes:

- **Star forming galaxies**: the radio emission is mostly as a result of the synchrotron emission of particles accelerated in supernova shocks and free-free emission from HII regions. This means that the radio luminosity is correlated with the star formation rate. For example, a radio luminosity of $L_{1.4\mathrm{GHz}} = 10^{22}$ W Hz$^{-1}$ corresponds to a star formation rate of about

5 M $_\odot$ yr$^{-1}$ (e.g. Condon 1992). Dusty HII regions that are heated and ionized by the same population of massive, short-lived stars that give rise to supernovae, re-process the radiation towards infrared wavelengths. Hence, far-infrared (FIR) emission is tightly correlated with radio emission (e.g. **?**helou); Condon 1992). Their 1.4 GHz radio luminosities range typically from from $10^{18}$ to $10^{23}$ W Hz$^{-1}$. Non-thermal emission in normal galaxies is also detected in the central regions of normal galaxies, and Seyfert galaxies form an almost continuous distribution in radio luminosity up to the radio-loud boundary.

- **Radio-loud AGN**: the radio emission in these systems is exclusively of non-stellar origin, associated with particles accelerated by the central active nuclei. Compared to star forming galaxies, RLAGN are more powerful radio sources hosted by mostly elliptical galaxies. Roughly 1% to 25% of giant elliptical galaxies are radio-loud. Basically, all sources with radio luminosities above $\sim 10^{24}$ W Hz$^{-1}$ are almost invariably associated with AGN (Condon 1992; Sadler et al. 2002; Best et al. 2005b). Throughout this work we will use the terms radio-loud AGN or radio galaxy interchangeably to designate the same type of object.

### 1.3.2 Radio Quasars

The quasar population can also be divided into two classes: radio-loud or simply radio quasars, and radio-quiet quasars. Radio quasars, like radio galaxies, are a minority among the the total quasar population. The precise definition of radio-loud is somewhat subjective and only $< 5\%$ of the sources are usually considered to be well into the radio-loud regime.

It is conventional to separate radio-loud quasars as those with total luminosities above $\mathrm{L_{5GHz}} = 2.5{\times}10^{24}$ W Hz$^{-1}$ or $10^{41}$ erg s$^{-1}$ (Kellermann et al. 1989). For these objects the ratio of 1.4 GHz radio luminosity to B-band optical luminosity, $R_{1.4GHz}$, ranges typically from $\sim 10$ and up to $\sim$1000. For all quasars with detected radio emission, the radio-to-optical luminosity ratio shows a smooth (and asymmetric) bimodal distribution, with a bright peak centered around $R_{1.4GHz} \sim 10^{2-3}$ and a much fainter peak clustered around $R_{1.4GHz} \sim 10$. A small fraction of quasars do not show radio emission even down to the $\mu$Jy level and the optical luminosity of most of the radio-quiet population varies by a factor of up to $10^4$. This suggests that there could be a distinction, in the physical mechanism responsible for the radio emission in the two regimes. High luminosity radio-loud quasars are thought to be result of well-collimated radio jets that originate from the accretion of cold gas. In radio-quiet quasars, the origin of the radio emission is less clear. One possibility is the thermal emission from supernova remnants in high density regions (Terlevich et al. 1992). But the most favored idea is that it is non-thermal emission from jets powered under a variety of physical conditions that could give rise to the apparent dichotomy. Differences in mass accretion rate, jet power, efficiency

of energy conversion, or different ignition/duration timescales of radio-optical AGN could explain the observed distributions. This is supported by parsec-scale radio observations (e.g. Kukula et al. [1998]) that resolve tiny jet-like structures around very faint radio-quiet quasars.

### 1.3.3 Observational Phenomenology of Radio AGN

Radio galaxies and quasars exhibit a wide range of sizes and morphological structures at radio wavelengths. There are extremely compact, steep spectrum radio sources ($\sim$15 kpc) with point-like morphologies. And there are complex structures with lobes, radio halos, compact nucleus, jets and filaments that in the most extreme cases extend up to $\sim 2$ Mpc from the nucleus.

In many cases the morphology is too complex to separate the different observed features, and not all of them appear in every radio galaxy or quasar. However, the most common elements found are:

- **Core**: present in about 80% of radio galaxies and in virtually all quasars, these are compact components –unresolved at typical subarcsec resolution– whose position usually matches with the associated optical counterpart. Cores have flat[2], self-absorbed spectrum. They contribute $\sim 1 - 100\%$ of the total radio luminosity.

- **Jets**: these are narrow beams that transport energy from the central AGN to the outer regions. Their extension ranges from a few pc up to several hundred kpc, in the largest radio galaxies. Jets can be one-sided or two-sided and present a smooth or knotty structure. As the jet radio luminosity is typically a small fraction of the total luminosity, most of the energy is in the form of bulk kinetic energy. In some cases, jets are also visible at optical wavelengths (e.g. the first case was M87 in 1918).

  Radio jets have steep spectra of almost constant spectral index along their longitude, and show the radiation generated shows polarization levels from 20% to >60%. Close to the core, jets are highly collimated and the magnetic field is parallel to the jet direction. At larger distances, the jets spread more and the magnetic field becomes perpendicular to the propagation vector (see Bridle and Perley 1984 for a comprehensive review about radio jets in AGN). Very long baseline interferometric radio maps have revealed tiny parsec-scale jets of knotty structure close the nucleus, whose apparent advance speeds often exceeds the speed of light (i.e. superluminal motion).

- **Lobes**: these are comparatively large radio-emitting regions, with linear sizes in the kpc-Mpc range. Quite often, two radio lobes are observed at opposite

[2]By convention, sources with spectral index $\alpha \leqslant 0.5$ are said to have flat power law spectrum, for $S_\nu \propto \nu^{-\alpha}$. Steep spectrum sources have $\alpha > 0.5$.

sides of the central source, in a roughly symmetrical configuration. The angle these two lobes form respect to the central component is called opening angle. It varies from 180 deg in ´classical" double sources to very small angles in narrow-angle-tail radio galaxies. In the last case, the jets/lobes are bent back by the ram pressure of the ICM flow, because of the high speed of the AGN moving through a galaxy cluster. Luminosities of radio lobes differ usually by a factor of $\sim 2$ at most, but sometimes extended structure is visible around only one side of quasars.

- **Hotspots**: these are small, $\sim 1$ kpc regions of maximum intensity located in the outer edges of radio lobes. Bright sources can display multiple, one or no radio hostpots at all, while sometimes the knotty structure of jets can render the definition of a hotspot much more difficult (see Bridle et al. 1994 for a complex empirical definition). Hotspots often display a spectrum less steeper than the hosting lobe, suggesting that they trace the region where the jet impacts the ambient medium and the bulk kinetic energy of the jet is converted into random motions.

### 1.3.4 Fanaroff-Riley Classification

In 1974, B.L. Fanaroff and J.M. Riley noted an intriguing correlation between radio luminosity and the relative location of the brightest peaks in radio maps of quasars and galaxies. Using a sample of only 57 resolved radio sources selected from the 3CR catalogue, they found that for the most luminous sources the ratio $R_{fr}$ of the distance between the regions of highest surface brightness on each side of the source, to the total extent of the source (up to the lowest radio countour observed), was greater than 0.5. They called objects with $R_{fr} > 0.5$ Fanaroff-Riley Class II (FRII) sources, while objects with $R_{fr} < 0.5$ where classified as Fanaroff-Riley Class I (FRI).

The luminosity boundary between the two classes at 1.4 GHz is around $10^{25}$ W Hz$^{-1}$ but there is significant overlap between the two classes. Nevertheless, various properties of FRI/FRII systems are different, suggesting, at least, different processes by which the energy is transported and converted into radio emission.

- **Fanaroff-Riley Class I (FRI)**: these systems become fainter toward the outer regions of the lobes, i.e the high intensity peaks are close to the central nucleus, while the regions of low surface brightness lie further away. This ´edge-darkening" is clearly visible in the radio map of the source 3C31, shown in Figure 1.2. Around 80% of FRI objects present radio jets and the steepness of the spectra increases toward the outer zones, indicating that the radiating electrons are comparatively old. FRI sources are often hosted by bright, elliptical D/cD galaxies, associated with rich clusters filled with hot, X-ray emitting gas.

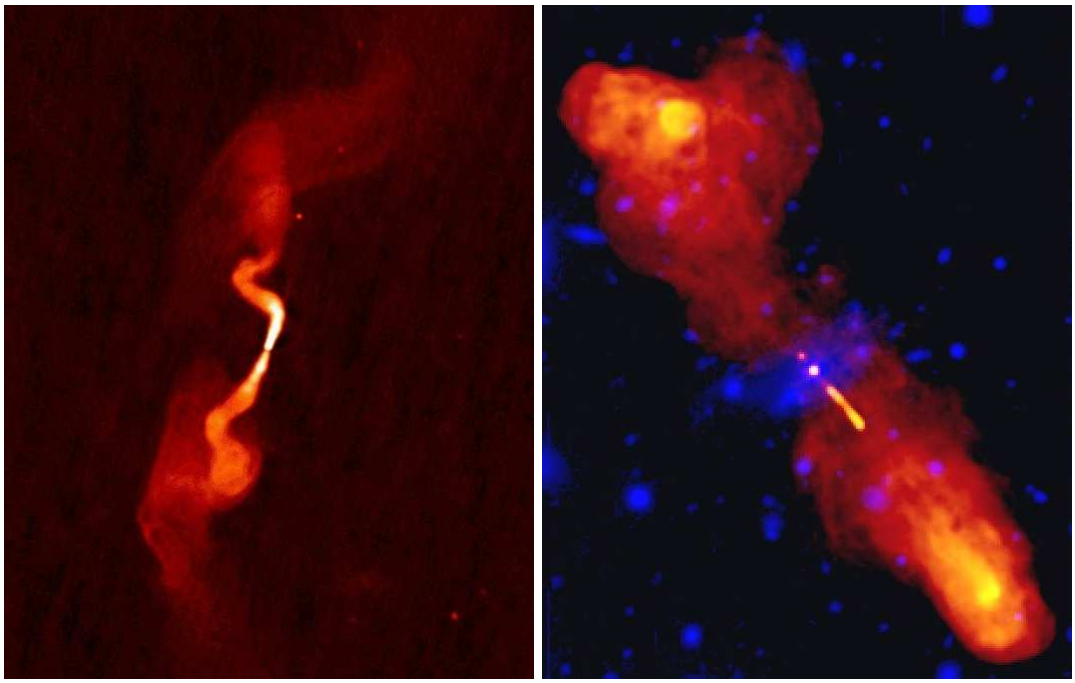

**Figure 1.2** • Left: VLA 21 cm radio image of 3C31 (NGC 383). It is a prototypical FRI radio galaxy, with conical short jets that bends in the outer regions, developing faint plumes extended out to ∼0.3 Mpc. The AGN is hosted by an elliptical galaxy at z=0.017. Right: composite image of 3C219, an double-lobed FRII radio galaxy at z=0.17. The optical V band image is in blue, while red/yellow is a 1.4-1.6 GHz radio composite, showing large, collimated radio jets and filamentary lobe structures that end up in bright hotspots a few hundred kiloparsecs away from the central AGN. Images courtesy of NRAO/AUI 1999.

- **Fanaroff-Riley Class II (FRII)**: this objects typically end up in bright hotspots, located at large distances when compared to the total extension of the radio source. Jets are found in about 10% of radio galaxies, but in almost all luminous quasars. FRII hosts are usually giant elliptical galaxies that are often not the first ranked galaxies of groups and clusters.

While the FRI/FRII classification scheme correlates with radio luminosity, the division between classes also depends on the optical luminosity of the host galaxy (Ledlow and Owen 1996). In the plane of $L_{rad}$ vs $L_{opt}$, the diagonal boundary that separates the two morphological classes follows the approximate relation $L_{rad} \propto L_{opt}^2$.

The physical distinction between FRI and FRII is still a matter of debate. One important clue comes from the jet properties: FRII jets are narrow, collimated, smooth, and end up in bright hotspots at the edge of well-defined lobes, suggesting they flow at supersonic speeds. FRI jets are wide, knotty and often distorted by the ambient, evidence that they have decelerated to subsonic speeds. Two different (but not mutually exclusive) scenarios could explain such behavior.

- **Environment**: all radio galaxies and quasars produce powerful, supersonic radio jets that quickly become disrupted and subsonic after impacting the ambient medium (e.g. De Young 1993).

- **Central Engine**: different properties or mechanisms intrinsic to the central engine powering FRI and FRII sources are responsable of the changes observed in radio jets. Briefly, Baum et al. [1995] found that at fixed absolute magnitude or radio luminosity FRII galaxies produce far more optical line emission than FRI sources, and orders of magnitude more than radio-quiet galaxies. Moreover, radio and emission line luminosity are correlated in powerful FRII, suggesting they are linked by some physical process. The bottom line is that differences in accretion rate, black hole mass, or black hole spin rate could potentially explain the differences between the two populations.

Whatever the case, FRI and FRII classes do not represent the whole diversity among extragalactic radio sources. Hine and Longair [1979] showed that FRII galaxies are not homogeneous: they can present strong, narrow, high excitation optical/UV emission lines; or weak-to-no emission lines, as in FRI systems. Also, a small fraction of FRI sources happen to display typical high excitation spectra. Other classes of radio sources include GHz-Peaked Spectum (GPS) and Compact Steep-Spectrum Sources (CSS). Table 1.1 resumes the different types of known extragalactic radio sources of non-stellar origin.

**Table 1.1** • Different populations of extragalactic radio sources.

| Population | Optical-UV Em. Line | Type |
|---|---|---|
| GPS | narrow | radio galaxy |
| | broad | quasar |
| CSS | narrow | radio galaxy |
| | broad | quasar |
| FRII high-excitation | narrow/broad | radio galaxy |
| | narrow | quasar |
| FRII low-excitation | weak/none | radio galaxy |
| | none | BL Lac |
| FRI | weak/none | radio galaxy |
| | none | BL Lac |

## 1.4 Basic Cosmology and the Emergence of Structure

The most favored cosmological theory predicts that a large "explosion" that we denominate The Big Bang gave origin to our universe about 14 billion years ago. Ever since then, it has been expanding and cooling.

Ordinary matter, i.e. that in form of baryons, represents only a minor fraction ($\sim$4%) of the total energy density budget of the universe. The next major contributor is the dark matter, accounting for $\sim$22% of the total content. However, the remaining 74% of the universe is in form of dark energy (commonly referred as the cosmological constant $\Lambda$) and actually dominates its geometry. The physical nature of dark energy is completely unknown, but its main effect is to counteract gravity by exerting an extra negative pressure. Type Ia supernovae can be used as standard candles and recent studies of these objects (e.g. Riess et al. 2004) confirm that the expansion rate of the cosmos has increased in recent times due to the presence of this unknown form of energy. With some assumptions (i.e. $\Omega_m = 0.3$), supernovae measurements indicate that $\Omega_\Lambda = 0.7$.

Over the last 50 years, the cosmological model of an expanding universe has developed steadily and converged to a model described basically by three parameters. It is remarkable that independent measurements largely agree in their numerical

values. These parameters are:

- **Hubble Constant**: it is defined in terms of the rate of change, as observed today, of the scale factor of the universe, which accounts for the overall expansion or contraction of the (homogeneous and isotropic) universe. The most recent determination of $H_0$ employing the period-luminosity relation of an homogeneous Cepheids population in hosts of Type Ia supernovae (Riess et al. [2009]) has estimated that $H_0 = 74.2 \pm 3.6$ km s$^{-1}$ Mpc, i.e. up to $\sim$5% accuracy.

- **Matter density**: the total matter density of the universe today $\rho_m(t_0)$ is contributed by both, dark and baryonic matter. It is usually expressed as $\Omega_m = \rho_m(t_0)/\rho_c$ in terms of the critical density of the universe $\rho_c = 3H_0^2/8\pi G$, which marks the limiting case between a high-density (closed) universe that will stop expanding and contract, and a low-density (open) universe that will expand forever if dark energy is neglected.

- **Cosmological Constant**: represents the dark energy content of the universe. It can also be expressed in terms of the critical density as $\Omega_\Lambda = \rho_\Lambda/\rho_c = \Lambda/3H_0^2$.

Very small anisotropies detected in the Cosmic Microwave Background (CMB) suggest that the structure originated from tiny seed fluctuations in the cosmic density field. One of the most important sources of information in cosmology is the power spectrum of the CMB, that combined with data on the spatial distribution of galaxies, have delineated the cosmic matter budget described above.

In the expanding universe, the growth of density fluctuations due to gravitational instabilities explains how bound objects such as galaxies and clusters formed at increasingly larger spatial scales. The most successful theory about cosmological structure formation is known as the cold dark matter model ($\Lambda$CDM), which states that the homogeneous universe turned into inhomogeneous by growing hierarchically from bottom to top : halos of cold dark matter collapse and merge together to form more massive structures. The $\Lambda$CDM paradigm is largely consistent with observations of very different nature such as the CMB temperature/polarization maps (Spergel et al. 2007) and the large-scale distribution of galaxies (Cole et al. 2005).

Throughout this work, the adopted values for the cosmological parameters are $\Omega_m = 0.3$, $\Omega_\Lambda = 0.7$, and $\mathrm{H}_0 = 70$ km s$^{-1}$ Mpc$^{-1}$.

## 1.5 Role of Radio AGN in Galaxy Formation

There is increasing evidence that AGN activity plays a key role in the process of galaxy formation, because during their short $10^6$-$10^8$ years lifetime AGN produce

an enormous amount of energy that is injected into their surrounding environment through ionising radiation and relativistic jets. Furthermore, the discovery that the black hole mass is correlated with the bulge mass and velocity dispersion (e.g. Ferrarese and Merritt 2000 and Gebhardt et al. 2000) also suggests a strong link between galaxy formation and black hole growth or AGN activity.

In the standard picture of hierarchical structure formation, the gas infalling into the gravitational potential well of merging dark matter haloes is heated to the virial temperature of the halo, and then gradually cools and condenses to form stars. Heated systems are supported by pressure, but in certain cases cold gas can fall into the equatorial plane forming stars and creating what can be observed today as disc galaxies (e.g. White & Rees 1978). It is the dissipation and collapse of gas that enables the formation of stars and galaxies. Hence, in order to describe galaxy formation at smaller scales, additional physical mechanisms other than gravitational interactions have to be taken into account.

The temperature of the gas is very important, as stars can form only from cold, dense gas. The gas can be easily heated by several processes, of which two of the most important are:

- UV Photo-ionization: in low mass halos, UV photons generated by quasars or massive stars can ionize and heat the gas to temperatures of $\sim 10^4$K, restricting further infall of baryons.
- Supernova feedback: in high mass halos, heating by newborn stars and supernovae can inject energy into the hot gas halo, preventing further cooling of the gas.

By running semi-analytic models (SAM) on top of large-scale numerical simulations of dark matter, it is possible to obtain the properties of galaxies sitting on different halos and then compare with observations. SAMS are just simple prescriptions that model physical processes like merging, cooling, feedback from supernovae, and chemical enrichment. Early versions of these models (e.g White and Frenk 1991 and Cole et al. 2000) were very successful in reproducing the observed properties of the baryonic component in the local universe, but a few important problems remained unsolved. For example, the fact that many more galaxies were predicted at both ends of the luminosity function compared to the observed quantities, was initially solved by invoking supernova feedback to reduce star formation in low mass systems (Dekel and Silk 1986; Benson et al. 2003), photoionization heating by the CMB (Efstathiou 1992) to reduce the formation of dwarfs, and artificially switching-off the cooling the most massive haloes to reduce gas condensation in massive systems (Kauffmann et al. 1999). The semi-analytical approach has been successful in predicting some of the key local observables (e.g. luminosity function, sizes, colours, Tully-Fisher relation, etc.), but reproducing all properties simultaneously for all types of galaxies remains challenging.

A promising (and much more elegant) solution to account for the mismatch between simulations and observations at the bright end of the luminosity function is the heating by radio-loud AGN. This mode of feedback works efficiently in high mass halos, where black holes accrete gas from the hot halo, releasing energy that heats the IGM and effectively suppresses cooling flows. AGN feedback is particularly important, as the suppression of cooling modifies the stellar mass, colors and clustering properties of galaxies. This turns the study of radio-loud AGN of particular interest. Tabor and Binney [1993] first suggested that radio galaxies could in principle regulate the cooling flows, preventing significant accretion of gas, and therefore limiting the mass of galaxies.

This effect has been incorporated (albeit with different prescriptions) in recent models of galaxy formation by Croton et al. [2006] (but also Bower et al. 2006) as the the ´´radio-mode" feedback by AGN. If AGN feedback is turned on in semi-analytic models, the resulting luminosity function has a steep high mass cut-off above which most systems are red, non star-forming elliptical systems. In Croton et al. [2006], radio emission is the result of hot gas being accreted at very low rates (well below the Eddington limit) into massive black holes sitting at the center of hot static haloes. The mechanical energy heating produced is such that is more effective in supressing the cooling flows at later times ($z < 2$) and in massive black holes, effectively shutting off the supply of gas to the disk, truncating star formation, and allowing the existing massive galaxies to redden and continue merging at later times. This model not only solves the luminosity function issue, but also explains the fact that the most massive galaxies tend to have red, old stellar populations, and exhibit a bulge-dominated morphology.

In the local universe, where high resolution observations are available, radio mode feedback has been directly observed. Recent X-ray data from the Chandra Observatory has shown the presence of bubbles and cavities, inflated in the ICM by high energy plasma carried out from the central AGN by radio jets (e.g. McNamara et al. 2000; Bîrzan et al. 2004). These cavities are clearly visible in the composite image in Figure 1.3, corresponding to the Hydra A cluster of galaxies.

## 1.6 This thesis

The importance (and success) of AGN feedback in recent semi-analytical models emphasizes the relevance that radio AGN have for the formation and evolution of galaxies.

However our understanding of the precise physical processes that take place and even of basic statistical properties of (low luminosity) radio galaxies, is still quite sketchy due the lack of comprehensive theories and adequate samples. For example, we do not know under which circumstances a black hole of a given mass can produce

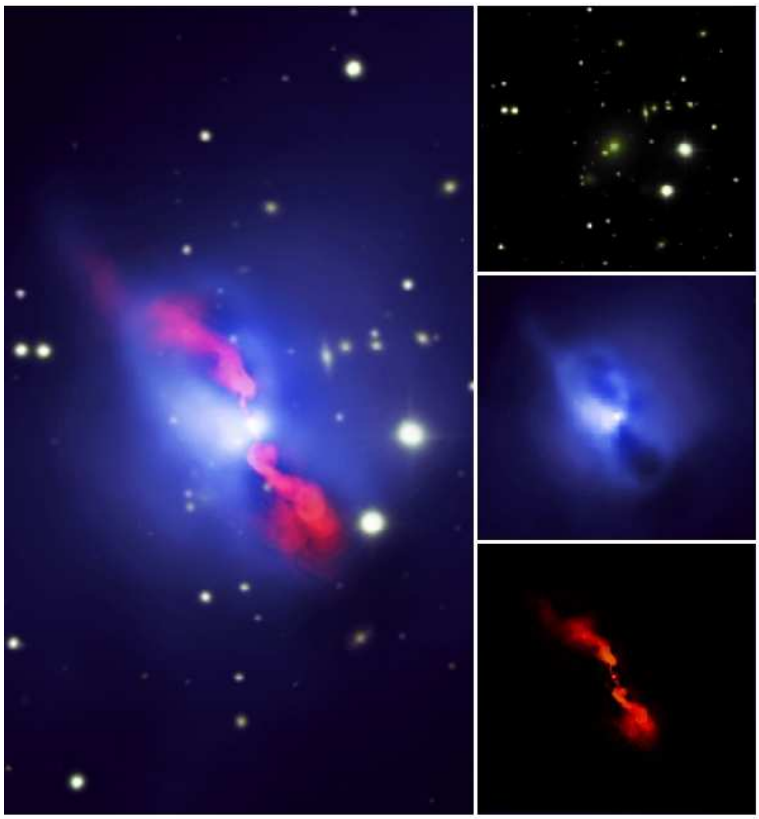

**Figure 1.3** • Left: composite image of the Hydra A galaxy cluster situated at ∼260 pc of distance. It shows $\sim 10^6$ K hot gas observed by Chandra (blue) and jets of radio emission observed by the Very Large Array (pink) that are inflating cavities in the ICM. Galaxies in the cluster are from the CFHT and the Digitized Sky Survey (yellow). Right: optical, X-ray and radio images. X-ray: NASA/CXC/U.Waterloo/C.Kirkpatrick et al.; Radio: NSF/NRAO/VLA; Optical: Canada-France-Hawaii-Telescope/DSS.

radio jets. Basically, an expanding radio source provides a direct way for the AGN output to be coupled to its environment. But, how often does this happen and in which galaxies? What is the dependency on stellar mass, black hole mass, radio luminosity and redshift? What are the evolutionary properties of the radio-loud population? In which environments do radio galaxies reside? This thesis presents additional evidence to characterize the radio population, its evolution and relation to hosts galaxies, based on statistical properties of large samples of radio-loud AGN and QSO. The structure of this thesis is as follows:

*Chapter 1*: this is the present chapter, aimed to provide a general overview of AGN and *radio* AGN/QSO properties, as well as present them in a cosmological context. As further motivation, I also present an overview of models of galaxy formation that taking into account the heating effects of radio sources successfully solve long standing issues in galaxy formation.

*Chapter 2*: here I will describe how to cross-match existing radio optical surveys to assemble a large samples of radio AGN that form the basis of posterior analyses. I explain the algorithm to select multiple radio components and associate it with one optical galaxy. I also estimate the efficiency and reliability of the methodology to assess the quality of the derived catalog.

*Chapter 3*: here I explain first how stellar masses and (k+e)-corrections are determined. Then, I turn to study the evolutionary properties of the radio population by comparing radio galaxies at different redshifts. I present new estimations of the radio luminosity function, radio-loud AGN fractions and the bivariate radio luminosity-stellar mass function, as well as quantify the impact of systematic biases.

*Chapter 4*: here I analyze the clustering properties of radio galaxies and quasars. First, I explain the methodology adopted to calculate the two-point auto and cross-correlation functions. I quantify how the clustering of radio-loud AGN depends on host galaxy properties and how it compares respect to that of control radio-quiet objects. I also compare the environments of radio AGN and radio QSO, and discuss the implications of the results in the framework of unification models of AGN.

*Chapter 5*: here I describe the implementation of a simple halo occupation model for RLAGN built on top of semianalytic models of galaxy formation that incorportate the feedback effect of radio AGN. I demonstrate that simple prescriptions to distribute radio galaxies in dark matter haloes which are shown to work in the local universe, can also account for the mass function and clustering of of radio-loud AGN. I combine the model predictions with previous results to estimated how much energy is being dumped by radio sources into haloes of different mass, and at different cosmic epochs.

*Chapter 6*: I present here a summary of the results and implications of this work, as well as discuss prospective ideas that are the subject of future investigations.

# 2

# Construction of Radio-Optical Galaxy Samples

In this chapter, I will address the problem of how radio and optical data are cross-matchted. While conceptually simple at first glance, this process is not immediately straightforward due to the nature of the different data, the spatial/angular scales involved, and the various survey setups. First, I will introduce the different catalogs that were used. Then I will proceed to explain the algorithm that selects candidate radio-optical associations, and the criteria used to accept or reject them. It should be noted that this involves associating the true (sometimes multiple) components observed in multiple radio surveys, to a single optical galaxy. I will also explain new techniques to improve the detection of sources below the nominal flux density limit adopted by radio catalogs. Finally, I will give an overview of the procedures to test the algorithm efficiency, assessing how many true objects are accepted, how many false matches are detected, and how many sources are missing from the catalogue.

The sample of radio-loud AGN assembled with these procedures forms the basis of the analysis described in the following chapters.

The contents of this chapter were published as Donoso, Best and Kauffmann, 2009, MNRAS, 392, 617.

## 2.1 The Sloan Digital Sky Survey

The Sloan Digital Sky Survey (SDSS; York et al. 2000; Stoughton et al. 2002) is a five-band photometric and spectroscopic survey started in the year 2000 that has mapped almost a quarter of the whole sky, providing precise photometry for more than 350 million objects and accurate redshifts for about a million galaxies and quasars. While the main scientific goals of the survey are studies of the large-scale structure of the universe and the properties of galaxies and quasars, it has proven extremely useful over a broad range of areas including mapping the structure and kinematics of the Milky Way (SEGUE; The SDSS-II SEGUE Collaboration: Brian Yanny et al.

2009), measuring accurate light curves of hundreds of Type Ia supernovae (Frieman et al. 2008), and discovering hundreds of new Jovian Trojan asteroids (Szabó et al. 2007).

Imaging data in the *ugriz* bands (Fukugita et al. 1996) was obtained with a wide-field 24×2048×2048 CCD camera (Gunn et al. 1998) mounted on a dedicated 2.5m telescope located at Apache Point Observatory in New Mexico. The observations were done in drift-scan mode, tracking great circles at the sidereal rate. Most images were taken good seeing conditions, with a median seeing of $\sim 1.4''$ in $r$ band. Astrometric coordinates are accurate to $\sim 0.1''$ per coordinate for typical extended objects, but close to half of that for bright point sources. The data is processed by a pipeline (Lupton et al. 2001; Stoughton et al. 2002) that reduces CDD images, performs the astrometric calibration, and detects objects, calculating position, brightness and shape. The imaging survey achieves a 95% completeness limit at ($u$,$g$,$r$,$i$,$z$)=(22.0,22.2,22.2,21.3,20.5) over most of the observed area and operational time.

The photometric system adopted is the AB system (Oke and Gunn 1983), calibrated by photometric standard stars observed by a companion 0.5 m telescope close to the main instrument. In this way, magnitudes are accurate to ∼2-3% level depending on the bandpass. Recently, a new calibration method that takes advantage of the overlapping area between adjacent imaging runs has been adopted (Padmanabhan et al. 2008), producing the so called *übercalibrated* magnitudes with $\sim 1\%$ uncertainty. Throughout this work we adopted the standard photometry because it was the only system available at the beginning of this work. In any case, it should be noted that for the purposes of this investigation the differences for the photometry of galaxies are largely irrelevant.

The SDSS pipeline calculates several types of magnitudes for each object. PSF magnitudes, based on the fitting of a gaussian profile, provide an optimal representation for the flux of stars and point sources. For extended objects (i.e. galaxies), a better representation of its flux is derived from the fitting of a two-dimensional model to the observed light distribution. Two models are fitted to the images of galaxies in each band: first, a de Vaucouleurs profile $I(r) = I_0 \times e^{-7.67(r/r_e)^{1/4}}$ that describes the bulge galaxy component; and second, an exponential profile $I(r) = I_0 \times e^{-1.68(r/r_e)}$ that fits the disk component ($r_e$ is the half-light radius). These are referred as *de Vaucouleurs* magnitudes and *exponential* magnitudes, respectively. A third magnitude type, *model* magnitude, is derived from the best-fit de Vaucouleurs or exponential profile in the $r$ band, with the amplitude scaled to fit the measurements in other filters. These magnitudes provide an unbiased estimator of galaxy colors in the absence of intrinsic color gradients since the same aperture is used in all passbands. Unless otherwise stated, model magnitudes are used in this work. Finally, a correction for foreground Galactic extinction was applied to all magnitudes following the dust extinction maps given by Schlegel et al. [1998].

A second instrument mounted in the SDSS telescope takes spectra of selected

objects. It consists of a twin 640 fiber multi-object spectrograph set up to give a spectral coverage from 3000$\mathring{A}$ to 9200$\mathring{A}$ at a resolution of $\lambda/\delta\lambda \sim 2000$. The imaging survey provides the targets selected for spectroscopy, which are arranged in tiles of radius 1.49 deg in order to maximize the number of allocated targets. It should be noted that due to mechanical constrains, the 3″ diameter fibers cannot be positioned closer that 55″, so spectroscopic coverage of dense regions such as clusters will be more incomplete. The vast majority of the spectra of galaxies and quasars yield reliable redshifts, with failure rates in of ∼1%. Around 88% of the targeted galaxies form the MAIN galaxy sample, with magnitudes $14.5 < r < 17.7$ and typical redshifts in the range $0.02 < z < 0.2$. The remaining 12% of targets are allocated to luminous red galaxies, fainter than the main sample, but extending out to $z \sim 0.38$. These are described in detail by Eisenstein et al. [2001], but they should not be confused with MegaZ LRGs, as they lie at different redshifts and are selected by different criteria.

The SDSS data have been made available to the scientific community in a series of cumulative yearly data releases (DR1, DR2, DR3, DR4, DR5, DR6 and DR7) that include new data, as well as data from previous releases re-processed with improved algorithms. This work uses data corresponding to the fourth Data Release (DR4), obtained before July 2004.

## 2.2 The MegaZ-LRG Galaxy Catalogue

The MegaZ-LRG (Collister et al. 2007) is a photometric redshift catalogue based on imaging data from the fourth Data Release (DR4) of the SDSS. It consists of ∼1.2 million Luminous Red Galaxies (LRGs) with limiting magnitude $17.5 < i_{deV} < 20$ over the redshift range $0.4 < z < 0.8$. MegaZ adopts various color and magnitude cuts to isolate red galaxies at $0.4 < z < 0.8$. The cuts are very similar to those adopted by the '2dF-SDSS LRG and Quasar' project (2SLAQ; Cannon et al. 2006). The specific color cuts are:

$$0.5 < g - r < 3 \tag{2.1}$$

$$r - i < 2 \tag{2.2}$$

$$c_{par} \equiv 0.7(g - r) + 1.2(r - i - 0.18) > 1.6 \tag{2.3}$$

$$d_{perp} \equiv (r - i) - (g - r)/8 > 0.5 \tag{2.4}$$

A further cut in $i_{fibre} < 21.4$ selects objects with sufficient flux to get enough S/N in the spectrograph (see later in this section). Essentially, $c_{par}$ isolates early-type galaxies (LRGs), while $d_{perp}$ selects galaxies with redshifts $z > 0.4$. This is illustrated in Figure 2.1, where the $g - r$ vs $r - i$ colors of 30000 randomly chosen MegaZ targets are plotted. These criteria are extremely efficient in selecting a homogeneous population of luminous red galaxies from the red sequence. More

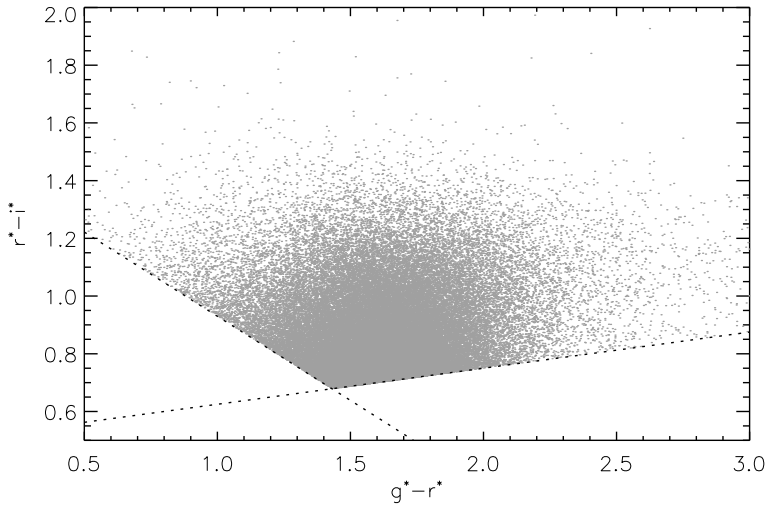


**Figure 2.1** • Distribution of (de-reddened) $g - r$ vs $r - i$ colors of target galaxies, selected by the MegaZ-LRG catalogue. The $c_{par} = 1.6$ (negative slope) and $d_{perp} = 0.5$ (positive slope) are indicated by dotted lines, which together with the plot limits, define color boundary criteria for the selection of luminous red galaxies. To improve visibility, only a subsample of the total catalogue is plotted.

than 95% of the targeted objects represent bona fide LRGs, while the remaining 5% are constituted mainly by M-type stars whose colors are very similar to those of LRGs.

The 2SLAQ spectroscopic survey applies almost the same photometric selection, but over a smaller 180 deg$^2$ equatorial stripe, in order to pick LRG candidates for follow-up spectroscopy. Figure 2.2 shows the spatial distribution of MegaZ and 2SLAQ sources in the sky. Using the Two-degree Field instrument on the 3.9m Anglo-Australian Telescope, 2SLAQ acquired spectra and redshifts for ∼13000 LRGs with the same selection function as MegaZ. This motivates the constrain on $i_{fibre}$ magnitudes of galaxies in the photometric catalogue.

Although only a small fraction of LRGs have spectroscopic redshifts measured by 2SLAQ, accurate photometric redshifts are available for the entire LRG sample. These were derived using an neural network photometric redshift estimator (ANNz, Collister and Lahav 2004). In general, photometric redshifts can be estimated from broadband photometry using two broad methodologies. The most traditional method is the *template matching* technique, where a set of of template spectral energy distributions (SED) derived from observations and/or population synthesis models are fitted in a $\chi^2$ sense to galaxy magnitudes. The accuracy depends on how well the templates are chosen in order to represent the diversity of the target galaxy population. The second approach aims to derive a parameterization of the redshift as function of photometric quantities. This parameterization

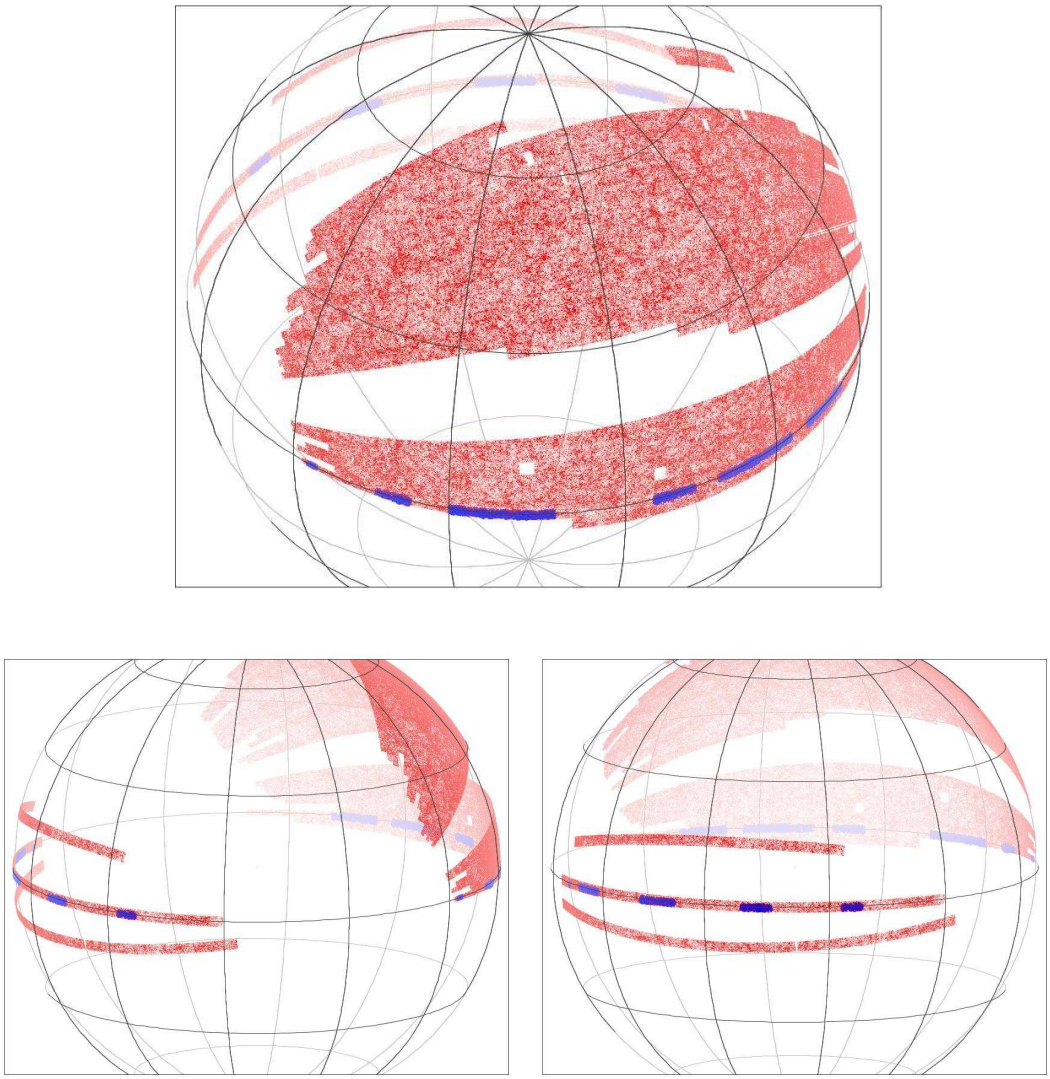

**Figure 2.2** • Spatial distribution of luminous red galaxies in the celestial sphere. Red dots mark the equatorial coordinates of MegaZ-LRG targets, while blue dots indicate targets selected by the 2SLAQ survey for spectroscopic follow-up observations (see text for details). The upper panel, along with two lower panels, focus in the northern and southern galactic parts of the survey, respectively. Celestial north points upward.

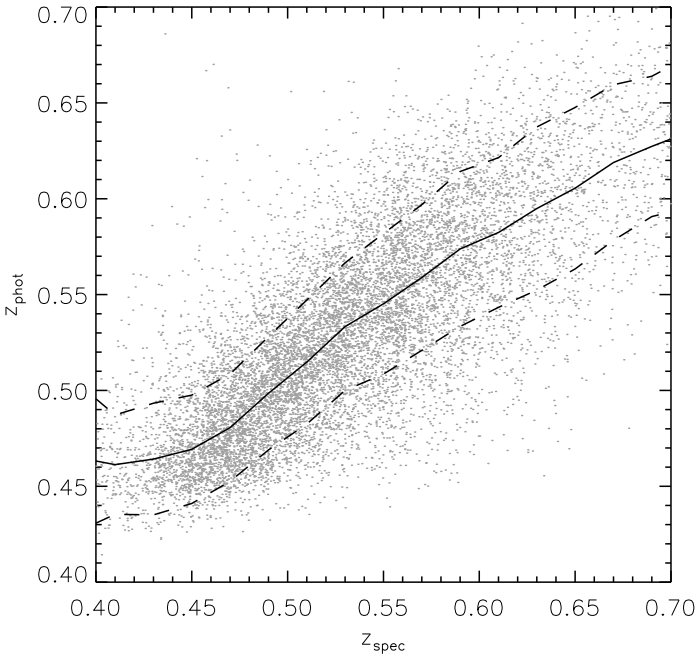


**Figure 2.3** • Spectroscopic redshift vs photometric redshift for the MegaZ sample, as calculated with artificial neural networks trained with spectroscopic data taken from the 2SLAQ survey. The mean and standard deviation, in bins of $\delta z = 0.02$ are indicated by the solid and dashed lines, respectively.

can be either explicit, for example expressing the redshift as a polynomial function of galaxy colors; or implicit, where the relation is not derived as a definite mathematical expression. One example of an implicit technique are *neural networks*. An artificial neural network is a set of interconnected software nodes or neurons, each one of which accepts an input, processes it, and feeds other nodes with partial output until a final output is produced. The network acts like a highly non-linear fitting function, mapping input *ugriz* magnitudes to an output estimate for the redshift, after being trained with a dataset where both input and output are known. Naturally, the best results are obtained when training and target datasets share the same selection effects, magnitudes, colors and redshifts. This is indeed the case for 2SLAQ and MegaZ.

Collister et al. 2007 used 2SLAQ to train a committee of four networks and used them to estimate photometric redshifts for MegaZ LRGs. Figure 2.3 shows the relation between spectroscopic and photometric redshifts. Over most of the redshift range, the ANNz $z_{phot}$ is an unbiased estimator of $z_{spec}$ with an error of $\sigma_z = 0.032(1 + z)$. They also estimated the contribution to the error budget that arises from noise in the photometry of faint objects. About $\sigma = 0.02 - 0.03$ of the total error, depending on the redshift, is due to variable photometric accuracy.

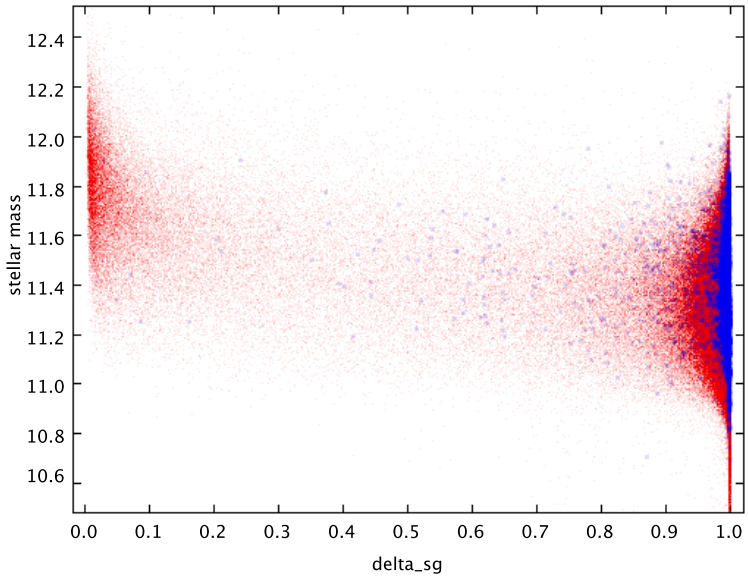


**Figure 2.4** • Stellar mass of galaxies as function of their probability parameter $\delta_{sg}$ as calculated by artificial neural networks after being trained with 2SLAQ spectroscopic data. Values of $\delta_{sg}$ close to 1 and 0 are typical of galaxies and stars, respectively. Red dots are for MegaZ-LRG targets and blue dots are for 2SLAQ galaxies. A number of miss-identified galaxies with large stellar masses are indeed stars, which are removed by setting $\delta_{sg} > 0.7$.

Another issue already noted is that about 5% of MegaZ objects are expected to be stars whose colors are almost indistinguishable from the real galaxy population. Neural networks were again used to derive an enhanced star/galaxy separation. In brief, ANNz was fed with de Vaucouleurs, exponential and model magnitudes, as well as a mixture of PSF fluxes, axis ratios and likelihood parameters, to derive for each object an output value $\delta_{sg}$, interpreted as its probability to be a galaxy or a star. $\delta_{sg}$ is a continuous variable that ranges from 0 (galaxy) to 1 (star), so a tradeoff must be made in choosing the threshold that discriminates between the two kinds of objects. If this value is set too low, stellar contamination persists, while if the value is set too high, true LRGs are discarded. We chose a threshold of $\delta_{sg} > 0.7$ that reduces the stellar contamination to $\sim$0.6%, discarding less than $\sim$0.8% of real LRGs. Figure 2.4 shows the galaxy stellar mass as function of $\delta_{sg}$ (the estimation of stellar masses is explained in Section 3.2). It can be appreciated that not applying such a cut would introduce a population of miss-identified galaxies with high stellar masses. Finally, it is worth to show where the remaining population of objects lies in color-magnitude diagram. Figure 2.5 illustrates the color-magnitude diagram for a random sample of SDSS Main galaxies and MegaZ targets. It can be readily appreciated that the latter populate a very well defined red sequence of galaxies.

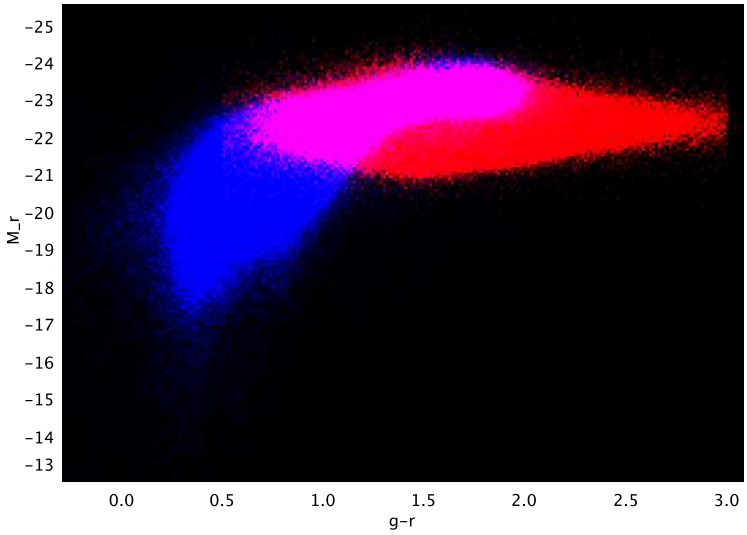


**Figure 2.5** • 2-D density histogram of $g - r$ vs $M_r$, k-corrected to z=0.1, corresponding to the SDSS DR4 Main galaxy sample plus the SDSS LRG sample (blue). The galaxies populate mostly two well defined sequences: the blue cloud and the red sequence. Overlaid are the high redshift MegaZ-LRG (red), forming an almost horizontal sequence that extends to much redder colors.

## 2.3 The NVSS and FIRST Radio Catalogs

The NRAO VLA Sky Survey (NVSS; Condon et al. 1998) is a radio continuum survey at 1.4 GHz carried by the 27-antenna Very Large Array (VLA) located in Socorro, New Mexico. It covers the whole sky at declinations $\delta_{J2000} > -40°$, providing total intensity ($I$) and polarization ($Q$,$U$) measurements down to a limiting point source flux density of $\sim 2.5$ mJy. The survey was carried out using the VLA in compact D and DnC configurations, which provides an angular resolution of around $45''$ and nearly uniform sensitivity. The rms noise and confusion limit in the total intensity maps is $\sigma_{RMS} \approx 0.45$ mJy beam$^{-1}$ FWHM, except near very strong sources or close the the Galactic Plane. Positional uncertainties in right ascention ($\sigma_\alpha$) and declination ($\sigma_\delta$) of the centroids grow for weak sources, but for objects brighter than the 3.5 mJy cutoff adopted in this work, these uncertainties are low ($\sigma_\alpha \cong \sigma_\delta < 4''$).

A catalogue of $\sim 1.8$ million point sources was derived by fitting elliptical gaussians to the discrete peaks in the images. In some cases, extended radio sources can be represented by multiple peaks. The catalogue lists peak flux densities and best-fit sizes for all sources with flux $S_{peak} \geqslant 2$ mJy beam$^{-1}$. The completeness of the NVSS survey is around 50% at $\sim 2.5$ mJy, but rises sharply to more than 99%

at 3.5 mJy. All images, catalogs and software are available online[1].

The VLA Faint Images of the Radio Sky at Twenty Centimeters (FIRST; Becker et al. 1995) is a survey that covers 10000 deg$^2$ of the Northern Galactic Cap, using the VLA in its B configuration at 1.4 GHz. This delivers a resolution of $\sim 5''$ and a typical noise of $\sigma_{RMS} \approx 0.13$ mJy, except in the vicinity of bright sources ($> 100$ mJy) where sidelobe interference can lead to an increased noise level. The sky coverage was chosen to overlap with most of the SDSS survey in the Northern Galactic Cap. Radio structures down to a few arcsec are resolved in FIRST, which is a valuable resource to match optical galaxies and radio sources.

As with the NVSS, a source catalogue including peak and integrated flux densities and sizes was derived from fitting a two-dimensional Gaussian to each intensity peak generated from the co-added images. Astrometric accuracy in this source catalogue is better than $1''$ for the faintest sources detected at the nominal flux threshold of 1 mJy.

FIRST was carried out during the mid-nineties and represented a factor of 50 improvement in sensitivity compared to other high frequency surveys at that time. Today, it still remains as the largest, most accurate wide-are survey available at 1.4 GHz. Reduced images and catalogs are available via the World Wide Web[2].

## 2.4 Cross-matching Radio and Optical Data

Over the last years, the amount of data available at different wavelengths for astronomical research has become so large, that it is relatively common to find optical, X-ray, radio or infrared for a set objects of interest. The techniques to correlate datasets across wavelength regimes have improved accordingly. The three important criteria that should be satisfied by a successful algorithm are the following : *maximum completeness*, *minimal contamination* and *full automation*. It is no longer possible to examine objects one-by-one. Hence, considerable care needs to be taken in choosing the various parameters that define whether observations in different catalogs correspond to a single true object.

This is particularly important when we try to identify the optical counterparts of radio sources. There are two reasons for this. First, radio sources often have extended structures, with sizes from a few arcsec up to tens of arcmins, and therefore in high angular resolution surveys, different components of the same source can split into different sources. Second, low resolution surveys can detect these multiple structures as a large, single component, but this makes it more difficult to reliably associate them with optical galaxies, whose surface density can be quite high (around 180 sources/deg$^2$ for MegaZ LRGs, but in the order of thousands per deg$^2$ for normal galaxies).

[1] http://www.cv.nrao.edu/nvss/
[2] http://sundog.stsci.edu/

The NVSS was the first radio survey with sufficient angular resolution to allow automated cross-correlation with optical surveys (Machalski and Condon 1999; Sadler et al. 2002). It has a resolution of 45″, making it sensible to diffuse large-scale emission. This beam size is large enough so that 99% of the radio sources are contained within a single NVSS component. However, such a low resolution results in an inevitably high percentage of missidentified objects, compromising the reliability of the sample.

A much lower contamination rate can be attained by correlating with radio surveys of higher resolution, such as FIRST, which has a resolution of 5″. Ivezić et al. [2002] constructed a sample matched to the SDSS with only 3% missclassified sources for a matching radius of 1.5″. FIRST is insensitive to very extended radio emission, and in fact resolves out large, faint radio structures. In some cases, FIRST can even miss the radio source completely. Nevertheless, as shown by Becker et al. [1995], the most important effects are that FIRST fluxes of extended objects are slightly underestimated, and that a single large source can be decomposed into multiple components.

Magliocchetti et al. [1998] first addressed the problema of how to define a single radio source from the multiple components listed by FIRST. They used a percolation technique to merge all neighboring sources of comparable flux, with separations below a linking length that varied as function of the total flux of the source. In this way clusters of bright components are combined into a single source, while faint sources remain as separate objects.

Best et al. [2005b] improved on this by using both NVSS and FIRST to carry out the cross-matching. The FIRST and NVSS surveys are highly complementary for identifying radio sources associated with nearby galaxies. NVSS provides the sensitivity to large-scale radio structures required to detect all of the emission from extended radio sources, while FIRST provides the high angular resolution required to reliably identify the host galaxy.

In this work, I have followed and improved the techniques given by Best et al. [2005b], and the reader is referred to their publication for a detailed explanation of the methods. Here, I give a broad overview of the steps involved, the criteria adopted, as well as the modifications that where implemented.

The following is a brief scheme of the cross-matching algorithm. Each stage is explained in more depth in subsequent sections in this chapter.

**1** | *Sky Coverage Mask*: exclude optical galaxies outside the area covered by the FIRST survey.
*Bright Source Mask*: exclude galaxies close to very bright radio sources, as the noise in NVSS image maps around such sources grows substantially. This is important, but the total area excluded is small, around 8.3 $\mathrm{deg}^2$.
*Redshift Cut*: exclude galaxies with redshifts below $z = 0.01$, because such

nearby galaxies appear very extended in the sky and their optical positions are consequently uncertain. This cut only applies to the construction of the low redshift DR4 comparison sample.

**2** | *NVSS Matching*: the remaining galaxies are cross-correlated with NVSS sources. Two sets of candidate objects are produced, those associated with a single NVSS component, and those associated with multiple NVSS sources.

**3** | *Multi-NVSS Source Testing*: candidates with multiple NVSS components are investigated, tested against a set of criteria, and either accepted or rejected. For accepted objects, the total radio source flux is the sum of the integrated flux densities of the NVSS components. A few sources that present very complex radio morphology are inspected visually.

**4** | *FIRST Matching*: single NVSS sources are matched against FIRST objects. Candidates are selected according the number of FIRST matches.

**5** | *Single FIRST Source Testing*: single NVSS sources with one FIRST component are tested and either accepted or rejected.

**6** | *Multi-FIRST Source Testing*: if multiple FIRST components are found in the vicinity of single NVSS sources, they are tested to determine if they satisfy the criteria for single FIRST sources, or if they form a multi-component radio source.

It should be noted that adopted flux densities are integrated quantities over the source extension. For a resolved source with peak flux $s_{peak}$, major axis $\theta_M$ and minor axis $\theta_m$, the integrated flux is

$$s_{int} = s_{peak} \left( \frac{\theta_M \theta_m}{\theta_{beam}} \right) \tag{2.5}$$

Similar expressions for unresolved sources are given by Condon et al. [1998].

Any accepted source (single or multiple), has an adopted final flux equal to the sum of component NVSS fluxes. FIRST is only used to validate the candidate associations, and does not provide flux data.

Best et al. [2005b] considered radio sources above a flux limit of 5 mJy. The major reason for this choice was to reduce any loss of sensitivity to multi-component NVSS sources. The MegaZ radio sources are more distant and their angular sizes are thus smaller, so there are fewer multi-component sources. In order to probe fainter radio galaxies out to higher redshifts, a (total) flux limit of 3.5 mJy was adopted. This value corresponds to approximately 7 times the noise level in the typical NVSS maps.

The parameters and criteria for rejection or acceptance of the various kinds of candidates were progressively refined in an empirical way using Monte-Carlo

simulations. Ten random catalogs of sources distributed over a 720 $\deg^2$ contiguous patch of the SDSS survey footprint, were constructed and then processed by the same algorithm treating real data. We evaluate the efficiency of the methodology by comparing how many associations are detected in the real dataset and how many are detected in random datasets. The numbers quoted in the following sections pertain to this test area.

### 2.4.1 Multi-component NVSS Sources

In order to find candidate multi-component NVSS sources, all NVSS detections within a 3 arcmin distance from each optical galaxy were identified. This radius smaller than the mean distance between NVSS sources ($\sim$8 arcmin) and is also larger than even the largest radio galaxies at $z > 0.3$. Candidates were tested according to the number of NVSS sources as follows:

### 2.4.2 NVSS doubles

Candidate NVSS doubles can be either true double sources, or single NVSS sources with a distant unrelated component. Figure 2.6 plots the offset of each pair member with respect to the optical galaxy, for both real and random catalogs. The numbers have been scaled to the same number of real sources). The two upper and lower panels show the cases before and after cross-correlation with FIRST, respectively. Note that subindices 1,2,3 refer to the first, second and third closest source from the MegaZ-LRG, respect to which all offsets are measured. Flux densities are denoted by $S$, FIRST as $F$ and NVSS as $N$. Our procedure is as follows:

- $\mathrm{off_{N1}} < 15''$: reclassified as NVSS single candidates.
- $15'' < \mathrm{off_{N1,N2}} < 90''$: selected as candidate doubles if the flux-weighted mean position is within $15''$ of the optical galaxy, and $\mathrm{off_{N1}} > \min[15'', \mathrm{off_{N2}} - 20'']$. These criteria are indicated by the solid lines in Figure 2.6. They enclose the region where there is an excess of sources, compared to random, with reasonably separated components and few spurious associations.
- Candidates are cross-matched with FIRST and classified according to:
  - ▷ *Accepted doubles*: if there is a FIRST component within $3''$
  - ▷ *Accepted doubles*: if (i) there are no FIRST components due to the flux being resolved out, (ii) $\mathrm{off_{N1,N2}} < 60''$, and (iii) the angle $\mathrm{NVSS_1}$-galaxy-$\mathrm{NVSS_2}$ is >135 deg. This accounts for mildly bent radio sources.
  - ▷ *Rejected doubles*: if there are $\leqslant$3 FIRST sources with $\mathrm{off_{F1,F2,F3}} > 15''$, and with $\sum \mathrm{S_{FIRST}} > 0.5(\mathrm{S_{NVSS1}} + \mathrm{S_{NVSS2}})$
  - ▷ *Visual cases*: remaining doubles are too difficult to classify automatically

and therefore were inspected visually using NVSS, SDSS and FIRST images simultaneously.

### 2.4.3 NVSS Triples

Candidate NVSS triples could be a true triple association, or they could be a double source plus an unassociated component. They are selected as possible triples if

- $\mathrm{off}_{\mathrm{N1,N2,N3}} < 120''$
- One of the following conditions is fulfilled
  - ▷ for all three components the offset between the optical galaxy and the flux weighted mean position is $< 15''$
  - ▷ for the two furthest components the offset between the optical galaxy and the flux weighted mean position is $< 15''$. This rule accounts for double-lobed objects plus a visible jet feature.
  - ▷ $\mathrm{off}_{\mathrm{N1}} < 15''$, $\mathrm{off}_{\mathrm{N2,N3}} < 90''$, and the angle $\mathrm{NVSS_2}$-$\mathrm{NVSS_1}$-$\mathrm{NVSS_3}$ is >135 deg. This selects double-lobed (possibly bent) galaxies, with a detected core component.

Triples satisfying these constrains were matched with FIRST and classified as

- *Accepted triples*: if there is a FIRST source with off $< 3''$
- *Rejected triples*: if there are $\leqslant$3 FIRST sources with $\mathrm{off}_{\mathrm{F1,F2,F3}} > 15''$, and with $\sum \mathrm{s_{FIRST}} > 0.5(\mathrm{S_{NVSS1}} + \mathrm{S_{NVSS2}} + \mathrm{S_{NVSS3}})$
- *Visual cases*: as for doubles, remaining triples were referred to visual analysis.

For the second and third nearest components of NVSS triples, Figure 2.7 plots the offsets from the optical galaxy for both, real (left) and random (right) datasets. Also for both cases, the candidates that were finally accepted, rejected (as triples), marked as potential doubles, or deferred to visual inspection, are indicated by the different symbols. As can be seen in the right panel, very few random matches are selected as true sources.

### 2.4.4 NVSS Quadruples

Candidate objects with 4 or more NVSS components within 3 arcmin where inspected visually in all cases, as it would be too difficult to define an efficient set of rules to accept or reject them automatically.

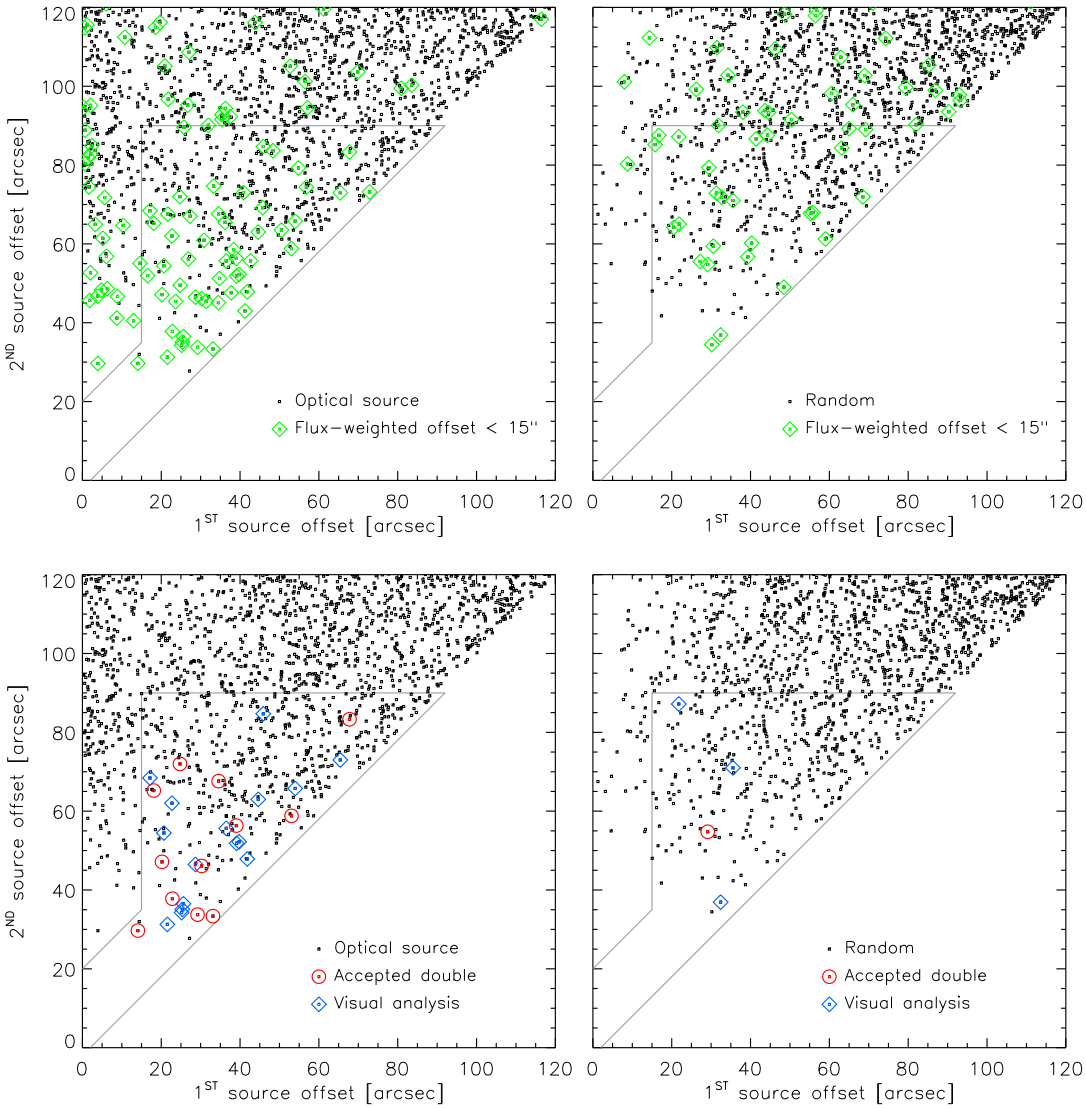


**Figure 2.6** • Positional offsets of the two NVSS component sources from the optical MegaZ galaxy, for candidate double NVSS matches selected from real data sample (left) and from the random catalogs (right). Upper panels show candidates selected on NVSS, and lower panels show the results after cross-matching with the FIRST catalogue. Green diamonds mark the cases where the flux-weighted mean position of the component pair lays within 15″ of the optical source. Also indicated are the candidates accepted as true double sources (red circles) or referred to visual analysis (blue diamonds). Section 2.4.2 explains in detail the criteria to accept or reject a source. They enclose a region (gray lines) where a large number of real candidate doubles are found, but only a small number of false matches get accepted in the random samples.

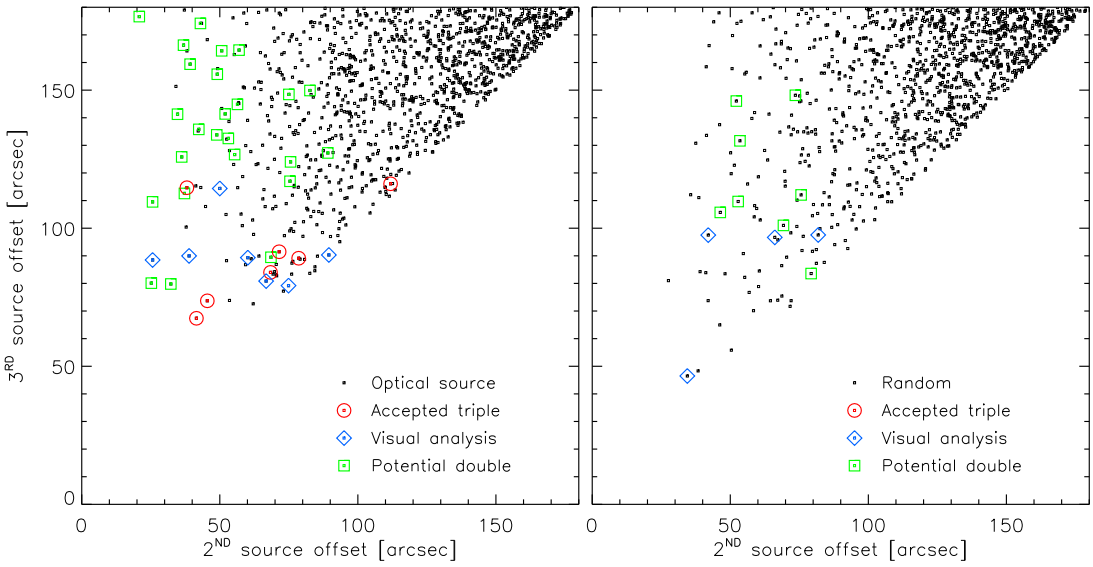


**Figure 2.7** • Distribution of offsets from the optical galaxy, for the second and third furthest NVSS components in triple source candidates. The left panel correspond to real candidate matches, while the right panel is for a comparable number of positions in the random samples. Objects finally accepted, rejected, marked as potential doubles, or deferred for visual inspection, are indicated by the different symbols.

### 2.4.5 Single-component NVSS Sources

Having dealt with complex multi-component NVSS sources, the next step is to analyze single NVSS objects. Most large radio sources are removed by the previous procedure, so that most (but not all) remaining objects are expected to be no larger than 15″.

Figure 2.8 shows the distribution of positional offsets between the MegaZ-LRGs and the NVSS source, for this population. There is a clear excess of galaxies, compared to random matches, for separations less than ∼10-15″, but the excess remains significant out to ∼70 ″. A significant part of the effect at larger angular separations is because galaxies are intrinsically clustered, while random samples are not (see Section 2.5 for a quantitative estimation of this effect). However, some part of the excess may consist of true associations between LRGs and extended NVSS sources. The subsequent FIRST cross-matching helps in pinpointing such cases. Best et al. [2005b] carried out this cross-matching for all optical galaxies with a single NVSS match within 30″. In this work, the limit is increased to 60″. Tests with random catalogs show that this identifies an extra 37 (2.8%) genuine radio galaxies at a cost of 0.8 false matches, i.e. a decrease of only ∼0.01% in reliability.

As before, by including information from the FIRST data, incompleteness can be lowered. Thus, all MegaZ galaxies with a single NVSS match were cross-correlated with the FIRST catalogue.

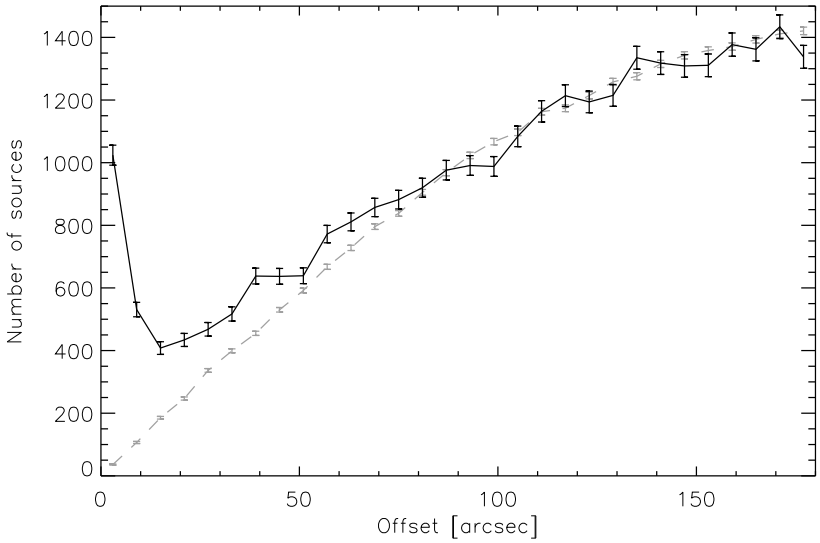


**Figure 2.8** • Distribution of offsets between the MegaZ-LRG galaxies and the closest NVSS source (solid line) and the corresponding offsets distribution derived from the random samples (gray dashed line). Most true matches clearly stand out at offsets less than 15 arcsec, but the excess remains significant out to separations of ∼70 arcsec. However, at these large separations this is mostly the result of the galaxy clustering.

### 2.4.6 NVSS Sources with 1 FIRST Match

Figure 2.9 plots the distribution of offsets between the FIRST component and the optical galaxy, for single NVSS sources with a single FIRST match within 30″. It can be seen that there is a clear excess of sources in the real dataset, at all separations compared to random samples. As noted before, at large scales this is mostly the result of the clustering of radio galaxies, but at small distances the peak corresponding to true associations stands clearly above the random matches. Up to a separation of 3″, the contamination by missidentified sources is well below ∼1%, so all candidates with offsets below this threshold were considered as true matches. Although the number of random detections with separations greater than 3″ rises sharply, just discarding all candidates above 3″ is not an option, as it would dramatically affect the sample completeness. Therefore, the selection criteria we adopt to accept real FIRST matches exploits also the geometrical information about the components in question as follows:

- $\mathrm{off_{F1}} < 3''$: classified as single NVSS, single FIRST source.
- $3'' < \mathrm{off_{F1}} < 10''$: classified as single NVSS, single FIRST source if
  - ▷ $\mathrm{angle[axis, offset]} < 30$ deg: the angle between the source major axis and the offset vector pointing to the optical galaxy is $< 30$ deg.
  - ▷ $\mathrm{off_{F1}} < 0.75 \times \mathrm{D_{proj}}$: the projected size of the source major axis along the offset direction, $\mathrm{D_{proj}}$, is a comparable fraction of the offset length.

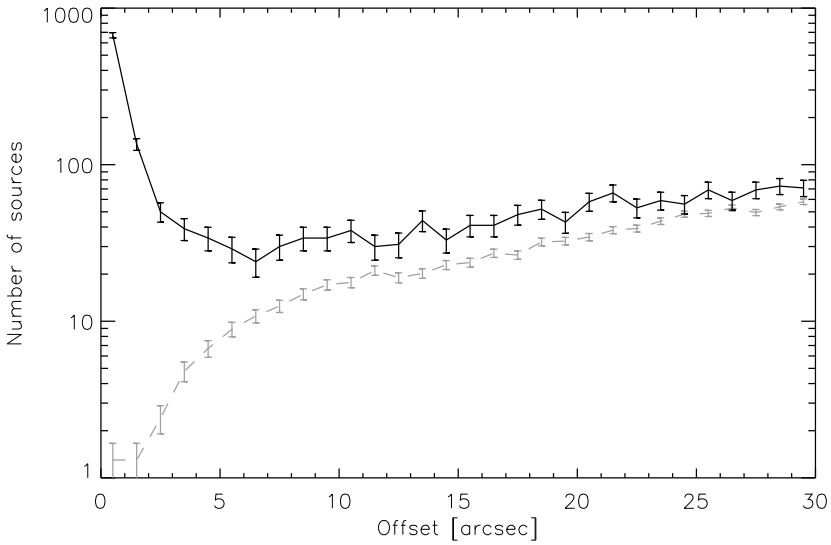


**Figure 2.9** • For galaxies with single NVSS source and a single FIRST match, this plot shows the distribution of MegaZ-FIRST offsets, for real data (solid line) and for random datasets (dashed gray line). The excess of true sources, compared to random, remains remains significant over all separations, but it is likely to be the result of galaxy clustering at large scales. Most true associations are expected to have offsets below 10-15″.

This selects sources that are extended along the direction defined by the optical and radio positions. Figure 2.10 plots the projected major axis length of the candidates as function of the MegaZ-FIRST offset, for real objects and for a comparable number of random objects. The selection rule is illustrated by the solid lines, and the diamonds mark the final accepted sources. Clearly, a large number of extended sources above 3″ are recovered, at the expense of very few false matches.

### 2.4.7 NVSS Sources with 2 FIRST Matches

The cases where a single NVSS source was matched to 2 FIRST components are naturally more complex. McMahon et al. [2002] analyzed in depth the properties of FIRST sources matched with optical galaxy catalogs, and found that genuine FIRST double sources could be identified by requiring: (i) the two sources to have comparable flux densities, (ii) the flux-weighted mean position of both components to be close to the optical galaxy, (iii) the sizes of the two sources to be comparable, meaning both are probably radio lobes. Based on this results, we adopted the following procedure:

- $\mathrm{off}_{\mathrm{F1}} < 3''$: accepted as NVSS singles with 2 FIRST components. As the nearest source is very close the optical galaxy, it can be interpreted as the core of of a core-jet source.

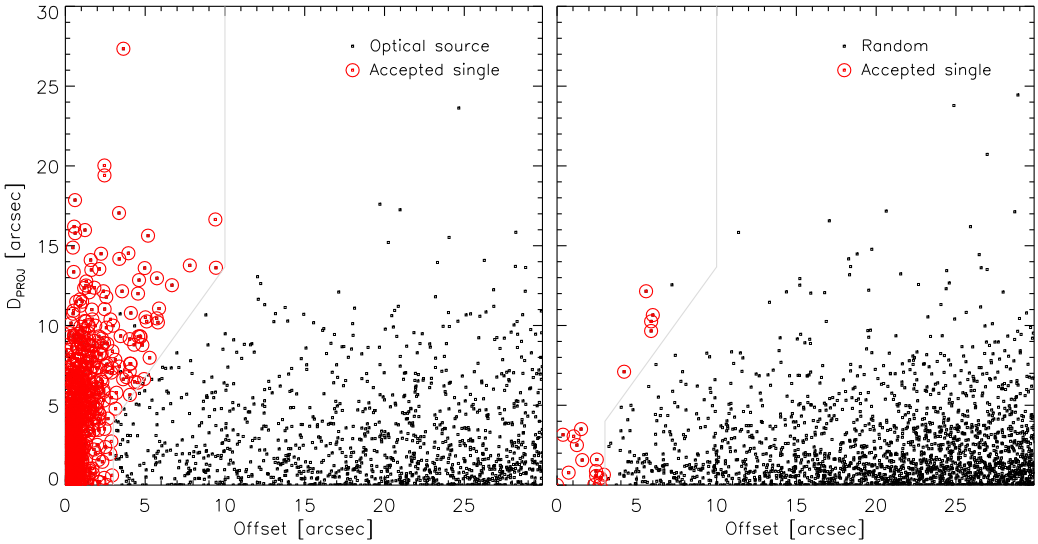


**Figure 2.10** • For single NVSS, single FIRST sources, this plot shows the FIRST major axis size projected in the direction to the the optical galaxy, as function of its separation. Left panel is for real candidates, and the right panel is for a comparable number of random positions. The gray lines enclose the region where there is an excess of possible true matches, compared to random. Such excess is clear for $\mathrm{off}_{\mathrm{F1}} < 3''$, but also for the range $3'' < \mathrm{off}_{\mathrm{F1}} < 10''$ and when the offset is less than 0.75 times the projected axis length. Red circles mark the objects finally accepted (i.e. those oriented within 30 deg from the offset vector, see Section 2.4.6).

- $\frac{\mathrm{D1}}{\mathrm{D2}} \times \frac{\mathrm{S1}}{\mathrm{S2}} \times \langle \mathrm{off}_{\mathrm{F1,F2}} \rangle_{\mathrm{fw}} < 5$: accepted as valid doubles if the ratio of the source sizes (d), multiplied by the ratio of the source flux densities (s), multiplied by the offset of the flux-weighted mean position, is less than 5. These rules identify most double-lobed extended radio sources with undetected cores. Figure 2.11 plots the offsets of the two components, and shows that very few objects pass these criteria in the Monte-Carlo simulations, while a large number of sources are recovered from the real data.

### 2.4.8 NVSS Sources with 3 and more FIRST Matches

The rules to select NVSS matches with 3 FIRST components are similar to the ones for double sources:

- $\mathrm{off}_{\mathrm{F1}} < 3''$: accepted as triple FIRST source.
- $\langle \mathrm{off}_{\mathrm{F1,F2,F3}} \rangle_{\mathrm{fw}} < 3''$: accepted as a triple source if the angle formed by three components is >135 deg, i.e. the triplet has a straight line configuration.
- pair rule: if any of the three possible component pairs meets the selection criteria for double FIRST sources, the candidate is accepted as a valid triple.

The cases of galaxies having 4 or more FIRST components can not be treated automatically without introducing more complex techniques, as we would then have

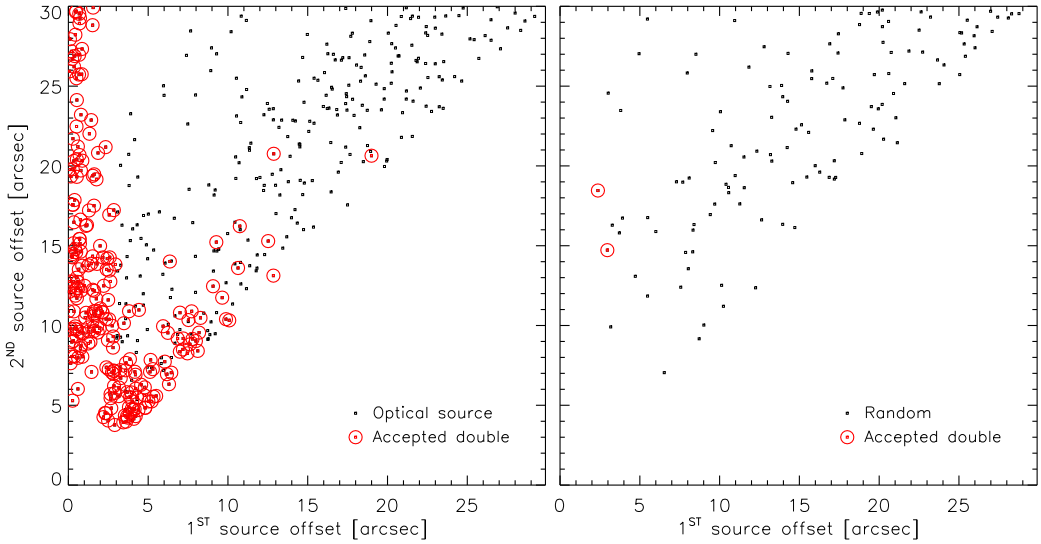


**Figure 2.11** • For single NVSS, double FIRST candidates, this plot shows the distribution of offsets between the two FIRST components and the optical Mega-Z galaxy. The left panel is for real candidates, while the right panel is for the same number of random matches. Accepted doubles are denoted by red circles. The exact criteria to accept or reject double sources is explained in detail in Section 2.4.7.

to start to describe the details of particular radio morphologies. Nevertheless, all objects in this category were tested by considering the closest components to the optical galaxy and testing them against the rules for triple, double and single sources. As before, rejected cases were not discarded, but sent to visual analysis.

### 2.4.9 Improved matching of sources without FIRST counterparts

Because the NVSS radio sources reach a fainter limit than those studied by Best et al. [2005b], more objects with no nearby FIRST match were found (8% compared to 5%). Most of these are likely to be extended sources missed by the low surface brightness sensitivity of FIRST. A small fraction may be variable radio sources whose flux density has changed between observations. To be retained in the catalogue, these objects are required to be associated with an optical counterpart.

As discussed before, the high resolution of the FIRST survey is essential to allow reliable cross-matching with dense optical samples. The NVSS sources without FIRST counterparts are the largest source of incompleteness in the final sample. However, blindly accepting all LRG candidates out to a separation of 20″ from the NVSS source introduces an average of 42.2 false detections in our random samples, reducing the reliability of the catalogue to 79%. Figure 2.12 plots the distribution of NVSS-MegaZ offsets in real and random data, for single NVSS candidates without FIRST matches. At large separations the excess caused by galaxy clustering is dominant, while random matches increase steadily with increasing separation. At

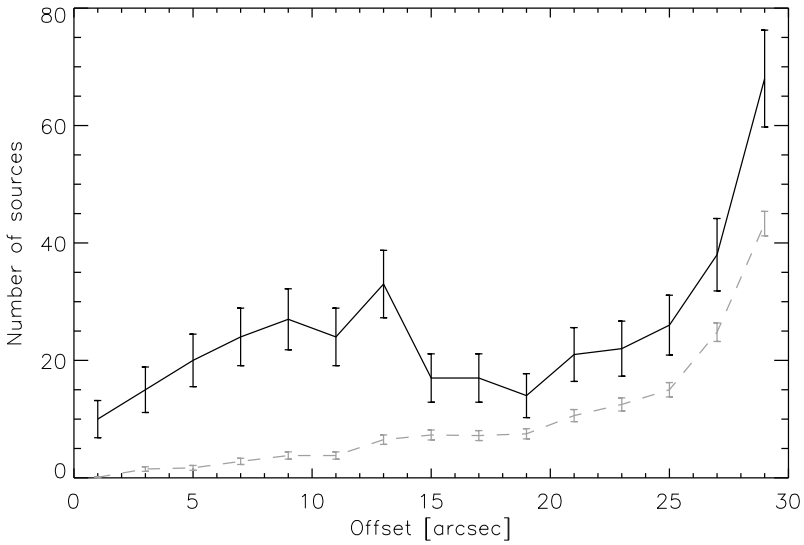


**Figure 2.12** • Distribution of offsets between MegaZ-LRG galaxies and NVSS candidates for sources that have no match in the FIRST catalogue. Results are shown for real (solid line) and random (gray dashed line) samples. Matches with separations larger than $\sim 15''$ are mostly the result of galaxy clustering, so most real sources are expected to lay below this threshold.

intermediate scales, there are still a number of objects that could in principle be recovered, provided the contamination can be controlled.

A careful inspection of FIRST images (along with NVSS and SDSS cutouts) around the positions of these objects revealed that in many cases there were bright spots near or slightly below the survey flux limit, that were clearly associated with a MegaZ galaxy. We have developed a method to use this extra information in order to increase the number of matches. Figure 2.13 shows FIRST cutouts of typical objects with no cataloged FIRST source, but with a nearby NVSS-MegaZ association. In many cases one or more bright "spots" matching the NVSS source and MegaZ galaxy can be seen, while in some cases two well-defined symmetric radio lobes centered around the optical galaxy are evident.

We took advantage of this additional information in deciding whether candidates should be accepted as true FIRST matches. For galaxies within $10''$ of the NVSS source we accepted all matches. In the test area, this provided 96 associations of which 9.9 are expected to be false (i.e. 10.3% contamination). For galaxies with offsets between 10 and $15''$, we accepted matches according to the following procedure:

**1** | The FIRST image was segmented using an initial threshold of $3\sigma_{rms}(\alpha, \delta)$, where $\sigma_{rms}(\alpha, \delta)$ is the *local* rms noise in the map. This provided a number of seed spots whose centroids were refined using the intensity-weighted moments in both directions.

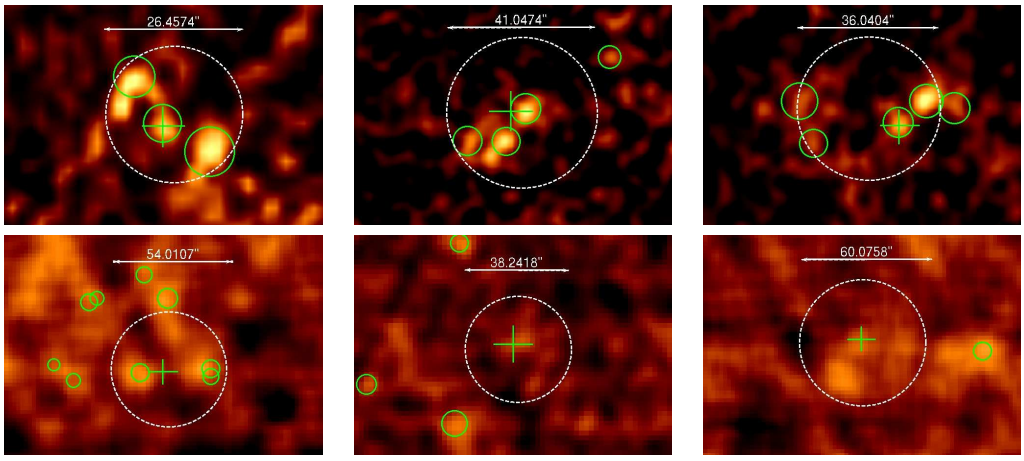


**Figure 2.13** • FIRST cutouts around sources without FIRST counterparts. The dashed circle marks the NVSS source position and size, while the plus sign indicates the MegaZ optical galaxy location. The small circles mark the detected spots. Top three panels are examples of accepted matches, while bottom panels are examples of rejected cases. A boxcar sliding average filter has been applied to enhance the visibility.

**2** | A brightness profile was derived for each spot and both the half light radius and the flux inside this radius were determined.

**3** | Any bright spot with a mean flux density greater than 0.4 mJy and within 5″ of the optical counterpart was considered to be a valid spot. These sources were accepted unless there were more than 4 bright spots inside a circle of 30″, in which case the match was rejected because it is then difficult to associate the source with a single MegaZ galaxy. Visual inspection of SDSS images confirmed this behavior.

To test this 'spot matching' technique we repeated the same procedure for candidates without FIRST components in the random samples. This constitutes a robust check, since we are in effect looking at random locations in the sky, so we can assess how probable it is to find a spot pattern by chance. In the sky test area, this procedure identified 13 additional FIRST for sources with NVSS-MegaZ offsets between 10 and 15″, at the cost of introducing only 2.4 false detections. This increases the overall completeness of the sample, for little cost in reliability. Our tests indicate that it is not possible to extract more matches beyond a ∼15″ offset with reasonable confidence.

### 2.4.10 Repeated Matches and Visual Classification

A fraction of the candidate sources (1093 objects, or 7.5% of the sample) with multiple NVSS or FIRST components were flagged as being too unreliable to classify by automated means. These were classified visually by simultaneous examination of SDSS, NVSS and FIRST images. Of these, 221 were accepted as genuine sources.

After running the procedures described above, the resulting catalogue was checked for the presence of two of more optical galaxies associated with the same radio source. This happened, for example, when two close radio sources appear merged together in NVSS due to its low angular resolution. In this case, the (NVSS) flux density was divided between the two galaxies according to the ratio of their FIRST flux densities. If the resulting flux density was greater than 3.5 mJy the source was retained. A total of 560 cases where visually examined to ensure that no NVSS source was linked to two different MegaZ-LRG galaxies.

Altogether, 564 positive matches (3.9%) result from the complete visual classification process.

## 2.5 Reliability, Completeness and Final Catalogue

Table 2.1 lists the number of accepted radio matches for different classes of radio sources found in the sky test area. Results are provided for both real and random samples, as well as reliability estimates. Note that even though this sample is much deeper and more than five times larger than the one of Best et al. [2005b], we were able to compile a catalogue with comparable reliability ($\sim$98.3%).

Because the true number of radio sources is unknown, the completeness is more difficult to estimate than reliability. Nevertheless, a reasonable estimate of the completeness can be obtained by considering the MegaZ-LRGs that have an NVSS source within a distance of $15''$. These can be assumed to be a mixture of true matches, random alignments from sources at different redshifts, and a contribution from sources that are associated with other galaxies which just happen, through clustering, to be close to the target galaxy. By using the Monte-Carlo simulations in the sky test area to estimate the latter two contributions, we can estimate the number of true matches and hence the completeness.

In the sky test area there are 1765 MegaZ-LRGs with an NVSS source within a distance of $15''$. In comparison, there are an average of 225 sources within the same distance to the galaxies in the random catalogs. Determining the contribution from clustered galaxies galaxies is more complicated. This was attempted in two ways.

First, we selected all NVSS-SDSS candidates with a single FIRST component within 15 arsec, but which were rejected by the matching algorithm. We then searched for other optical MegaZ galaxies in a $3''$ region around these FIRST radio positions (a standard search radius for FIRST matching, e.g. Obrić et al. 2006). From a total of 359 LRGs, 40 (11.1%) had a nearby LRG with an associated FIRST source. The corresponding fraction in the random sample was 0%. This means 11.1% of the 1765 sources ($\sim$200) within $15''$ are due to clustering.

To check this result, we estimated the excess number of LRG-LRG pairs over random by integrating the angular correlation function $w(\theta)$ given by Ross et al.

[2007] for the 2SLAQ catalogue out to 15″. This yielded value of 1.66, i.e. $\sim 150$ extra sources due to clustering. These two values are in rough agreement; the fact that the first method gives a slightly larger number can be explained by the fact that radio galaxies are in general more massive than the underlying LRG population, so we would expect them to be more strongly clustered. This is demonstrated in detail in Chapter 4. For our final completeness estimate, we assume that 180 sources are due to clustering.

The expected number of true matches is then estimated as $1765 - 225 - 180 = 1360$. Our matching procedure detects 1309 objects, of which 21.7 are predicted to be false detections. The completeness can therefore be estimated as $100 * (detected - false)/expected$ or $100 * (1309 - 21.7)/1360 \approx 95\%$. This value is comparable to that obtained by Best et al. [2005b], for a much lower redshift sample. It should be noted that this completeness estimate applies only to the MegaZ-LRG sample and does not take into account missing radio-loud QSOs or radio galaxies that do not pass the MegaZ-LRG color cuts. [3]

Table 2.2 lists the final number of radio galaxies found in the MegaZ-LRG sample and included in the catalogue. This catalogue is by far the largest sample of radio galaxies of its kind. Out of a total of 14553 sources, the majority (78.6%) have single counterparts in both FIRST and NVSS, and a significant fraction (11.5%) are resolved by FIRST into multiple components. Only 253 (1.7%) sources have multiple NVSS counterparts, to be compared with the 6.2% found by Best et al. [2005b]. This is again expected, because the radio galaxies lie at larger distances.

Finally, it is important to note that M-type stars with similar colors as those of faint LRGs were removed when compiling the radio galaxy catalogue, as explained in section 2.2. To give a visual impression of the different kind of objects detected by the procedure, Figures 2.14, 2.15 and 2.16 show radio and optical images of typical multiple FIRST, multiple NVSS and single NVSS/FIRST radio sources. They demonstrate how important is FIRST to correctly associate the optical galaxy, and why NVSS is needed to capture the flux of giant radio structures.

## 2.6 The Local Radio Galaxy Comparison Sample

In the following chapters, most results obtained for the MegaZ-LRG catalogue of radio AGN will be compared to those obtained for galaxies selected from the main spectroscopic galaxy sample of SDSS DR4.

These two datasets are comparable as they are selected essentially by the same set of procedures. They have redshifts in the range $0.01 < z < 0.30$, with a mean

[3] A preliminary comparison with a complete spectroscopic catalogue at similar redshifts indicates that $\sim$ 20% of all galaxies with $M_* > 10^{11}$ $M_\odot$ are too blue to fall within the MegaZ-LRG color boundaries. Since radio AGN are biased towards the higher mass galaxies, the corresponding percentage should be smaller for this population.

**Table 2.1** • Numbers of different classes of accepted MegaZ-LRG radio galaxies, as well as the corresponding numbers found in the random samples. The numbers are for a 720 deg$^2$ patch of the total survey area. Values in parentheses indicate the number of sources accepted using the spot-matching technique (see section 2.4.9).

| NVSS type | FIRST type | MegaZ | Random | Reliability(%) |
|---|---|---|---|---|
| NVSS single | 0 comp. | 109(13) | 12.3(2.4) | 88.7 |
| NVSS single | 1 comp. | 1068 | 7.8 | 99.3 |
| NVSS single | 2 comp. | 88 | 1.2 | 98.7 |
| NVSS single | 3 comp. | 38 | 0.3 | 99.2 |
| NVSS single | 4+ comp. | 6 | 0.1 | 98.3 |
| NVSS mult. | | 24 | 0.8 | 96.7 |
| **Total** | | **1333** | **22.5** | **98.3** |

**Table 2.2** • Total number of MegaZ-LRG radio galaxies with 1.4 GHz flux above 3.5 mJy in the different classes.

| NVSS type | FIRST type | MegaZ |
|---|---|---|
| NVSS single | 0 comp. | 1176 |
| NVSS single | 1 comp. | 11445 |
| NVSS single | >1 comp. | 1679 |
| NVSS mult. | | 253 |
| **Total** | | **14453** |

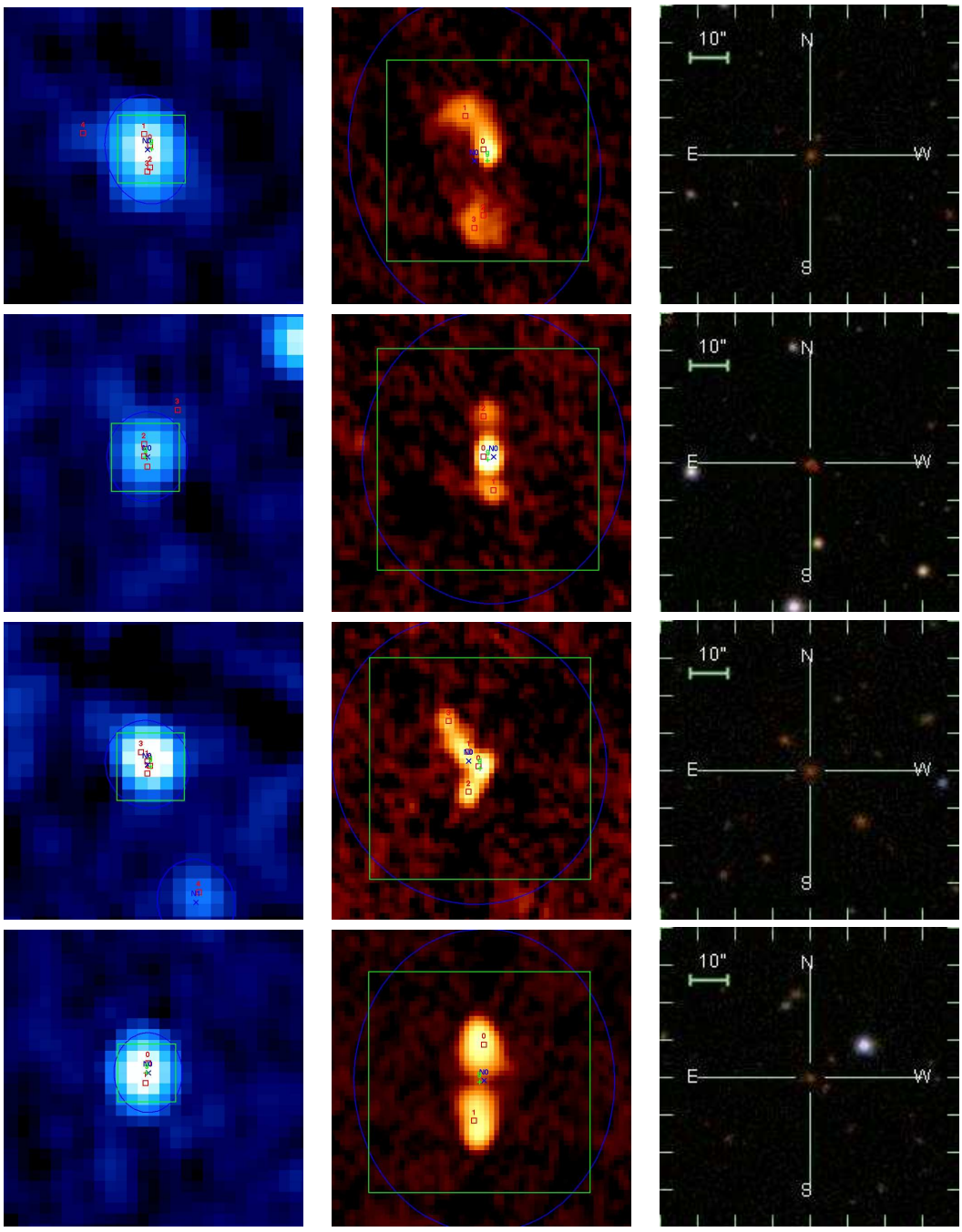


**Figure 2.14** • NVSS (left), FIRST(center) and SDSS(right) cutouts around radio sources with multiple FIRST counterparts. The optical galaxy position is marked by the green (g) plus symbol and the FIRST components are indicated by the successive (0,1,2,...) red squares. NVSS sources are shown in blue. The large green square measures 80x80 arcsec and corresponds to the field of view of the optical image.

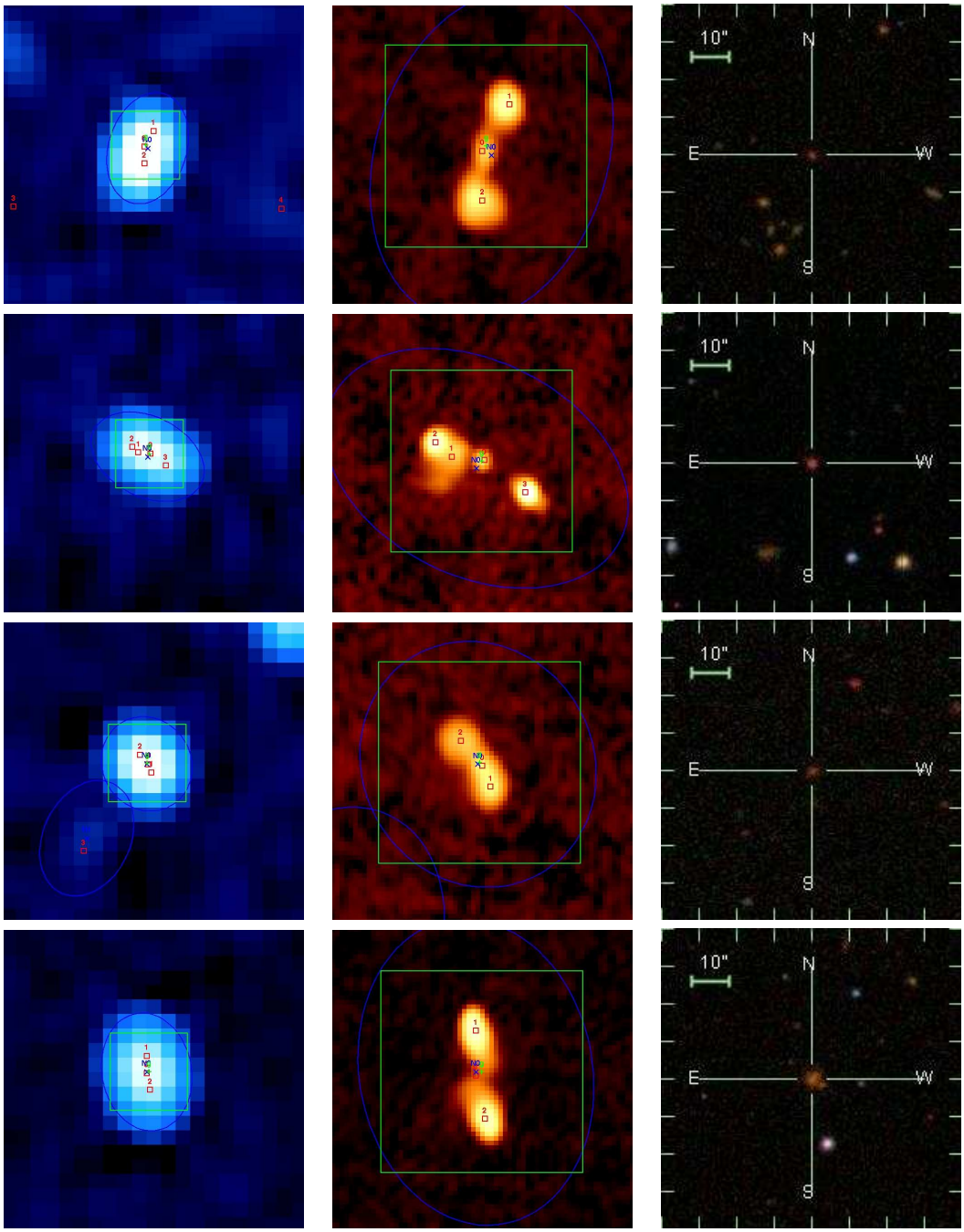


**Figure 2.15** • Continuation of Figure 2.14.

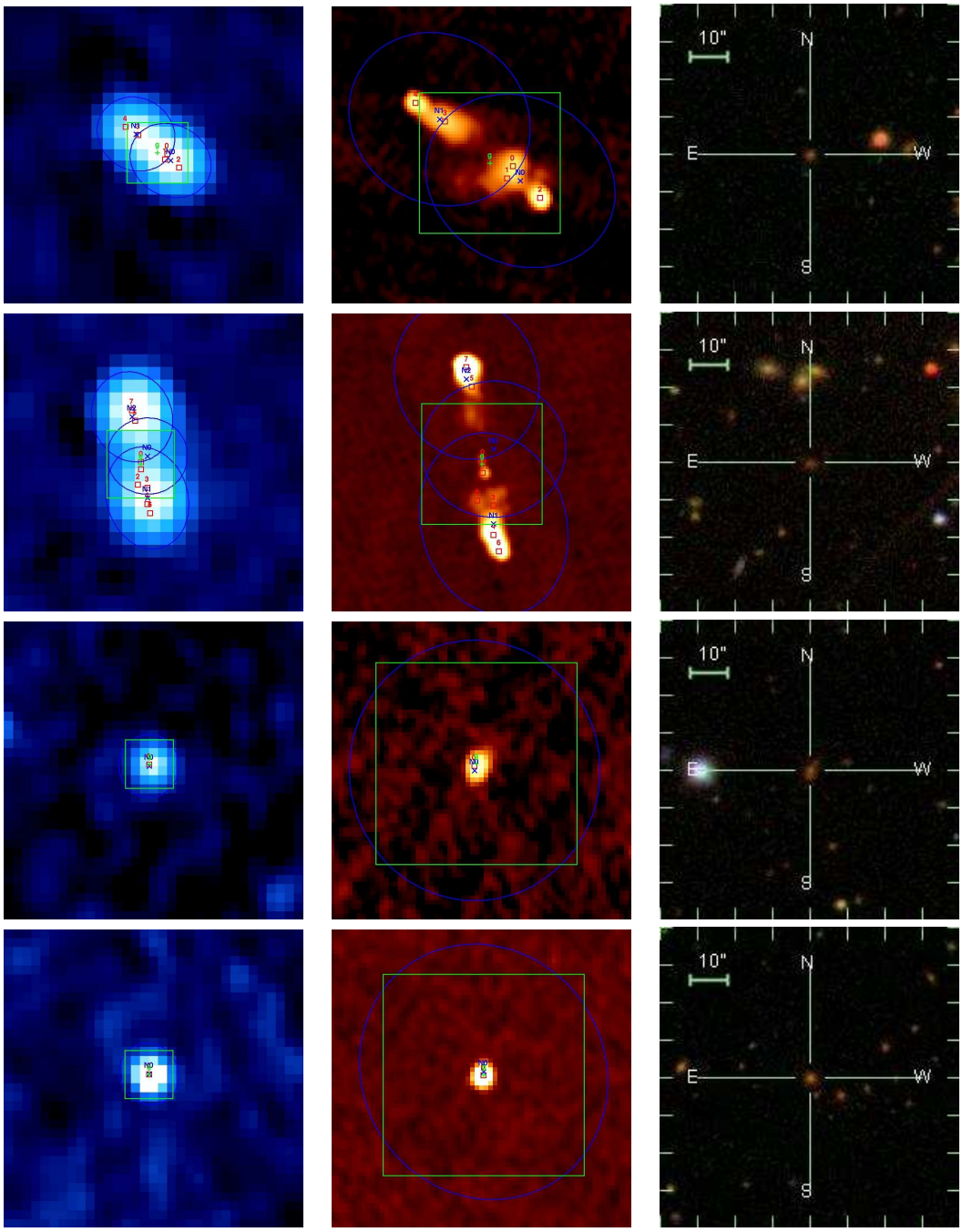


**Figure 2.16** • NVSS (left), FIRST(center) and SDSS(right) cutouts around radio sources with multiple NVSS counterparts (upper two rows), and single NVSS/FIRST matches (lower two rows). The optical galaxy position is marked by the green (g) plus symbol and the FIRST components are indicated by the successive (0,1,2,...) red squares. NVSS sources are shown in blue. The large green square measures 80x80 arcsec and corresponds to the field of view of the optical image.

redshift of $\langle z \rangle \sim 0.14$. This sample represents an extension to the fourth Data Release of the original DR2 radio-matched catalogue by Best et al. [2005b]. This sample is composed of two populations of radio-emitting galaxies: the radio-loud AGNs that dominate at high radio powers, and the star forming galaxies, which are usually much fainter. The radio emission of the latter is mostly the result of the synchrotron emission of particles accelerated in supernova shocks, so they are associated with star formation activity. To investigate the radio AGN phenomena alone it is necessary to discriminate between these two populations.

Normal star-forming galaxies and AGN are often separated using optical emission-line properties, as they occupy different regions in the BPT (Baldwin et al. 1981) diagnostic diagram of NII/H-$\alpha$ vs OIII/H-$\beta$. However, as pointed by Kauffmann et al. [2003a], a significant fraction of emission-line selected AGN also have associated star formation. This means that using emission-line ratios to separate radio-loud AGN is not ideal, as radio-quiet AGN could be mistaken as radio-loud due to the emission associated with star formation processes. In addition, this would limit the classification to galaxies with well measured optical spectral lines.

Best et al. [2005b] proposed a radio AGN/SF division based on the location of galaxies in the $L_{1.4\mathrm{GHz}}/M^*$ vs $D4000$ plane. They adopted a 3 Gyr exponential star formation track derived from Bruzual and Charlot [2003] stellar population models to discriminate between the two populations. This methodology is shown in Figure 2.17, as applied the DR4 low redshift sample. The left panel shows the location of the galaxies in the $L_{1.4\mathrm{GHz}}/M^*$ – $D4000$ plane (restricted to $0.03 < z < 0.1$ for the plot). Star-forming galaxies lie below the exponentially decaying star formation curve (dashed line), while true radio-loud AGN lie above it, at higher $D4000$ or stellar ages. The right panel shows the location of radio-emitting galaxies in the BPT diagram. The colors indicate the different classifications of objects according to their position in the BPT plane. Together, these plots demonstrate the reliability of the AGN-starburst separation for radio galaxies, which is estimated to be accurate by about$\leqslant$1%. For more details about the methodology we refer to Kauffmann et al. [2003a] and Best et al. [2005b]. Finally, it is worth to recall that in our sample of high redshift radio galaxies it is not necessary to apply this separation, as it is composed of very luminous radio sources ($> 10^{24}$ W hz$^{-1}$) which can only be powered by the central AGN.

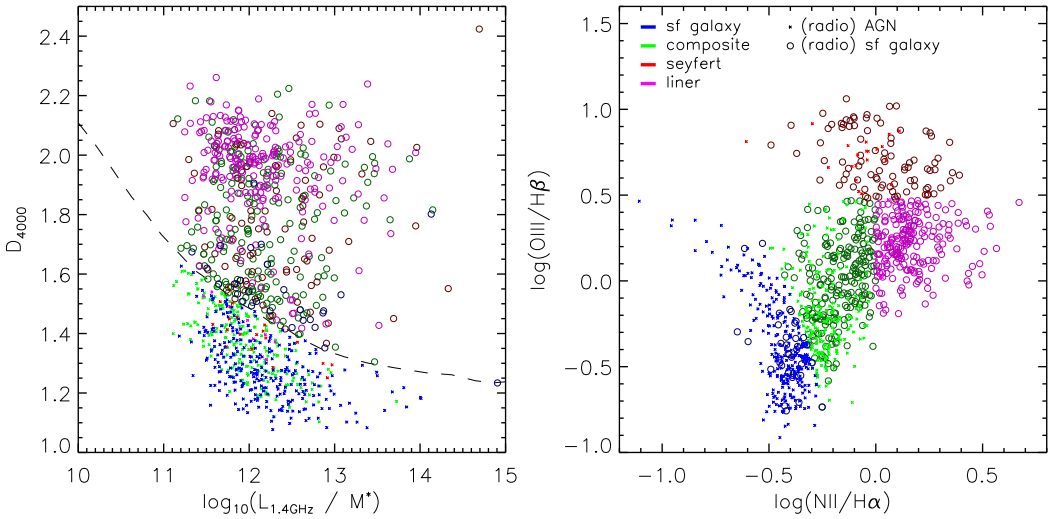


**Figure 2.17** • AGN-starburst separation for radio galaxies in the SDSS DR4 sample. The left panel shows the $L_{1.4\mathrm{GHz}}/M^*$ vs $D4000$ plane, divided by the 3 Gyr exponentially decaying star formation track derived from Bruzual and Charlot [2003] stellar population synthesis models (dashed line). Objects below the curve are mostly star-forming galaxies (small dots), and objects laying above it are radio AGN (circles). Colors indicate the classification of galaxies in the BPT plane. To improve the visibility, the plot is restricted to $0.03 < z < 0.1$.

# 3

# Evolution of Radio-Loud Active Galactic Nuclei

In this chapter I will turn to the study of the evolution of radio galaxies, exploiting the large samples of radio AGN constructed in the previous chapter. By using uniform methodologies and algorithms, it is fair to compare low redshift radio AGN selected from SDSS DR4 with their high redshift counterparts drawn from the MegaZ-LRG sample.

I begin by describing the techniques used to derive (k+e)-corrections and stellar masses for each galaxy, based on fits to broad-band photometry, as well as the tests performed to check those estimates. Then, I present a new determination of the radio luminosity function, which is the main tool to study the evolution of (radio) galaxies. This constrains the overall statistics of the radio AGN population.

Then I proceed to calculate the probability for a galaxy to become a radio-loud AGN, as function of its stellar mass and radio power. By comparing estimates in the high and low redshift datasets, I trace how this relation changes as function of cosmic time. To get further insight into these relations, I also estimated the bivariate radio luminosity-mass function, which gives the probability that a galaxy in a given stellar mass range hosts an AGN with radio power above a certain value. This is an effective way to combine the information of the radio luminosity function and of the radio-loud AGN fractions in a single diagram, to pinpoint in which galaxies does most of the evolution takes place. This complements the analysis of the properties of galaxies that host radio AGNs.

Finally, I address the issue of systematic biases that might affect the results. These biases come from photometric redshift errors and errors on the photometry of distant LRGs measured by SDSS, potentially altering the derived luminosities and stellar masses. By convolving low redshift samples with typical errors of high redshift LRGs, I estimate that such biases, while present, do not significantly affect the results.

The contents of this chapter were published as Donoso, Best and Kauffmann, 2009, MNRAS, 392, 617.

## 3.1 Introduction

Ever since the first studies of Longair [1966], it has been widely accepted that evolution is required to explain the radio source counts. Strong cosmological evolution of the high luminosity radio source population has been established out to at least $z = 2 - 3$ (e.g. Dunlop and Peacock 1990), with the space-densities of the most powerful radio sources increasing by a factor $\sim 10^3$ relative to their densities at $z \sim 0$. However, the evolution of the low-luminosity radio galaxy population remained more uncertain. Clewley and Jarvis [2004] found that the low luminosity population of radio sources with $L_{325\mathrm{MHz}} < 10^{25}$ W Hz$^{-1}$ sr$^{-1}$ exhibits no evolution out to $z \sim 0.8$. In contrast, Brown et al. [2001] found significant cosmic evolution out to $z \sim 0.55$, which they modelled using a pure luminosity evolution model as $P(z) = P(0)(1+z)^{k_L}$, with $3 < k_L < 5$. More recently, similar results were obtained by Sadler et al. [2007], who analyzed radio galaxies in the '2dF-SDSS Luminous Red Galaxy and Quasar' (2SLAQ) survey (Cannon et al. 2006). They found that the number density of radio sources below $\mathrm{P}_{1.4\mathrm{GHz}} = 10^{26}$ W Hz$^{-1}$ grows by a factor of $\sim 2$ between $z = 0$ and $z = 0.55$. These results confirm that the cosmic evolution of low power radio sources is considerably weaker than that of their higher radio power counterparts. However, because of the relatively small sizes of samples, none of these studies was able to accurately constrain the luminosity dependence of the evolution.

Over the same period, our physical understanding of radio galaxies has developed steadily. Fanaroff and Riley [1974] showed that radio galaxies exhibit a dichotomy in radio morphology. Low radio luminosity sources are usually 'edge-darkened', with radio jets that quickly decelerate and flare as they advance through the interstellar medium (Fanaroff-Riley class I sources, or FRIs). In contrast, most higher luminosity sources have jets that remain relativistic over kpc and up to Mpc scales, ending in bright hotspots ('edge-brightened' sources, or FRIIs). The dividing line between FRIs and FRIIs occurs around a monochromatic power of $\mathrm{P}_{1.4\mathrm{GHz}} \sim 10^{25}$ W Hz$^{-1}$, although Ledlow and Owen [1996] showed that it occurs at higher radio luminosity in more optically-luminous galaxies. This division is close to the break in the radio luminosity function, and has led to the hypothesis these two populations of radio galaxies correspond to the different populations of cosmologically-evolving sources, FRIIs being strongly evolving and FRIs much less so (e.g. Jackson and Wall 1999).

A more important division in the radio source population, however, appears to relate to the radiative properties of the AGN. Powerful FRIIs and a small subset of the more powerful FRIs (e.g. see Heywood et al. 2007) show strong emission lines and either a visible or hidden quasar-like nucleus (Barthel 1989), indicative of radiatively efficient accretion. In contrast, most FRIs and a sub-population of weak-emission-lined low luminosity FRIIs show no evidence for a powerfully radiating nucleus (see Hardcastle et al. 2007 and references therein) suggesting radiatively

inefficient accretion. This implies that a fundamental difference exists between high and low power radio sources that is distinct from the radio morphological dichotomy. Instead, it is likely to be related to different origins or mechanisms of gas fueling.

Understanding this low luminosity radio source population, and its cosmic evolution, is not only important for understanding the physical origin of the radio activity, but also for understanding galaxy evolution. There is growing evidence that low-luminosity radio-loud AGN play a critical role in regulating the masses and star formation rates of galaxies. Semi-analytic models of galaxy formation (for example see White and Frenk 1991 and Cole et al. 2000) successfully reproduce many of the the observed properties of galaxies. However, these models over-predict the abundance of galaxies at the bright end of the luminosity function. This problem arises because many massive galaxies are predicted to sit at the center of hot hydrostatic halos, in which cooling flows are expected to develop. If the gas cools and forms stars, central group and cluster galaxies are too massive by the present day and have much bluer colors than observed. Tabor and Binney [1993] first suggested that radio galaxies could in principle regulate these cooling flows, preventing significant accretion of gas and limiting the mass of galaxies. This concept of AGN feedback has now been successfully incorporated into the semi-analytic models of Bower et al. [2006] and Croton et al. [2006].

Observational support for a scenario in which radio AGN play an important role in regulating the growth of massive galaxies has slowly been accumulating. Both luminous FRII and low power FRI sources can in principle inject a significant amount of energy into the surrounding gas, as their radio lobes expand and interact with the surrounding medium ($\sim 10^{42}$ ergs$^{-1}$ for the jets of a borderline FRI/FRII object, see Bicknell 1995). This has been directly observed in clusters of galaxies, where the expanding radio lobes create buoyant bubbles and drill cavities in the hot intracluster medium (Boehringer et al. 1993; McNamara et al. 2000; Fabian et al. 2003). In nearby systems, which can be studied in detail, the energy supplied by the radio source is well-matched to that required to balance the cooling (e.g. Fabian et al. 2003).

With the availability of large redshifts surveys like the 2-degree-Field Galaxy Redshift Survey (2dFGRS, Colless et al. 2001) and the SDSS it has become possible to obtain the sky and redshift coverage needed to define sufficiently large samples of nearby radio sources to study population statistics and global energetics. Best et al. [2005b] constructed a sample of 2215 radio-loud AGN brighter than 5 mJy with redshifts $0.03 < z < 0.3$ using the SDSS Data Release 2 (DR2) in combination with the Very Large Array NVSS and FIRST surveys. Best et al. [2005a] found that the fraction of radio-loud AGN, $f_{RL}$, is a strong function of black hole and stellar mass, with dependencies $f_{RL} \propto M_*^{2.5}$ and $f_{RL} \propto M_{BH}^{1.6}$. Twenty-five percent of the most massive galaxies (with $M_* \sim 10^{11.7}$ M$_\odot$) host radio sources more powerful than $10^{23}$ W Hz$^{-1}$. By combining these results with estimates of the energetic output of

these sources, Best et al. [2006] showed that the time-averaged mechanical energy output of radio sources in elliptical galaxies is comparable to the radiative cooling losses from the hot halo gas, for ellipticals of all masses. Radio sources can therefore provide sufficient energy to suppress cooling flows and regulate the growth of massive galaxies in the nearby Universe.

The role of powerful (radiatively-efficient) FRII objects could not be addressed by Best et al. due to the scarcity of such systems in the low redshift catalogue. Another open question is how the heating-cooling balance in massive galaxies evolves with redshift. In order to address these issues, we require a large radio galaxy sample at higher redshifts. By comparing with a sample of local radio sources selected from SDSS DR4 with a very similar algorithm, we aim to study not only of the evolution of the radio galaxies, but also the evolution of the duty cycle of radio AGN activity in galaxies as a function of their stellar mass.

## 3.2 Stellar Masses and (K+e)-corrections

One of the most important observables in understanding galaxy formation and evolution is the stellar mass content in galaxies. It is a sensitive tracer of the physical processes governing the evolution of the baryonic matter, and provides information on the coupling between the galaxy growth as dark matter halos collapse and merge. The stellar content in galaxies is regulated by a multitude of factors, e.g. intrinsic star formation within galactic disks, accretion of nearby satellites, close encounters, and merging of galaxies. Many physical processes combine to determine the mass assembly of galaxies.

However, the stellar mass of a galaxy is relatively difficult quantity to measure. Mass estimates based on direct measures of the dynamics of systems, like the stellar velocity dispersion, are available only for some objects at relatively high observational cost. They measure the total mass of the systems, usually requiring adequate models to account for the contributions of dark matter and gas.

The alternative is to convert the luminosity of a galaxy into a stellar mass by means of a model of its stellar population, derived either from photometry or spectroscopy, that predicts a mass-to-light ratio ($M/L$) in a certain wavelength band. Near-infrared luminosities of galaxies are thought to be ideal for this approach, as the derived $M/L$ varies only by a factor of $\sim$2 for a wide range of star formation histories (e.g., Bell and de Jong 2001). But again, IR data is available only for limited areas of the sky.

Measuring the stellar masses of galaxies in the local universe by modeling their stellar populations has been successfully attempted using newly available wide-area galaxy surveys. Kauffmann et al. [2003b] used spectroscopic data from the SDSS to derive accurate stellar masses of galaxies. At $z \sim 0$, Bell et al. 2003 used the

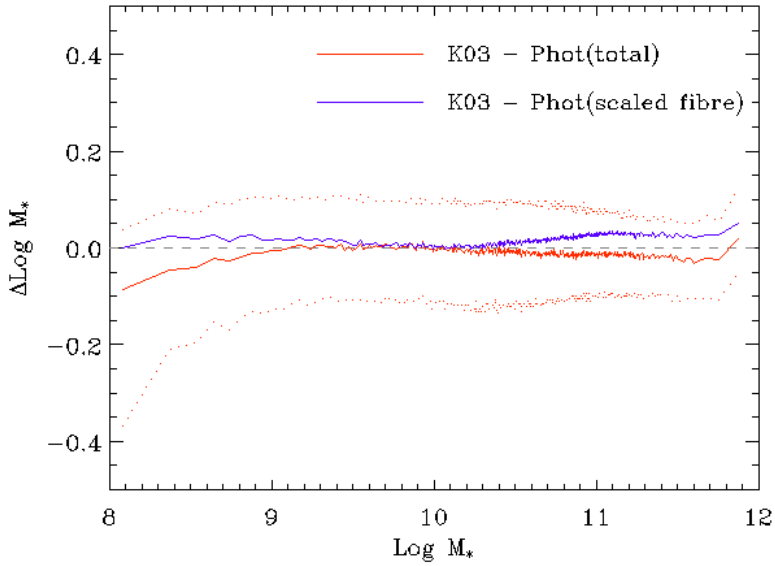


**Figure 3.1** • Comparison for DR4 data of mass estimates based on fits to the photometry and on fits to spectral indices. The x-axis shows the stellar mass from Kauffmann et al. [2003b], derived from spectral data. The y-axis shows the median difference between that estimate and the one obtained from fitting to total magnitudes (red), and to fiber magnitudes scaled to total (blue). Dotted lines show the 1 sigma variation. In general, both estimates are in good agreement. Adapted from `http://www.mpa-garching.mpg.de/SDSS/DR7/Data/stellarmass.html` .

concentration and colors of galaxies derived from SDSS to classify galaxies as early or late type and derived separate mass functions for each class, demonstrating that early types dominate at higher masses. Baldry et al. [2004] found similar results, but used the bimodal color distribution to separate early from late-type populations.

To derive stellar masses for each galaxy, we used the KCORRECT algorithm (Blanton and Roweis 2007), which finds the non-negative linear combination of spectral templates that best matches the flux measurements of each galaxy in a $\chi^2$ sense. These templates are based on a set of Bruzual and Charlot [2003] synthetic stellar population models that span a wide range of star formation histories, metallicities and dust extinctions, so they can be used to estimate the mass-to-light ratio of a galaxy. This method yields stellar masses that differ by less than 0.1 dex on average from estimates given by other techniques, for example the method using the 4000Å break strength and $H\delta$ absorption proposed by Kauffmann et al. 2003b. Figure 3.1 illustrates this point, showing a comparison of two different mass estimates for SDSS DR4 data: one derived from fits to the broad-band photometry, and the other derived from the spectral indices of galaxies.

In order to compare radio galaxies at different redshifts in a fair way, we need to compute the volume over which the MegaZ sources are visible, given the magnitude and color cuts of the survey as well as the 3.5 mJy radio flux limit. In

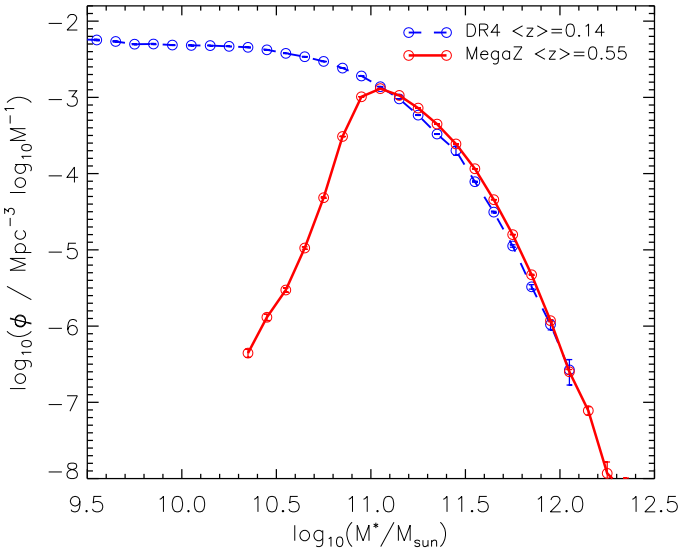


**Figure 3.2** • Mass function for galaxies in the MegaZ-LRG (solid red line) and the DR4 sample (dashed blue line). There is no significant evolution in mass between the two redshift intervals of the samples.

this work we generated $(K+e)$-corrections using a library of Bruzual and Charlot [2003] evolutionary stellar population synthesis models. LRGs constitute a nearly homogeneous population of old, red, early-type galaxies with spectral energy distributions that are reasonably well described by a single stellar population (SSP) model that forms all its stars in an instantaneous burst at high redshifts (we choose $z = 9.84$) and then passively evolves (Wake et al. 2006). We use these models to compute $K$-corrections, which account for the redshifting of the spectra through the different rest-frame bandpasses, and $e$-corrections, which account for the intrinsic evolution in the spectral energy distribution of galaxies because stars are younger at higher redshifts. With these corrections in hand, we are able to predict the $u, g, r, i, z$ magnitudes as well as the radio luminosities of each MegaZ LRG as function of redshift, which then allows us to determine the precise minimum ($z_{min}$) and maximum ($z_{max}$) redshift that a particular object enters and then leaves the radio-optical sample. The weight for each $i$-th galaxy is then $1/V_{max,i}$, where $V_{max,i}$ is the integral of the comoving volume between $z_{min,i}$ and $z_{max,i}$, calculated as

$$V_{max,i} = \Omega \frac{c}{H_0} \int_{z_{min,i}}^{z_{max,i}} \frac{dV_c}{dz} dz \tag{3.1}$$

where $\Omega$ is the survey area in sterads, $z_{min,i} = z_{min,i}^{optical}$, and $z_{max,i} = \min[\mathrm{z}_{\mathrm{max,i}}^{\mathrm{optical}}, \mathrm{z}_{\mathrm{max,i}}^{\mathrm{radio}}]$.

As a check, we have computed the stellar mass function and the luminosity function of the LRGs in the MegaZ catalogue, and we compare our results with

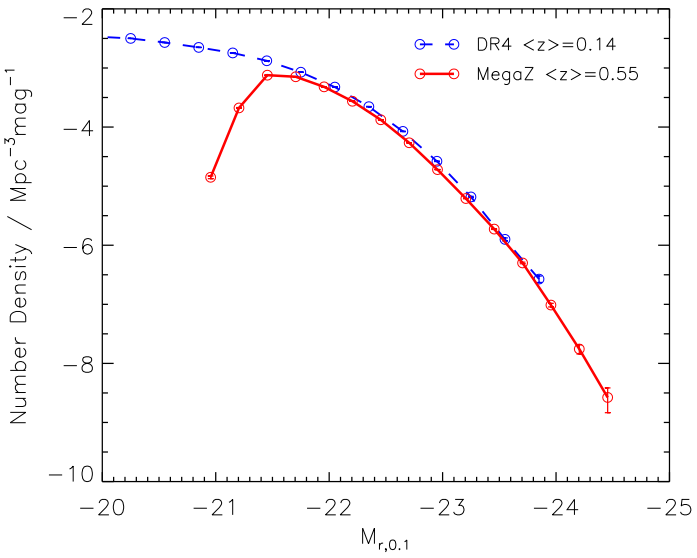


**Figure 3.3** • Luminosity function for galaxies in the MegaZ-LRG (solid red line) and the DR4 sample (dashed blue line). Luminosities in the $r$ band are $(k+e)$-corrected to $z = 0.1$ as explained in Section 3.2 There is very little change in the comoving space density of the two samples.

analog estimates derived for low redshift galaxies drawn from SDSS DR4. These are shown in Figure 3.2 and in Figure 3.3. The MegaZ-LRG sample probes the high mass end of the stellar mass function, spanning a range in stellar mass from $10^{11}$ to $10^{12.2} M_{\odot}$. Over this range in mass, there is essentially no evolution in the stellar mass function out to $z \sim 0.55$. This is in accord with recent results presented by Brown et al. [2007] and Cool et al. [2008], who show that the upper end of the stellar mass function has apparently changed very little out to a redshift of $z \sim 0.9$. The same is true regarding optical luminosities of galaxies, as we do not find significant evolution in the comoving space density of objects. As expected, the LRGs extend to significantly brighter magnitudes up to $M_{r,0.1} \sim 24.5$.

## 3.3 The Radio Luminosity Function

A standard technique for quantifying the rate of evolution of a population of galaxies is to compare the radio luminosity function of such objects at two different epochs. In this section, we will determine the evolution of the radio-loud AGN population by comparing the luminosity function of MegaZ-LRG radio galaxies with that derived from the SDSS DR4 sample. These functions were calculated for radio sources above a 1.4 GHz flux density limit of 3.5 mJy using the standard $1/V_{max}$ formalism

proposed by Schmidt [1968], given by the expression

$$\Phi(\mathrm{P_{1.4GHz}}) = \sum_{\mathrm{i}} \frac{1}{\mathrm{V_{max,i}}} \tag{3.2}$$

where the sum is computed for the galaxies in a given luminosity bin. We estimate $V_{max}$ for each galaxy as the maximum comoving volume within which it would be visible given the radio flux and optical magnitude limits and the color cuts used to define the MegaZ-LRG sample (see Section 3.2). We have included both $K$-corrections and $e$-volutionary corrections in this computation as described in the previous section. Radio luminosities are calculated using the formula

$$\log_{10}[\mathrm{P_{1.4GHz}}] = \log_{10}[4\pi \mathrm{D_L^2(z) S_{1.4GHz}}(1+\mathrm{z})^{\alpha-1}] \tag{3.3}$$

where $\mathrm{D_L}$ is the luminosity distance in the adopted cosmology, $\mathrm{S_{1.4GHz}}$ is the measured radio flux, $(1+\mathrm{z})^{\alpha-1}$ is the standard $k$-correction used in radio astronomy, and $\alpha$ is the radio spectral index ($S_\nu \propto \nu^{-\alpha}$) for which we adopted a value of 0.7, as is usually assumed for radio galaxies (Condon et al. 2002).

The normalization of the luminosity function requires knowledge of the precise intersection area of all three surveys: NVSS, FIRST and the SDSS DR4 photometric sample. We used the footprint services of the Virtual Observatory[1] (Budavári et al. 2007) to derive a total area of 6164.6 deg$^2$. A further 8.3 deg$^2$ was subtracted to avoid noisy regions around bright NVSS sources, resulting in an effective area of 6156.3 deg$^2$. In the MegaZ sample, the maximum variation of the mean redshift as we go from our second luminosity bin to the highest luminosity one, is $\sim 0.025$. If we include the first bin, this difference increases to a value $\sim 0.08$. We nevertheless decide to keep the lowest luminosity bin to avoid introducing further luminosity cuts.

In Figure 3.4 we plot the radio luminosity function measured for the MegaZ-LRG catalogue and the results are also tabulated in Table 3.1. For comparison we reproduce the luminosity function calculated by Sadler et al. [2007] for the 2SLAQ LRG sample. There is very good agreement, but the new determination has considerably smaller error bars, because our sample is very much larger. This is especially important for determining the number density of radio sources with radio powers greater than $\mathrm{P_{1.4GHz}} = 10^{26}$ W Hz$^{-1}$.

A further issue that could potentially bias the luminosity function comparison is mix of galaxies that enter the two samples at high and low redshift. The color and magnitude selection cuts of MegaZ basically restrict to red, luminous early-type galaxies, while SDSS main sample is much less restricted in this sense, allowing a different mixture of blue and red galaxies to pass the selection criteria. To separate these two populations Baldry et al. [2004] and Li et al. [2006a] adopted a tilted

[1] http://www.voservices.net/footprint

color cut motivated by the color-magnitude diagram. We follow the procedure of the latter, fitting bi-Gaussian functions to the $g-r$ color of galaxies, in different luminosity bins. Specifically, the dividing point of the two Gaussian is fitted by a linear equation of the form

$$(g-r)_{div} = A + B \times M_{r,0.1} \tag{3.4}$$

where $M_{r,0.1}$ is the absolute $r$-band magnitude, and $A = -0.832 \pm 0.021$ and $B = -0.078 \pm 0.001$ are the best-fitting linear coefficients. Galaxies with $g-r$ values greater (smaller) than $(g-r)_{div}$ are classified as red (blue).

Motivated by this, we also plot in Figure 3.4 two determinations of the radio luminosity function for SDSS DR4: the first without color restrictions, and the second restricted to red galaxies as defined by a luminosity dependent $g-r$ color cut explained above. As expected, by restricting to red galaxies, the radio luminosity function is slightly shifted toward lower comoving densities, particularly at radio powers above $10^{25.9}$ W Hz$^{-1}$. In any case, this color effect is minor and does not alter our conclusions. For reference purposes, we also show the radio luminosity function obtained by Best et al. [2005b] for the SDSS DR2 sample.

The evolution of the luminosity function of a population of objects is often characterized in terms of simplified density or luminosity evolution models. In a pure density evolution model, the underlying luminosity distribution of the radio sources remains fixed, but the number density of the sources increases at higher redshifts. This might be the case if a larger fraction of galaxies harbor radio jets at higher redshifts, but the intrinsic properties of the jets do not evolve with time. In a pure luminosity evolution model, there is a fixed population of radio AGN with luminosities that dim as the radio sources age.

In the two lower panels of Figure 3.4, we plot the ratios $f_{\rm PDENS}$ and $f_{\rm PLUM}$ as a function of radio luminosity. $f_{\rm PDENS}$ is the ratio of the comoving number densities of radio sources in the MegaZ and DR4 catalogs at fixed radio luminosity, while $f_{\rm PLUM}$ is the factor by which the low redshift number densities should grow in order to match the values found at higher redshift. If either model is a correct description of the data, one should find constant $f$ values as a function of radio luminosity. We find that neither model is a good description of the data. Both plots show a sharp increase near $\rm P_{1.4GHz} \sim 10^{25}$ W Hz$^{-1}$.

In Figure 3.4, we also plot the radio luminosity function for steep-spectrum sources at z=0.55 predicted by the luminosity-density evolution model of Dunlop and Peacock [1990]. This model is based on high frequency data, and has been shown to provide an accurate description of the radio source counts and redshift distributions. Briefly, the model treats the radio luminosity function as composed of two parts: an evolving population of powerful elliptical radio galaxies ($\rho_h$), and a non-evolving

spiral/irregular galaxy population ($\rho_l$)

$$\rho(P,z) = \rho_l(P) + \rho_h(P,z) \tag{3.5}$$

The evolving component $\rho_h(P,z)$ is fitted by a double power-law of the form

$$\rho_h(P,z) = \rho_0(z)\left\{\left(\frac{P}{P_c(z)}\right)^{\alpha} + \left(\frac{P}{P_c(z)}\right)^{\beta}\right\}^{-1} \tag{3.6}$$

where $\alpha$ and $\beta$ are the two power-law exponents. This expression in similar to the optical luminosity function of quasars. $P_c(z)$ and $\rho_0(z)$ are the redshift dependant break and normalization of the radio luminosity function, modeled respectively as

$$\log_{10}(P_c(z)) = a_0 + a_1(1-(1+z)^{-\eta})/\eta \tag{3.7}$$

$$\log_{10}(\rho_0(z)) = \sum_{i=0}^{5} 0.1 c_i z \tag{3.8}$$

Finally $\rho_l(P)$ is parametrized as a power-law expansion in radio luminosity as

$$\log_{10}(\rho_l(P)) = \sum_{i=0}^{6} 0.1 b_i (\log_{10} P - 20) \tag{3.9}$$

The best-fitting coefficients $a_i$, $b_i$, $c_i$, and the exponents $\alpha$, $\beta$, $\eta$, are listed in Table C4 of Dunlop and Peacock [1990].

At the redshifts corresponding to our MegaZ-LRG sample, the models are only strongly constrained above $10^{26}$ W Hz$^{-1}$ due to the high flux limits of their radio samples, which are then extrapolated to the lower radio powers. We note that Dunlop and Peacock [1990] provide a range of different parameterizations in their paper, but all give very similar results at moderate redshifts. As can be seen, our data matches the model reasonably well. In particular, the extrapolation to lower radio power appears to provide a reasonable fit to our data, but our estimate appears to be 0.2-0.3 dex lower that that of Dunlop and Peacock [1990] over the luminosity range from $10^{25}$ to $10^{26.5}$ W Hz$^{-1}$.

It is important to note that if radio galaxies fall outside the MegaZ-LRG color selection criteria, they will be missed in our radio luminosity function determination. Such an effect is visible for our low redshift luminosity function at radio powers above $10^{26}$ W Hz$^{-1}$; the luminosity function of bright sources in the red galaxy population is 0.1-0.2 dex lower than for the DR4 sample as a whole. Neither the DR4 sample nor the MegaZ-LRG sample includes radio-loud quasars, which would likely increase the amplitude of the radio luminosity functions by $\sim 0.1$ dex above a radio luminosity of $10^{25}$ W/Hz$^{-1}$. Nevertheless, it is clear from our comparisons that a large fraction (i.e $> 50\%$) of all radio galaxies at $z = 0.55$ do reside in the LRG population. In the rest of the chapter, we will be comparing radio AGN

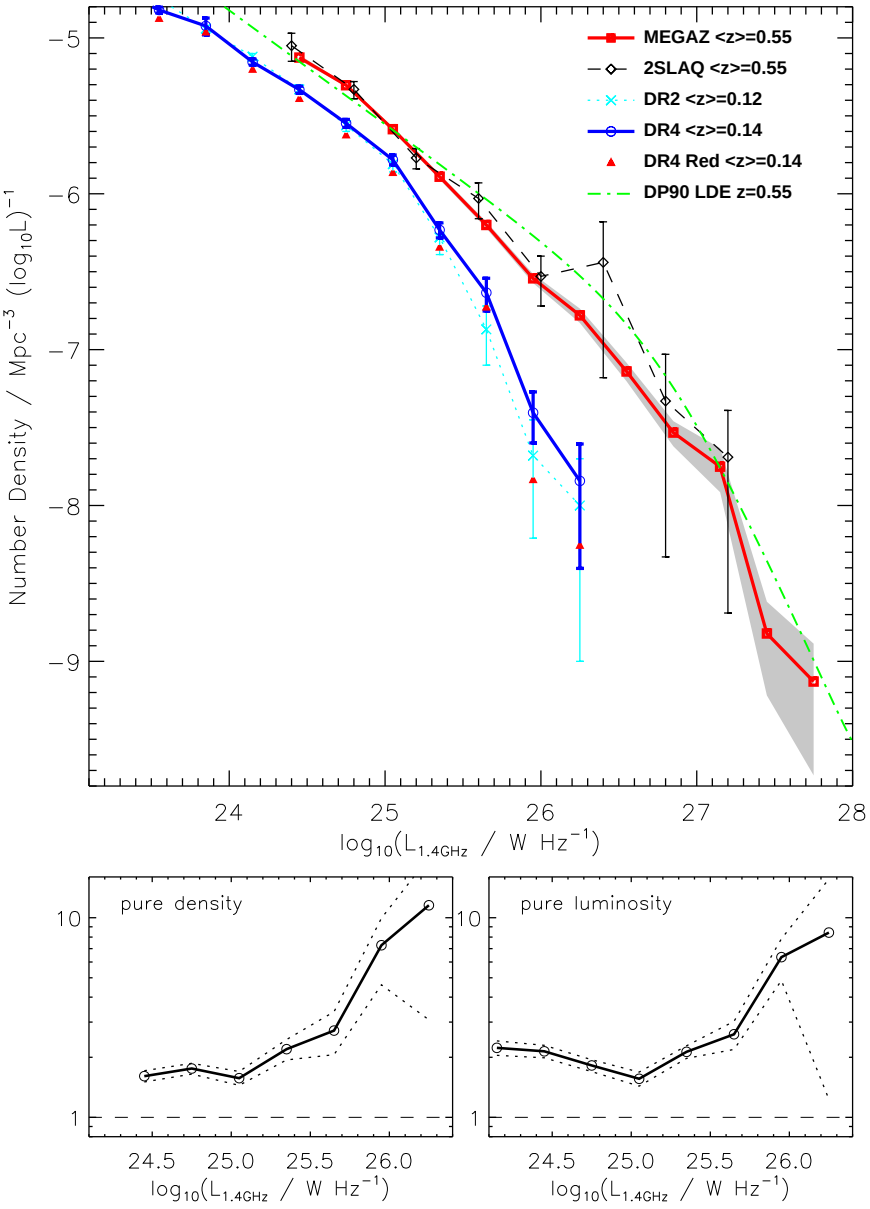


**Figure 3.4** • The radio luminosity function at 1.4 GHz derived for MegaZ-LRG and DR4 samples (thick line with square and circle symbols, respectively). An additional DR4 radio luminosity function restricted only to red sequence galaxies (triangles) is also plotted. Likewise shown are the calculations by Sadler et al. [2007] for 2SLAQ (thin line and diamond symbols), and by Best et al. [2005b] for SDSS DR2 (dashed line and crosses). Results are in good agreement at both redshift intervals. The luminosity function based on the luminosity/density evolution model of Dunlop and Peacock [1990] is also overplotted (dash-dotted line). The right panels show the factors by which luminosity and density should increase in order to match the DR4 curve at $\langle z \rangle \sim 0.14$ with the MegaZ-LRG curve at $\langle z \rangle \sim 0.55$. No evolution scenarios are indicated by the horizontal dashed lines. Error bars are poissonian, except for the right upper panel where they are calculated via statistical bootstrapping of each sample.

**Table 3.1** • The MegaZ-LRG AGN radio luminosity function at 1.4 GHz

| $\log_{10}(P_{1.4GHz})$ [W Hz$^{-1}$] | $\log_{10}(\rho)$ [Mpc$^{-3}$ $(\log_{10}L)^{-1}$] | N |
|---|---|---|
| 24.45 | -5.13 $^{+0.02}_{-0.02}$ | 2218 |
| 24.75 | -5.30 $^{+0.01}_{-0.01}$ | 5438 |
| 25.05 | -5.59 $^{+0.01}_{-0.01}$ | 3506 |
| 25.35 | -5.89 $^{+0.02}_{-0.02}$ | 1742 |
| 25.65 | -6.20 $^{+0.02}_{-0.02}$ | 840 |
| 25.95 | -6.54 $^{+0.03}_{-0.03}$ | 365 |
| 26.25 | -6.78 $^{+0.04}_{-0.05}$ | 185 |
| 26.55 | -7.14 $^{+0.06}_{-0.06}$ | 87 |
| 26.85 | -7.53 $^{+0.07}_{-0.09}$ | 41 |
| 27.15 | -7.75 $^{+0.12}_{-0.16}$ | 18 |
| 27.45 | -8.82 $^{+0.20}_{-0.40}$ | 3 |
| 27.75 | -9.13 $^{+0.24}_{-0.60}$ | 1 |

*fractions* at low and high redshifts, and we will show that such fractional estimates are much less sensitive to any incompleteness in our sample.

## 3.4 The Fraction of RL-AGN

We are now in a position to investigate the relation between radio-loud AGN and their host galaxies. Over the redshift range covered by the MegaZ-LRG sample ($0.4 < z < 0.8$), radio sources have 1.4 GHz powers well above $10^{24}$ W Hz$^{-1}$ (the faintest radio galaxies in our sample are $\sim 10^{24.4}$ W Hz$^{-1}$). It is well known that radio emission above this luminosity is rarely associated with star-formation, but rather an AGN (Sadler et al. 2002; Best et al. 2005b). In addition, luminous red galaxies are photometrically defined so that the majority of star-forming galaxies are excluded, so we can safely assume that our sample is dominated by an AGN population.

Figure **??** shows the fraction of MegaZ LRGs with radio luminosities above different threshholds, as a function of their stellar mass. The fraction of LRGs with radio AGN more luminous than $10^{24.4}$ W Hz$^{-1}$ rises from $\sim$0.04% for galaxies with stellar masses around $10^{10.8}M_{\odot}$, to $\sim$25% for the most massive LRGs with $M_* \sim 10^{12.2}M_{\odot}$. Results for radio power cuts of $10^{25}$ W Hz$^{-1}$, $10^{25.5}$ W Hz$^{-1}$ and

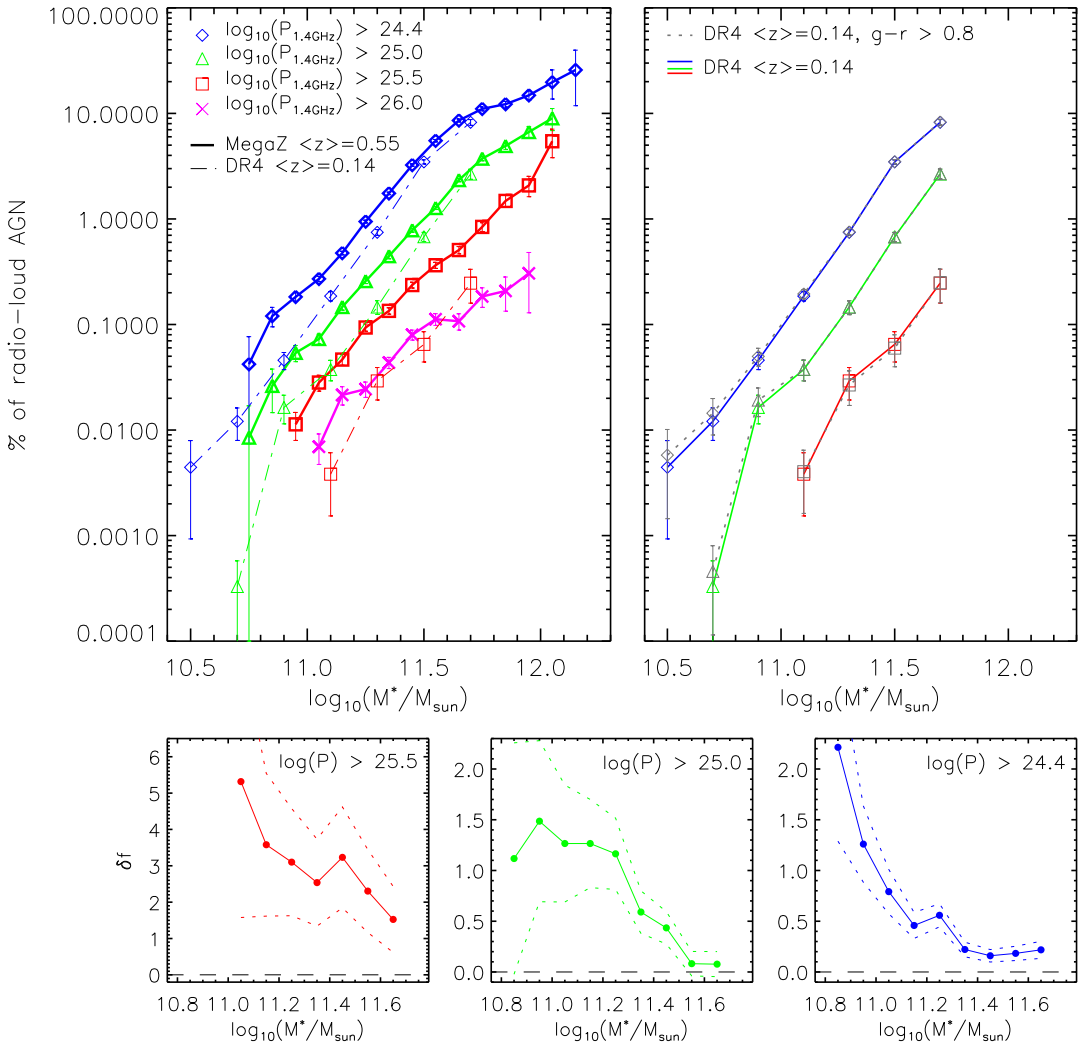


**Figure 3.5** • The left upper panel shows the percentage of galaxies have radio luminosities above a given threshhold, as a function of stellar mass. Results are shown for the high redshift MegaZ-LRG sample (thick solid lines), and for the low redshift SDSS DR4 sample (thin dashed lines). The right upper panel shows the radio-loud fractions for the SDSS DR4 sample, but including a color constraint of $g - r \geqslant 0.8$. Lower panels show the relative variation $\delta f$ between high redshift (MegaZ) and low redshift (DR4) radio-loud fractions as a function of stellar mass. Errors are poissonian and are propagated via standard error propagation theory.

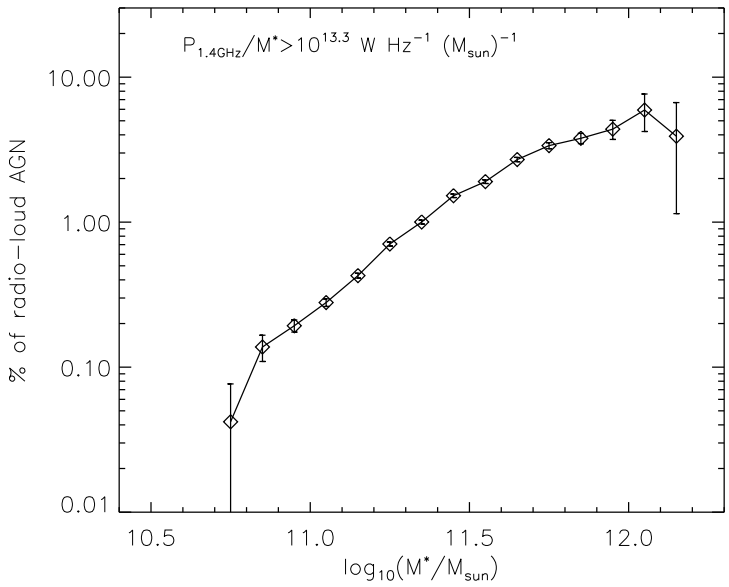


**Figure 3.6** • Fraction of radio-loud AGN as function of stellar mass, for galaxies above a fixed limit of radio luminosity per unit stellar mass ( $\mathrm{L/M^* > 10^{13.3}\ W\ Hz^{-1}\ M_\odot^{-1}}$).

$10^{26}$ W Hz$^{-1}$ are also included in the plot and a similar mass dependence is found. The dotted lines connecting light symbols on the plot show the corresponding dependence of the radio loud fraction on stellar mass for the low-redshift SDSS DR4 sample. We find that there is an increase at higher redshifts in the fraction of of radio-loud AGN hosted by galaxies of all stellar masses. The increase is larger at higher radio luminosities and for galaxies with lower stellar masses. This is shown in more detail in the bottom three panels of Figure 6, where we plot the relative ratio $\delta f$ between the high redshift and low redshift data ($\delta f = (f_{\mathrm{MegaZ}} - f_{\mathrm{DR4}})/f_{\mathrm{DR4}}$) as a function of mass and for our three radio luminosity thresholds.

Once again it is important to recall that the DR4 sample includes all galaxies regardless of color, whereas the MegaZ sample is restricted to red galaxies. Best et al. [2005a] showed that the probability for a galaxy to host a radio-loud AGN was not influenced by its stellar population. In the top right panel of Figure 3.5 we compare the radio-loud AGN fraction versus mass relation for the full DR4 sample to the results obtained if the sample is restricted to galaxies with $g-r$ colors greater than 0.8. As can be seen, the results are almost identical. The effect of the color cut is much smaller than the evolutionary trends we find between the low redshift and MegaZ LRG sample. To check whether the increase in the fraction of radio-loud AGN with mass is not simply the result of the fact that more massive galaxies harbor more massive black holes and hence produce more radio emission, we have also calculated the fraction of radio-loud AGN that are above a given limit in radio luminosity per unit stellar mass. For our sample, this is equivalent to choosing only

those sources that produce radio emission above a fixed fraction of the Eddington limit. For reasonable values of the chosen limit (e.g. $L/M^* > 10^{13.3}$ W Hz$^{-1}$ $M_\odot^{-1}$), the strong mass dependence persists, although the slope of the relation is somewhat shallower, as illustrated in Figure 3.6.

It is also important to check if the small percentage of galaxies that might be missclassified due to random superposition (∼1.7%, see Section 2.5) could affect these results. As ∼1.2% of objects in MegaZ are radio-loud, only 0.02% of galaxies might be false matches. For the most massive systems, such contribution to the radio-loud fraction is negligible. For low mass galaxies around $10^{10.9} M_\odot$, only ∼0.1% are radio-loud, so that the error due to false detections is at most 20%, a value that is well below the observed change factors of 2-5 in evolution.

## 3.5 Bivariate Radio Luminosity-Mass Function

The first determination of the bivariate radio-optical luminosity function was carried out by Auriemma et al. [1977] for a sample of 145 galaxies of type E and S0, and there were subsequent studies by Sadler et al. [1989] and Ledlow and Owen [1996].This (integrated) function measures the probability that a galaxy in a given optical absolute magnitude range hosts an AGN with radio power above a certain value. Best et al. [2005a] calculated the bivariate radio luminosity-stellar mass function of radio sources in the SDSS DR2, and parameterized the behavior using a broken power with characteristic luminosity $P_\star = 2.5 \times 10^{24}$W Hz$^{-1}$. A single fitting function was found to hold for for all masses below $10^{11.5} M_\odot$.

Our MegaZ radio galaxy sample is over 100 times larger than the one of Auriemma et al. [1977] and picks up close to the break luminosity found by Best et al. [2005a]. Following Best et al. [2005a], we will use stellar mass instead of optical luminosity. We can thus interpret our calculation as the fraction of radio-loud AGN of a given mass emitting above a certain certain radio power. Figure 3.7 shows the bivariate functions at high and low redshift in mass bins from $10^{11} M_\odot$ to $10^{12.25} M_\odot$. The most striking result shown in this plot is that for galaxies of all stellar masses, the high redshift fractions lie only slightly above the low redshift ones at faint radio luminosities, but there has been much stronger evolution at higher radio luminosities. This is shown in more detail in the lower panel of Figure 3.7, where we plot the ratio of the radio-loud AGN fraction derived for the MegaZ LRGs to that derived for the DR4 galaxies, as a function of radio power. We show results for the four mass bins for which there is reasonable overlap between the two surveys (there many fewer galaxies with $12 < \log M_* < 12.25$ in the DR4 sample, because the volume covered is much smaller). It is striking that for all the mass bins, the ratio remains approximately constant up to a radio luminosity of $10^{25}$ W Hz$^{-1}$ and then turns up sharply. As discussed in Section 1, $10^{25}$ W Hz$^{-1}$ corresponds to the approximate dividing line between low excitation and high excitation sources, and

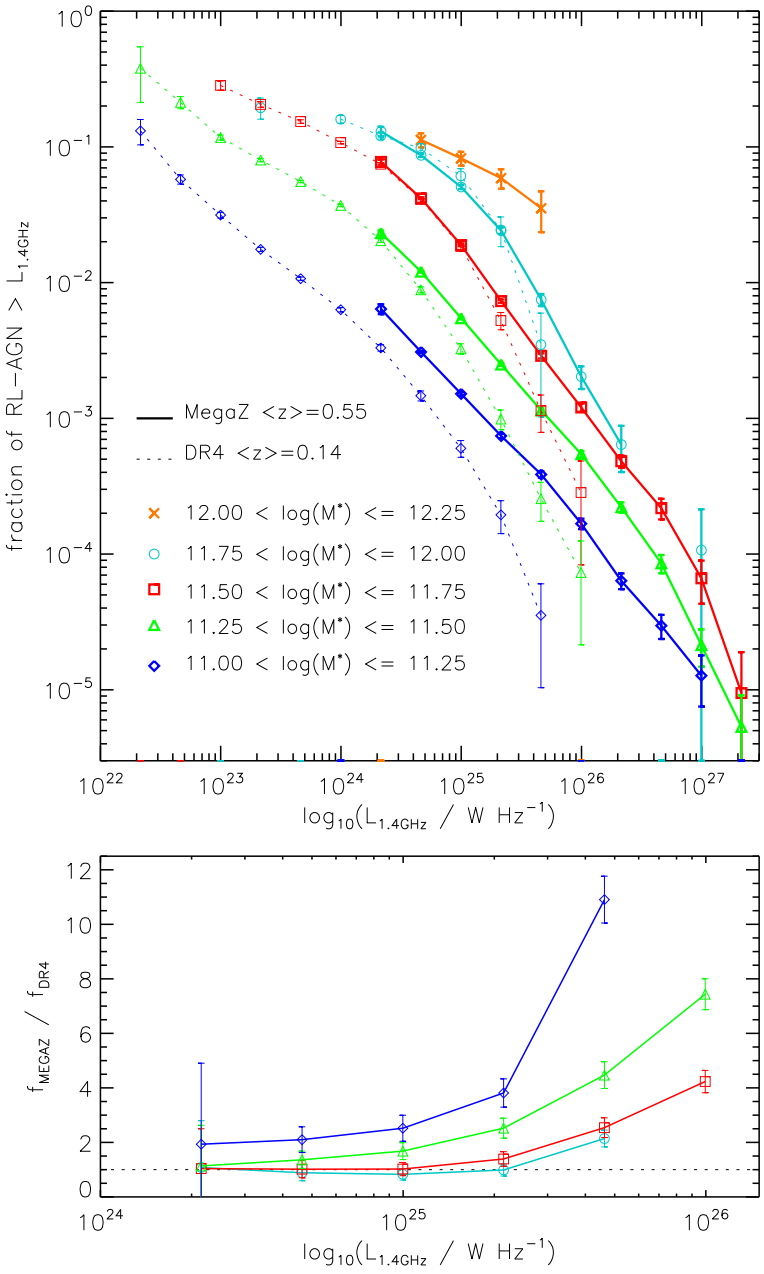


**Figure 3.7** • Integral bivariate radio luminosity-mass function in several bins of stellar mass (symbols) for high redshift MegaZ-LRG sources (thick solid lines) and low redshift SDSS DR4 sources (thin dashed lines). The bivariate function gives the fraction of radio-loud AGN brighter than a given radio luminosity, as a function of the luminosity. The right panel shows the ratios of the bivariate functions derived for the MegaZ-LRG sample to those derived for the SDSS DR4 sample. These results show that radio sources evolve strongly across cosmic time depending on their stellar mass and radio luminosity. The dashed horizontal line marks the no-evolution scenario.

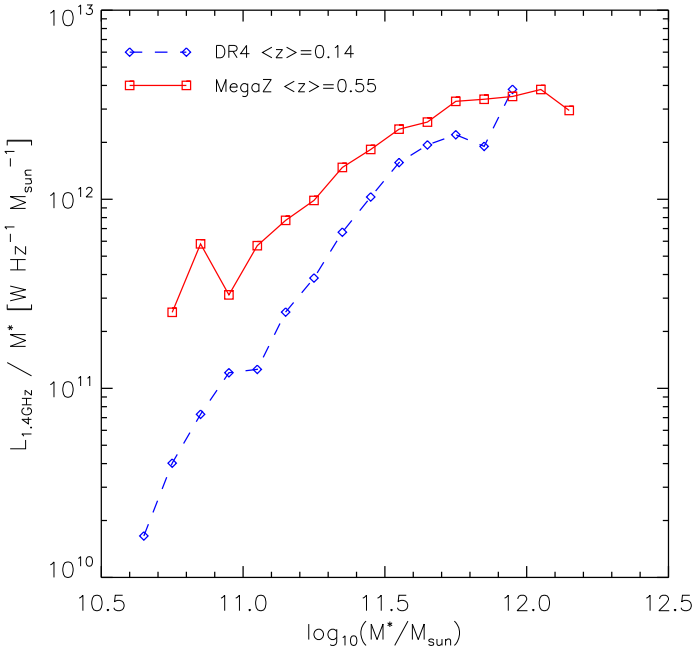


**Figure 3.8** • Integrated volume-weighted radio luminosity per unit stellar mass, as function of stellar mass, for MegaZ-LRG radio-loud AGN (solid line with square symbols) and DR4 sources (dashed line with diamond symbols).

also delineates the boundary between strongly-evolving and less strongly-evolving radio sources found in previous studies. The main new result shown in this plot is that the strongest evolution in the radio source population apparently occurs *in the lowest mass galaxies*.

Another way of showing the same effect is to plot the integrated radio emission per unit stellar mass for galaxies of different stellar masses in the DR4 and MegaZ samples. Heckman et al. [2004] used the volume-weighted distribution of [OIII] 5007 line luminosity per unit black hole mass to study the average rate at which black holes are accreting and growing. They find that low mass black holes are currently growing at substantially higher rates than high mass black holes. Best et al. [2005a] extended this analysis by computing the integrated radio luminosity per unit black hole mass, demonstrating that radio and emission line luminosities are produced in black holes of quite different masses (see Figure 11 in Best et al. 2005a).

In the present work, we do not have direct estimates of black hole mass, so we carry out the computation as a function of stellar mass. In Figure 3.8 we plot the volume-weighted radio luminosity per unit stellar mass, as a function of $\log M_*$, for our high and low redshift samples. The plot is constructed by taking at each mass bin, the ratio of the integrated (and weighted) radio luminosity, to the integrated

(and weighted) stellar mass in that bin. As can be seen, radio activity has been boosted at all masses at high redshift, but the boost factor is considerably higher for low mass galaxies.

## 3.6 Stellar masses and colors of the host galaxies of radio-loud AGN

It has long been known that powerful high redshift radio galaxies are hosted by very massive galaxies with predominantly old stellar populations. This conclusion arises from the fact that there is a well defined relation between the K-band magnitude of radio galaxies and redshift (the famous K-z relation) that agrees with the predicions of a passively evolving model galaxy of high mass ($> 10^{11} M_{\odot}$), and that there is relatively little scatter about this relation for the most luminous radio sources (e.g. Lilly and Longair 1984; Jarvis et al. 2001).

So far we have phrased our analysis of the relationship between radio AGN and their host galaxies in terms of the *probability* for a galaxy of a given mass to host such an AGN. We have shown that this *probability* evolves most strongly in low mass galaxies. Note, however, that the fraction of radio loud AGN is a strongly increasing function of galaxy mass both at $z = 0.55$ and at $z = 0.14$. This means that radio galaxies in massive elliptical hosts always dominate *by number*.

This is shown in more detail in Figure 3.9 where we plot the median stellar masses of both the MegaZ and the SDSS DR4 radio AGN as a function radio luminosity. As can be seen, radio AGN are hosted by galaxies with median masses of $\sim 3 \times 10^{11} M_{\odot}$ in both surveys. There is a weak increase in the median mass at higher radio luminosities.

In Figure 3.10, we plot the color distributions of the MegaZ radio AGN. One must of course bear in mind that the MegaZ sample is selected so as to occupy a restricted range in color space, but we can nevertheless check whether there are any color differences between different types of radio AGN. We split the sample into 3 different redshift bins and show results for low luminosity ($< 10^{25.3}$ W Hz$^{-1}$) and high luminosity ($> 10^{25.3}$ W Hz$^{-1}$) radio sources. As was found previously by Smith and Heckman [1989], there is a tendency for the more powerful radio galaxies to have slightly bluer colors at fixed redshift, but the effect is very weak.

In summary, we conclude that the majority of both low luminosity and high luminosity radio AGN are hosted by massive (3 $L_*$) galaxies with red colors. This is in good agreement with past work on this subject.

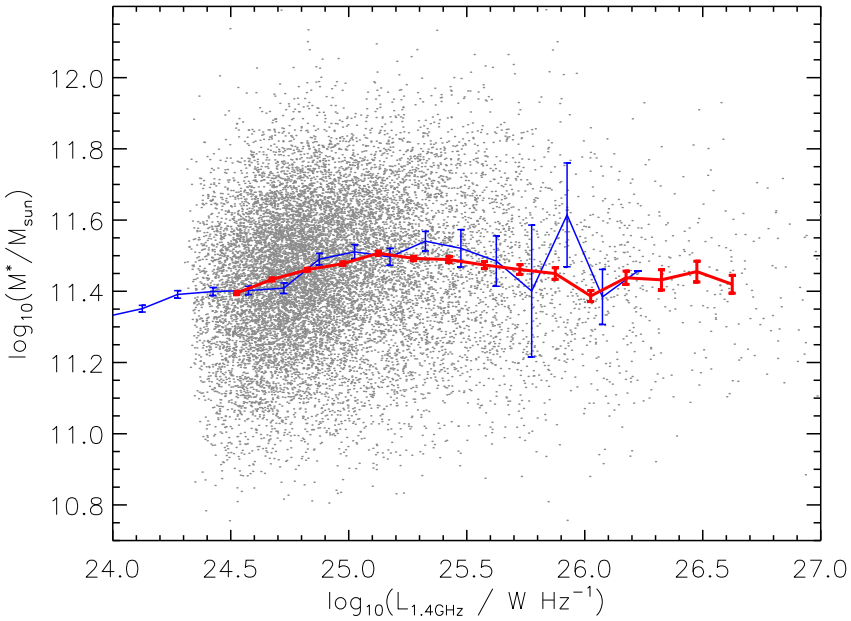


**Figure 3.9** • Median stellar mass of radio-loud AGN in the MegaZ-LRG (solid line) and SDSS DR4 (dotted line) samples as function of radio power. Gray dots represent the actual values for each MegaZ galaxy and errors are calculated by the bootstraping technique.

## 3.7 Systematic Effects

Photometric redshift codes have improved vastly over the years and the resulting redshift estimates are useful for a broad range of studies. Even though the neural network photometric redshift estimator used in the MegaZ catalogue has been throughfully calibrated using spectroscopic redshifts, it is important to test the sensitivity of our results to photo-z errors. Such errors could translate into systematic offsets in our estimates of stellar mass. In addition, the errors in the Sloan $u, g, r, i, z$ magnitudes increase with redshift, so one might worry that this would translate into apparent (as opposed to real) evolution of the radio loud fraction with redshift.

In order to test for such effects, we artificially redshifted our SDSS DR4 sample from their observed redshifts near $\langle z \rangle \sim 0.14$ out to the mean redshift of the MegaZ-LRG sample, $z = 0.55$. To do this, we applied the *kcorrect* algorithm in conjunction with the $e$-corrections described above. We then added an error to the redshift using the distribution of $z_{phot} - z_{spec}$ of 2SLAQ galaxies. In practice, for each MegaZ LRG, we extracted the 100 closest neighbors in $g, r, i, z$ magnitude space in the 2SLAQ catalogue and we draw the redshift error, $z_{phot} - z_{spec}$, at random from this set of galaxies. Magnitude errors were assigned to each DR4 object in the same way. We then ran our code for estimating stellar mass on this "artificially redshifted" data set, first applying just the redshift error, and second, incorporating errors on both

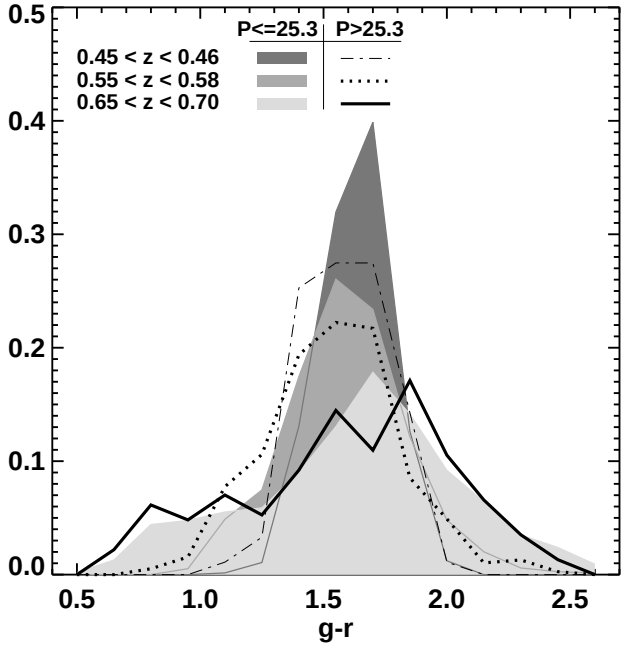


**Figure 3.10** • Color distribution of MegaZ-LRG in three different redshift bins, split into a high luminosity population of radio sources with $\log_{10}[P_{1.4\mathrm{GHz}}/(\mathrm{W\ Hz^{-1}})] \leqslant 25.3$, and a low luminosity population with $\log_{10}[P_{1.4\mathrm{GHz}}/(\mathrm{W\ Hz^{-1}})] > 25.3$.

the photometry and the redshifts. The whole procedure was repeated 25 times.

The solid line in Figure 3.11 shows the difference between the mean fraction of radio-loud AGN measured in the 25 artificially redshifted samples and the "true" value for the DR4 galaxies as a function of stellar mass. The difference $\delta f$ is expressed in fractional terms, i.e. $\delta f = (\bar{F}_{\rm artificial} - F_{\rm true})/F_{\rm true}$. The shaded contours respesent the $1\sigma$ scatter among the 25 samples. It can be seen that small systematic shifts in the derived radio loud fractions do occur at the two ends of the stellar mass distributions. They also occur in our estimates of the fraction of the most luminous radio galaxies. On the whole, these effects are small ($< 20\%$). Note also that $10^{25.5}$ W Hz$^{-1}$ sources are much rarer in the DR4 catalogue than in the MegaZ sample, so the bottom right panel overestimates the size of the true effect at this radio luminosity and is likely to apply only to very much higher luminosity cuts at $z = 0.55$.

## 3.8 Summary

The main results presented so far can be summarized as follows:

A catalogue of 14453 radio-loud AGN with 1.4 GHz fluxes above 3.5 mJy in the redshift range $0.4 < z < 0.8$, has been constructed from the cross-correlation of NVSS and FIRST radio source catalogs with the MegaZ-LRG catalogue of luminous red galaxies. The vast majority of the radio AGN are single component sources in both NVSS and FIRST. However, there is a significant fraction of objects without high S/N FIRST detections, which are required for accurate identification of the optical counterpart. We thus introduced a method for analyzing the FIRST radio maps around the candidate positions of these sources. This allowed us to dig deeper into the FIRST survey and use lower S/N detections to pinpoint the location of the host galaxy.

We have presented a new determination of the luminosity function of radio-loud AGN at $z \sim 0.55$ that is in excellent agreement with other results in the literature, but with notably smaller error bars. By comparing our radio luminosity function at $z \sim 0.55$ to that derived for a large sample of nearby radio AGN from the SDSS DR4, we find compelling evidence for strong cosmic evolution of radio sources. The comoving number density of radio AGN with luminosities less than $10^{25}$ W Hz$^{-1}$ increases by a factor of $\sim 1.5$ between $z = 0.14$ and $z = 0.55$. At higher luminosities, this factor increases sharply, reaching values $\sim 10$ at a radio luminosity of $10^{26}$W Hz$^{-1}$. Neither a pure luminosity evolution nor a pure density evolution scenario provides a good description of the data.

We then turn to an analysis of how the relation between radio AGN and their host galaxies evolves with redshift. The fraction of galaxies with radio luminosities above

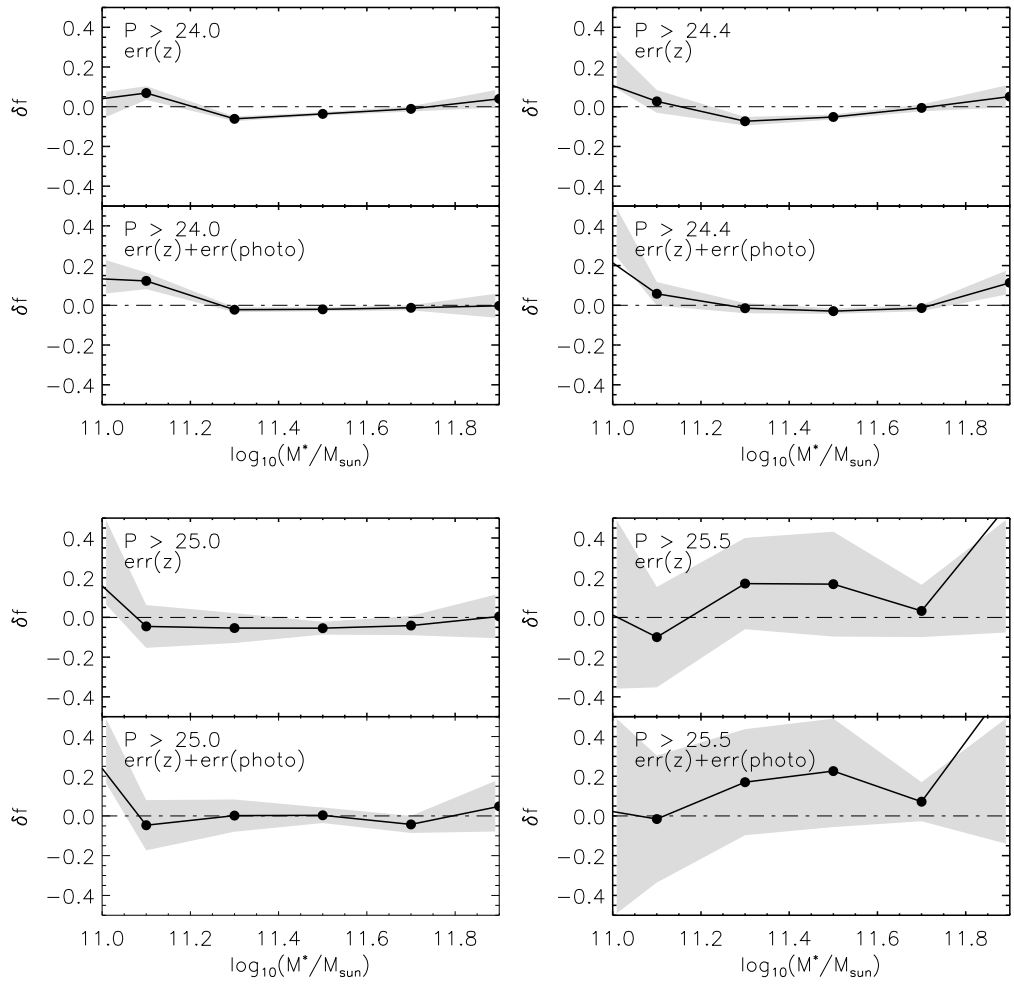


**Figure 3.11** • The difference between the true radio-loud AGN fraction and the one calculated for the artificially redshifted samples is plotted as function of stellar mass. Results are shown for increasing luminosity cuts. The solid line shows the mean difference for the 25 random samples, and the gray area is the 1-$\sigma$ scatter in this variation. Very few sources have masses higher than $10^{11.7} M_{\odot}$.

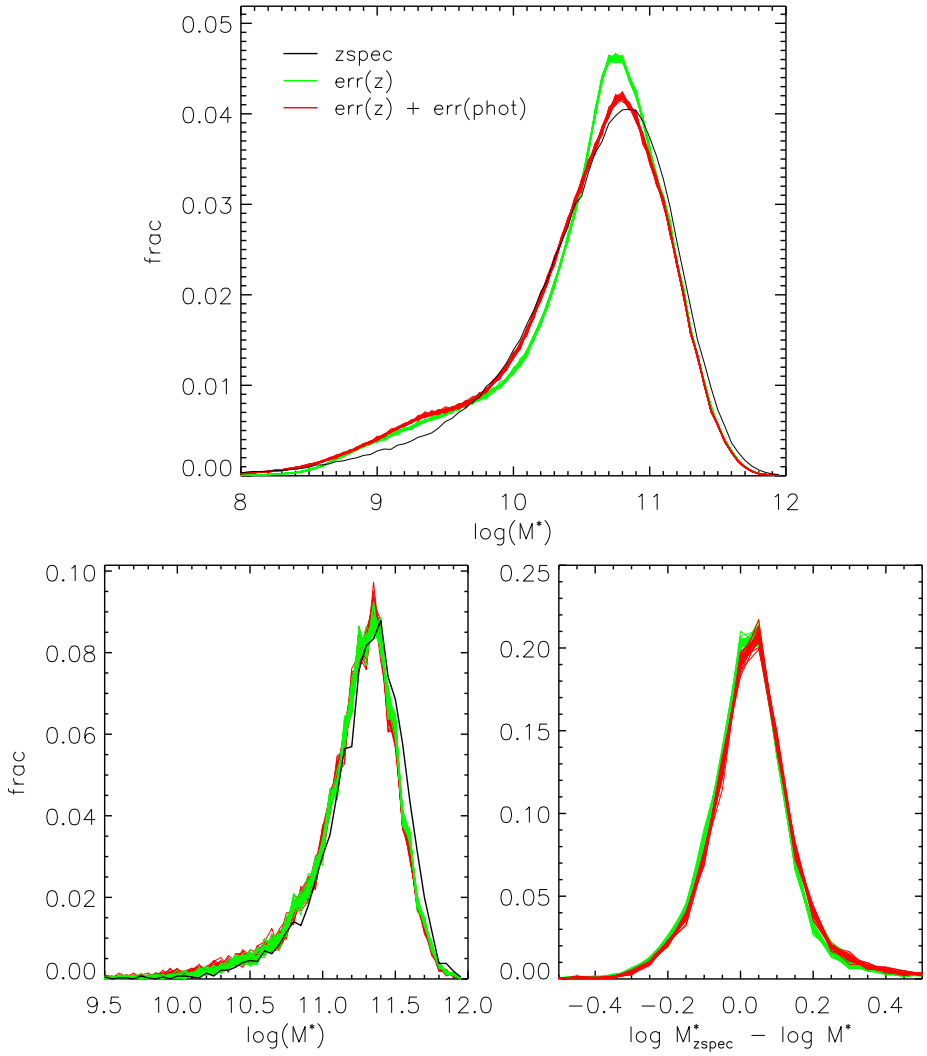


**Figure 3.12** • Stellar mass distributions for the DR4 low redshift comparison sample derived with the KCORRECT algorithm (Blanton and Roweis 2007). The upper panel is for all galaxies in the DR4 Main sample and the two lower panels are for the radio-matched population. Stellar masses are derived using: spectroscopic redshifts (black), artificial redshifts convolved with photometric redshift errors (green), and artificial redshifts convolved with photometric redshift errors plus typical errors of LRG photometry at $0.4 < z < 0.8$. Color lines are thick as they are the result of 25 Monte-Carlo realizations. See Section 3.7 for details of the methodology.

a given threshhold is a steeply increasing function of stellar mass at both $z \sim 0.1$ and at $z \sim 0.55$. The fraction of radio loud AGN increases with redshift and this increase is largest at the highest radio luminosities and also for lower mass galaxies. We have also calculated the bivariate radio luminosity-mass function at $z \sim 0.14$ and $z \sim 0.55$. Its shape does not appear to depend on mass at either redshift, but there is strong evolution in the shape at the *bright-end* of the function. The fraction of galaxies brighter than $10^{25}$ W hz$^{-1}$ declines with significantly shallower slope at higher redshifts. Within the range $10^{25-27}$ W hz$^{-1}$, simple power law fits to the DR4 bivariate function in Figure 3.7 (frac $\propto \mathrm{L}^{\gamma}_{1.4\mathrm{GHz}}$), produce slopes $\gamma$ of $-1.84 \pm 0.21$, $-1.66 \pm 0.02$ and $-1.83 \pm 0.04$ for the first, second and third mass bins. In MegaZ, we obtain $-1.05 \pm 0.02$, $-1.16 \pm 0.05$ and $-1.20 \pm 0.02$ for the same luminosity range and mass bins.

In short, two main conclusions have emerged from these analysis:

- There is a characteristic luminosity of $\sim 10^{25}$ W Hz$^{-1}$ below which the radio source population appears to evolve only very weakly with redshift. Above this characteristic luminosity, there is strong evolution, with the most powerful radio sources undergoing the largest increase in co-moving number density. These results are in broad agreement with past studies.
- The strongest evolution in the fraction of galaxies that host radio-loud AGN takes place in the lower mass galaxies in our sample.

The most plausible explanation of these trends is that there are two classes of radio galaxy, likely associated with the high excitation/low excitation "dichotomy") that have different fueling/triggering mechanisms and hence evolve in different ways. This has also been argued by Tasse et al. [2008], whose analysis of a sample 1% of the size of ours in the XMM-LSS region provided hints of similar evolutionary properties. As discussed before, it has been hypothesized that the class of low luminosity AGN is likely associated with massive ($\sim 10^{13} M_{\odot}$) dark matter halos with quasistatic hot gas atmospheres. The abundance of such halos is predicted to remain approximately constant out to redshifts $\sim 1$ (Mo and White 2002) and this is broadly consistent with the very weak evolution we see in this population. These "hot-halo" triggered sources at $z \sim 0.5$ would then produce radio emission that roughly compensates the radiative losses of the hot gas.

The reason for the remarkably strong evolution in the comoving abundance of high-luminosity radio AGN is somewhat more difficult to understand. As shown in Figure 3.7, this evolution is most dramatic in galaxies at the low stellar mass end of our sample. It is thus tempting to link this population with the strongly accreting (and evolving) population of luminous quasars, whose space densities also increase by factors of more than 10 over the redshift range studied in this work. Recent work has shown that quasars are hosted in dark matter halos of masses $\sim 10^{12} M_{\odot}$, independent of redshift or the optical luminosity of the system (e.g. Croom et al.

2005; Shen et al. 2007). Only $\sim$ 10% of optical quasars are radio-loud, however, and this raises the question as to whether there is simply a short radio-loud phase during the lifetime of every optical quasar, or whether optically luminous AGN and powerful radio galaxies are triggered under different physical conditions. If, as in quasars, these sources are not regulated by cooling from a surrounding hot gaseous halo, but by other mechanisms like interactions/mergers, then we would not expect to find them in an equilibrium state like in low excitation AGNs.

One way to shed further light on these matters is to compare the clustering properties of quasars to those of the luminous radio galaxies in our sample. If their clustering properties are identical, this would favor the hypothesis that all quasars experience a radio-loud phase. Recently, Kauffmann et al. [2008] found that nearby radio-loud AGN were more strongly clustered than matched samples of radio-quiet AGN with the same black hole masses and extinction corrected [OIII] line luminosities. It will be interesting to see if the same conclusion holds at higher redshifts and for more powerful systems. This will be the subject of the following chapter.

# 4

# Clustering of Radio Galaxies and Quasars

In this chapter I analyze the clustering properties of radio galaxies and quasars. First, I explain the construction of the radio-loud and radio quiet quasar samples and the calculation of quasar radio luminosities with extended emission. Then I discuss the methodology adopted to calculate the two-point auto-correlation and cross-correlation functions.

We have shown that radio-loud AGN are more massive than the typical LRGs present in the MegaZ sample. Coupled with redshift or luminosity-dependant effects, this makes difficult to compare the true clustering between radio-loud and radio-quiet samples. We explain how we constructed control radio-quiet samples matched in stellar mass, redshift and luminosity to control for these effects.

Then, I quantify how the clustering of radio-loud AGN depends on host galaxy properties like stellar mass and radio luminosity. Using the same methodology, I also compare the environments of radio AGN and radio-loud quasars, and discuss the implications of the results in the framework of unification models of AGN.

The contents of this chapter were submitted for publication as Donoso et al., 2009, MNRAS (arXiv:0910.3667v1).

## 4.1 Introduction

Radio-loud active galactic nuclei (RLAGN) are known to be hosted by massive early-type galaxies, preferentially sitting at the center or clusters and groups of galaxies. This turns them into excellent probes of the large-scale structure, as they are biased tracers of the underlying dark matter mass distribution. In recent years, galaxy formation models have become increasingly interested in the radio AGN phenomenon, because it is hypothesized that these objects may regulate the star formation history and mass assembly of the most massive galaxies and black holes in the Universe. Nearby radio galaxies in clusters are observed to inject a significant

amount of energy into the surrounding gas. As the radio jets expand and interact with the surrounding medium, they are believed to heat the gas and prevent further accretion onto the central galaxy.

The precise conditions that determine whether an AGN develops radio jets/lobes are still a matter of debate. Several studies have shown that the probability for a galaxy to become radio-loud is a strong function of stellar mass and redshift (e.g. Best et al. 2005a; Donoso et al. 2009). The role that the environment plays in triggering or regulating the RLAGN phenomenon is not as well established.

Ledlow and Owen [1996] found that the fraction of radio sources and the shape of the bivariate radio-optical luminosity function was the same for objects in cluster and field environments. This means that, while the morphology and properties of radio galaxies in rich and poor clusters might differ, the total radio power output and lifetime of radio sources were the same. Best et al. [2007] found that group and cluster galaxies had similar radio properties to field galaxies, but the brightest galaxies at the centers of the groups where more likely to host radio-loud AGN than other galaxies of the same stellar mass. In the local universe, Mandelbaum et al. [2009] analyzed a large sample of RLAGN at z$\sim$0.1. They showed that RLAGN inhabit massive dark matter halos ($> 10^{12.5}$ $M_\odot$) and that, at fixed stellar mass, radio-loud AGN are found in more massive dark matter halos than control galaxies of the same mass selected without regard to AGN properties. This result implies that RLAGN follow a different halo mass - stellar mass relation than normal galaxies. Mandelbaum et al. [2009] also found that the boost towards larger halo masses did not depend on radio luminosity. Hickox et al. [2009] investigated the clustering in a small sample of higher redshift (and low luminosity) radio-loud AGN selected from the AGN and Galaxy Evolution Survey (AGES). They found no difference in the clustering amplitude of radio galaxies when compared to normal galaxies matched in redshift, luminosity and color.

Most nearby RLAGN lack any of the standard accretion-related signatures that would indicate that their black holes are growing significantly at the present day (Hardcastle et al. 2006). In contrast, quasars are thought to be powered by supermassive black holes accreting at close to the Eddington rate. Large redshift surveys like the Two Degree Field Galaxy Redshift Survey (2dFGRS) and the Sloan Digital Sky Survey (SDSS) now provide angular positions, accurate photometry and spectra for tens of thousands of QSOs. Recent determinations of the quasar two-point correlation function have demonstrated that at $z < 2.5$ quasars cluster like normal $L_*$ galaxies (Croom et al. 2005; Coil et al. 2007) and populate dark matter halos of $\sim 10^{12}$ $M_\odot$, with the clustering only weakly dependent on luminosity, color and virial black hole mass (Shen et al. 2009).

As one moves out in redshift, the radio-loud AGN population evolves very rapidly in radio luminosity. Whether the RLAGN population also evolves strongly in black hole accretion rate, is considerably less clear. In particular, our understanding of

whether there is a relationship between powerful, high redshift radio-loud AGN and quasars is quite sketchy. Around 10% of the quasar population is radio-loud. Numerous investigations have found that radio-loud quasars and at least *some* powerful radio galaxies share a number of common characteristics, such as excess infrared emission, comparable radio morphologies and luminosities, optical emission lines, large evolutionary rates, and host galaxies with similar properties. It has thus been tempting to link both phenomena under the hypothesis that they are the same active nuclei viewed at different orientations (e.g. Barthel 1989; Urry and Padovani 1995).

A few facts are believed to be key in any attempt to understand the transition from the population of low-luminosity radio AGN produced by weakly accreting black holes at low redshifts, to a population of high-luminosity radio AGN that may be produced by strongly accreting black holes at high redshifts. Fanaroff and Riley [1974] found an important correlation between radio morphology and radio power: low luminosity sources (Fanaroff-Riley Class I, FRI) show emission peaking close to the nuclei that fades toward the edges, whereas more luminous sources (Fanaroff-Riley Class II, FRII) are brightest toward the edges. Hine and Longair [1979] discovered that radio galaxies could also be classified according to the strength of their optical emission lines: low excitation (weak-lined) radio galaxies or LERGs, and high excitation (strong-lined) objects or HERGs. Modern unification models usually associate quasars with the most powerful HERGs, and low luminosity LERGs with BL Lac objects. Although there is a notable correspondence between RLAGN luminosity, morphology and spectral type, i.e. lower luminosity FRIs with LERGs, and higher luminosity FRIIs with HERGs, the correlations between these properties are not straightforward. There are populations of FRI sources with high excitation nuclear lines, and conversely, FRII galaxies with low excitation spectra are also common.

It has been known for years that very high redshift ($z > 2$), powerful radio galaxies are often surrounded by galaxy overdensities with sizes of a few Mpc (e.g. Pentericci et al. 2000; Miley et al. 2006). Since we know that quasars at the same redshift are clustered like normal $L_*$ galaxies, this would seem to throw some doubt on a simple unified scheme for explaining both phenomena.

In view of this highly complex situation, a more statistical approach to comparing the properties of quasars and radio galaxies may yield further insight. In this chapter we present measurements of the projected cross-correlation between our sample of $\sim$14,000 radio-loud AGN with a median redshift of $z = 0.55$ with the surrounding population of massive galaxies ($M_* > 10^{11}$ $M_\odot$). The large size of our samples allows us to investigate in detail how clustering depends on stellar mass and on radio luminosity. By comparing the RLAGN clustering with results from control samples matched in redshift, luminosity and mass, we isolate the effect that the radio AGN phenomenon has on the clustering signal. We cross-correlate radio quasars

drawn from the SDSS with the same reference sample of massive galaxies. Again, by using control samples matched in black hole mass and radio luminosity, we ensure that we compare RLAGN and RLQSOs in as uniform a way as possible.

## 4.2 The Radio-loud and Radio-quiet Quasar Samples

In this work we use quasars selected from the fourth edition of the spectroscopic quasar catalogue (Schneider et al. 2007). This contains 77,429 quasars drawn from SDSS DR5, with luminosities larger than $M_i = -22$, that have at least one broad emission line with FWHM>1000 km s$^{-1}$ in their spectra. The catalogue also identified radio-loud quasars with FIRST components within a 2 arcsec radius.

Most of the objects targeted as quasars were initially selected using the algorithm of Richards et al. [2002], which pick candidates using *ugriz* broadband photometry and by matching with unresolved FIRST sources. As the survey progressed, the quasar selection software was modified to improve its efficiency at high redshift. This is reflected in two spectroscopic target selection flags listed as TARGET and BEST (for the final algorithm). Photometry of quasars is also available in two versions, TARGET measurements (values used at the time of targeting), and BEST measurements (values derived with the latest pipeline). We note that the selection of UV-excess quasars at low redshifts ($z < 3$) has remained essentially unchanged, so that only small differences arise from using TARGET or BEST versions. In addition, the bias introduced by selection of targets via FIRST radio detections is significant only at high redshift.

In this work we are interested in cross-correlating the quasars with the LRGs described above. We therefore selected an homogeneous quasar sample consisting of all quasars with $0.35 < z < 0.78$ and psf magnitudes in the range $15 < i < 19.1$. We only consider primary objects ($primary = 1$) with point source morphology ($morphology = 0$), that were also targeted as primary science objects ($scienceprimary = 1$). This yields a sample of 7128 quasars.

Of these 7128 quasars, 684 (9.6%) have radio identifications in the FIRST survey down to the 1 mJy flux density limit. One issue that could affect the derived radio luminosities of the QSOs in our sample is that a fraction of them present a truly extended FRII-like morphology, and the total radio flux is distributed over many components. The exclusion of such structures might lead to an underestimation of the total radio luminosity. We visually examined NVSS/FIRST radio maps of the 678 QSO with FIRST detections and added the NVSS fluxes of the associated component(s), if present, or of the FIRST component(s) when no NVSS source was found in the nearby. For some radio QSO the derived radio luminosities increase by a factor of ∼2-3. Figure 4.1 shows a few examples of extended radio structures around target quasars detected in FIRST maps. Nevertheless, we note that we

repeated the clustering analysis described in Section 4.4.4 using only the central (core) component flux, and we verified that this has no significant influence on any of our results.

According to convention, we define radio-loud quasars as those with total integrated 1.4 GHz radio power (after adding all associated components) above $10^{25}$ W Hz$^{-1}$. With this definition, there are 307 radio-loud quasars in our sample. We consider objects below this luminosity (or non-detections) as radio-quiet quasars.

### 4.2.1 Sample Properties

Shen et al. [2008] have derived virial black hole mass estimates for SDSS DR5 quasars. These are based on H$\beta$, MgII, and CIV emission lines, and the continuum luminosities around these lines. We adopt these estimates for our quasar sample (at $z < 0.7$, these are mostly derived from H$\beta$). For RLAGN we adopted the relation between black hole mass-bulge mass derived by Häring and Rix [2004], $\mathrm{M}_{bh} = 0.0014\mathrm{M}_{bulge}$, where we replace $\mathrm{M}_{bulge}$ by the stellar mass of the galaxy. At the lower end of our galaxy mass distribution ($\sim 10^{11} M_{\odot}$), use of the stellar mass instead of the bulge mass may cause the black hole mass to be overestimated by a factor of $\sim 1.2 - 1.4$. We note that the majority of RLAGN in our sample are more massive than this.

For reference, Figure 4.2 shows the radio luminosity and black hole mass distributions derived for all the radio-loud AGN and radio-loud QSO in our samples. In the upper panel, we also plot the ratio of the number of RLQSOs to RLAGN and show that this increases from $\sim 1\%$ at $10^{25}$ W Hz$^{-1}$ up to $\sim 50\%$ at $10^{27}$ W Hz$^{-1}$. This is broadly consistent with the results of Lawrence [1991] who found similar relative proportions between broad-lined and narrow-lined 3CR sources. One scenario that has been introduced to explain this varying fraction (at least at luminosities where the relative numbers of RLQSO and RLAGN are similar) is the receeding torus model (e.g. Simpson 1998), in which the inner radius of the obscuring torus (which is identified with the dust sublimation radius) scales with luminosity as $L^{0.5}$. This model predicts that a larger fraction of more luminous objects are classified as quasars.

## 4.3 Clustering Analysis

### 4.3.1 The Cross-correlation Function

A standard way to characterize the clustering of galaxies is with the two-point correlation function $\xi(r)$, which measures the excess in the numbers of pairs with separation $r$ in a volume $dV$, respect to a random distribution with the same mean

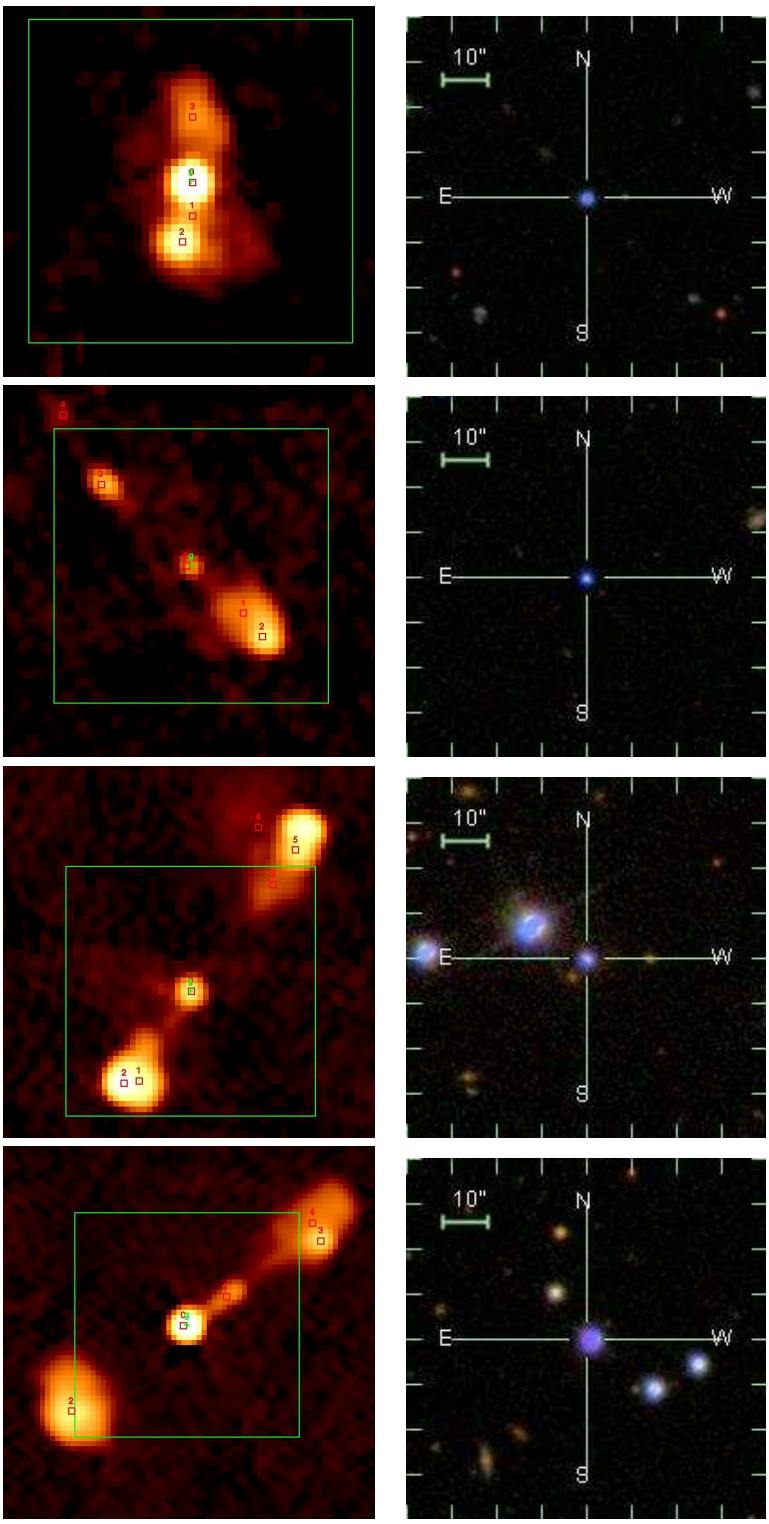


**Figure 4.1** • FIRST cutouts around quasars with multiple radio counterparts (left) and the corresponding SDSS images (right). The QSO position is marked by the green (g) plus symbol and the FIRST components are indicated by the succesive (0,1,2,...) red squares. The large green square measures 80x80 arcsec and correspond to the field of view of the optical image.

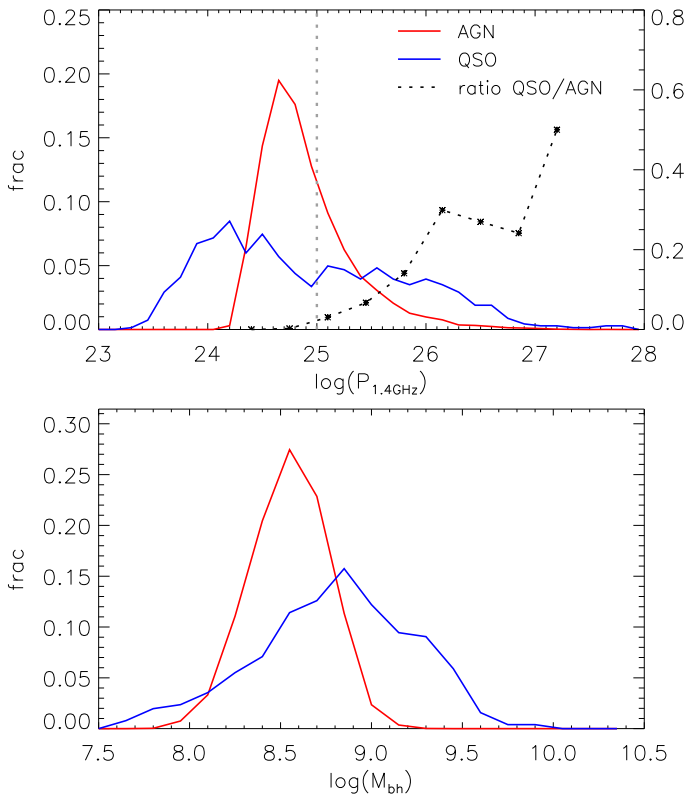


**Figure 4.2** • Top: normalized distribution of radio luminosity ($P_{1.4GHz}$) corresponding to radio-loud AGNs (red), and to QSOs detected down to 1 mJy in the FIRST survey (blue). The vertical line at $10^{25}$ W Hz$^{-1}$ marks the adopted threshold between radio-quiet and radio-loud QSOs (dotted). Also shown is the ratio of the number of radio-loud quasars relative to radio AGN (scale on the right axis). Bottom: distribution of black hole mass ($M_{bh}$) for radio-loud AGNs and radio-loud QSOs.

number density of objects $n$ (Peebles 1980). This can be expressed as

$$dP = n^2[1 + \xi(r)]dV^2 \tag{4.1}$$

Objects are said to be clustered if $\xi > 0$. The amplitude and shape of the correlation function yield a variety of different information. On scales larger than a few Mpc, the amplitude is a measure of the mass of dark matter halos that the galaxies inhabit (e.g. Sheth and Tormen 1999). On intermediate scales, the shape of the correlation function is sensitive to how galaxies are distributed within their halos (Li et al. 2006b), while at scales smaller than a few hundred kpc it probes processes such as mergers or interactions (Li et al. 2008).

Several estimators for the (auto)correlation function have been proposed in the literature. In this work we calculate the auto-correlation function of the LRGs using the estimator of Hamilton [1993],

$$\xi(r) = \frac{DD(r)RR(r)}{[DR(r)]^2} - 1 \tag{4.2}$$

where $DD(r)$, $RR(r)$, $DR(r)$ refers to the normalized number of (LRG-LRG), (random-random), and (LRG-random) pairs as function of the spatial separation $r$ (see the next section for details about the construction of the random sample).

To estimate the cross-correlation function of radio-loud AGN or quasars with the MegaZ-LRG galaxy sample, we count the number of LRGs around each AGN or quasar as a function of distance, and divide by the expected number of pairs for a random distribution,

$$\xi(r) = \frac{CD(r)}{CR(r)} - 1 \tag{4.3}$$

where $CD(r)$ stands for the number of (RLAGN/QSO-LRG) pairs, $CR(r)$ is the number of (RLAGN/QSO-random) pairs, and the quantities have been normalized by the number of objects in the LRG and random catalogues. The advantage of our procedure is that it does not require full knowledge of the QSO or RLAGN selection function. Only the LRG selection function is needed for the construction of the random sample, and this is well quantified. Another reason for calculating cross-correlations rather than auto-correlations, is that it allows us to overcome shot noise when the sample size is small. We note that the LRG sample ($D$ in the notation above) remains fixed throughout this work. The error bars of the auto and cross-correlation functions are calculated via statistical bootstrapping by drawing $n = 100$ random samples with replacement.

In practice, photometric redshift errors as well as distortions due to peculiar velocities along the line of sight will introduce systematic effects in our estimate of $\xi(r)$. Therefore, to recover real-space clustering properties we decompose $\xi$ in two directions, along the line of sight ($\pi$) and perpendicular to it ($r_p$). Integrating over the $\pi$-direction allows to define the projected two-point cross-correlation function

$w_p(r_p)$, a quantity that is independent of such distortions (Davis and Peebles 1983). A detailed description of the method can be found in Li et al. [2006b].

We note, however, that Li et al. [2006b] integrated along the line of sight up to 40 Mpc $h^{-1}$ of distance, which is typical in spectroscopic samples with accurate redshifts. In our sample, the photometric redshift errors of LRGs is $\delta z \sim 0.049$, which corresponds to $\sim$110 Mpc $h^{-1}$ at $z = 0.5$. And since, both the radio-loud AGN and reference galaxies have photometric redshifts, the relative distance between them is uncertain by another factor of $\sqrt{2}$ or $\sim$150 Mpc $h^{-1}$. We have therefore integrated up to 200 Mpc $h^{-1}$ along the line of sight in order to include all correlated galaxies.

### 4.3.2 Construction of the Random Sample

In order to infer statistically meaningful results about clustering from pair counts in observed samples, one must have complete understanding of the sample selection function, so that the random sample being used has the same selection effects as the observed galaxies.

To do that, we follow the method by Li et al. [2006a]: we take observed LRG sample inside the coverage mask of SDSS DR4 and randomly re-assign the sky coordinates of each galaxy. All other quantities such as like redshift, stellar mass and luminosity are kept fixed. Because the survey covers a very wide area (>6000 $deg^2$ for SDSS DR4), this procedure is sufficient to remove any coherence in the radial direction and it ensures that the geometry of the random catalogues are exactly the same as the real one, and that all redshift-dependent selection effects are accounted for. We generate N=10 random samples in this way.

## 4.4 Results

### 4.4.1 Radio-loud AGN clustering

It is well known that the clustering amplitude of galaxies varies as a function of mass, luminosity and redshift. Radio AGN are usually hosted by very massive, $> 3L_*$ galaxies (Best et al. 2005a; Donoso et al. 2009). To take this into account, we select control samples of radio-quiet MegaZ-LRG galaxies with redshifts, stellar masses and absolute magnitudes that closely match the radio AGN sample. For each RLAGN we randomly select 10 radio-quiet LRG (or 5, depending on the number of available candidates) within a tolerance of $\Delta z = 0.02$ in redshift, $\Delta M = 0.1$ in log stellar mass, and $\Delta M_i = 0.05$ in absolute magnitude, where $M_i$ is the extinction and k-corrected $i$-band absolute magnitude. By constraining this parameters we make sure that host galaxies are roughly similar. Figure 4.3 shows the distributions of these parameters for radio-loud, radio-quiet and control objects.

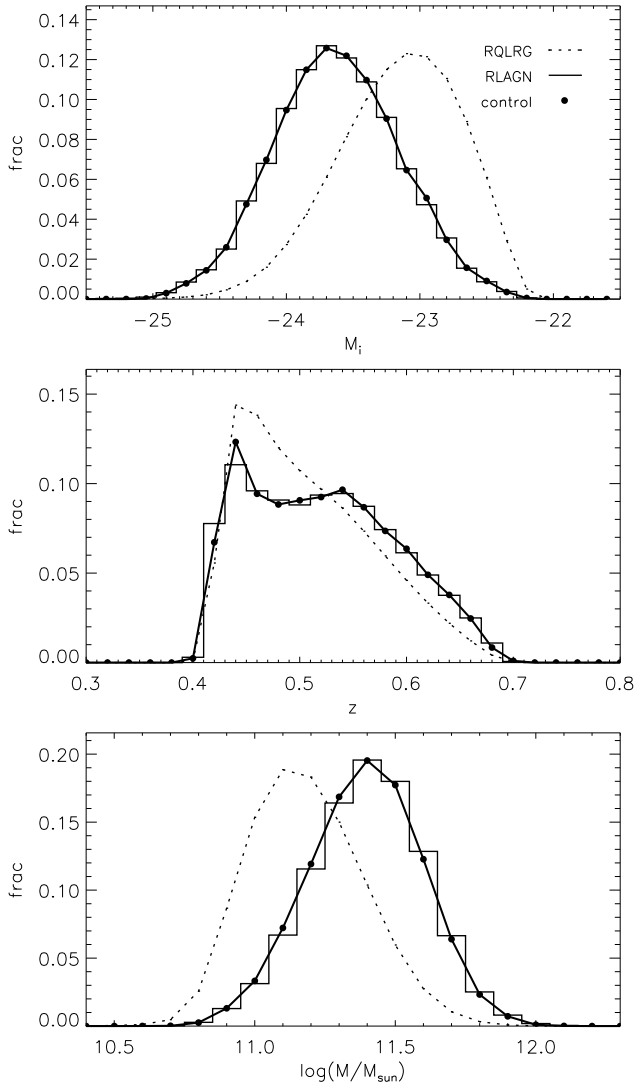


**Figure 4.3** • Normalized distributions of $i$-band absolute magnitude, redshift and stellar mass for radio-quiet LRGs (dotted), radio-loud AGN (histogram), and control radio-quiet LRGs (large dots).

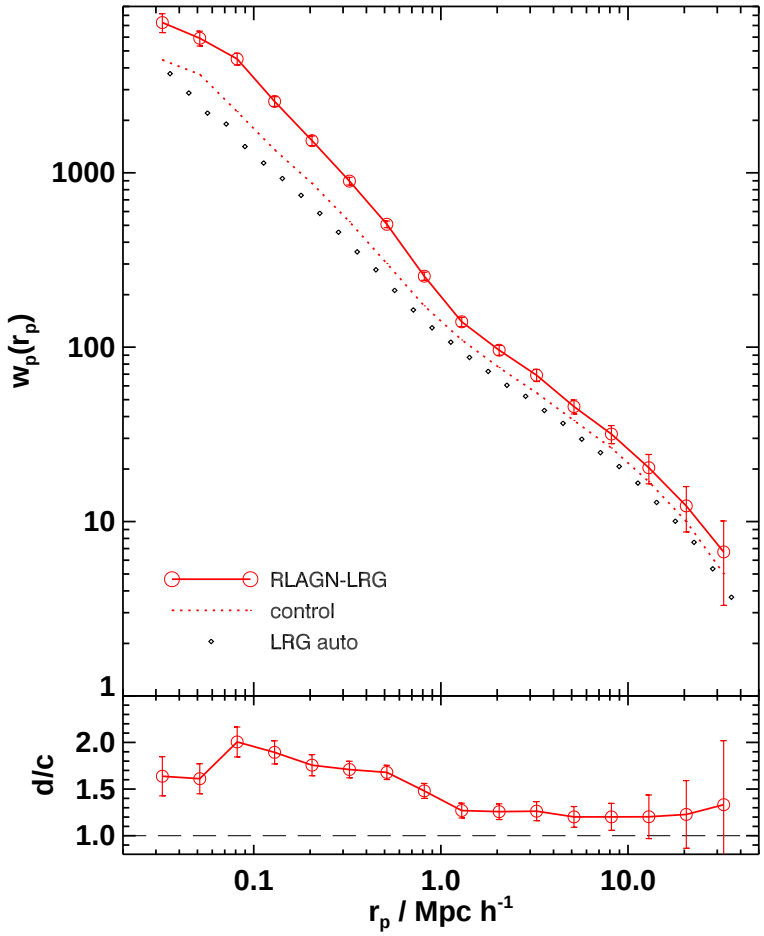


**Figure 4.4** • Projected cross-correlation function $w_p(r_p)$ between radio-loud AGN and MegaZ luminous red galaxies (red, solid) in the range 0.3 to 30 Mpc $h^{-1}$. The LRG-LRG auto-correlation is indicated by small diamond symbols. Also shown is the cross-correlation of a control sample of radio-quiet LRG (red, dashed) with the same distribution of redshifts, luminosities and stellar masses as the radio-loud population. The bottom panel shows the ratio of $w_p(r_p)$ for the RLAGN to that for the control sample.

Using the methods described in the previous section, we first calculate the auto-correlation function for our reference sample of luminous red galaxies selected from the MegaZ-LRG catalogue. We then cross-correlate the radio-loud AGN with the LRG parent sample. This is shown in Figure 4.4, where it can easily be appreciated that RLAGN are significantly more clustered than the LRG population on all spatial scales. The two terms of the clustering signal, corresponding to galaxies within the same halo (1-halo) and in different halos (2-halo), are clearly visible with the transition occurring around 1 Mpc $h^{-1}$. The boost in clustering signal exhibited by the RLAGN is significantly stronger on scales less than 1 Mpc $h^{-1}$, which tells us that RLAGN must occupy special positions within their dark matter halos. We intend to model this in more detail in upcoming work.

If we compare the clustering of RLAGN with that of control galaxies with the same redshifts, luminosities and stellar masses, we see that RLAGN are still signifi-

cantly more clustered. The ratio between the cross-correlations $w_p(r_p)$ corresponding to RLAGN and its corresponding control radio-quiet sample, is plotted in the bottom panel. This proves that the probability of a galaxy to become radio-loud depends on environment as well as on black hole or galaxy mass.

### 4.4.2 Dependence on Stellar Mass

We want to investigate in detail how clustering depends on stellar mass in radio-loud AGN. We split the RLAGN sample into two subsamples with $\log(M/M_\odot) < 11.3$ and with $\log(M/M_\odot) > 11.6$. We also applied the same split to the corresponding control samples. Figure 4.6 shows the relevant distributions for radio-loud, radio-quiet and control objects. The resulting cross-correlations are plotted in Figure 4.5. As expected, more massive radio galaxies are more strongly clustered on all scales. When compared to control galaxies, both subsamples show roughly the same relative clustering strength on scales larger than 1-2 Mpc $h^{-1}$. On small scales the difference between control and data samples is more significantly boosted for RLAGN in less massive galaxies. These results are in good agreement with those of Mandelbaum et al. [2009] for RLAGN at lower redshifts.

We now investigate how the clustering of RLAGN and their control galaxies varies *as a function* of stellar mass. We fit two power laws of the form $w(r_p) = A\ r_p^{(1-\gamma)}$ to the cross-correlation function, one over the range $0.1 < r_p < 0.8$ Mpc $h^{-1}$ and the other over the range $1 < r_p < 20$ Mpc $h^{-1}$. This division allows us to quantify separately the clustering signal contributed by LRGs within the same halo as the RLAGN and by LRGs residing in different halos. For the complete RLAGN sample, the best fitting parameters are $A = 233.9 \pm 15$ and $\gamma = 2.18 \pm 0.05$ on scales less than 1 Mpc $h^{-1}$ and $A = 173.2 \pm 10$ and $\gamma = 1.81 \pm 0.05$ on larger scales. We then divide the sample into 8 mass bins and perform new fits, keeping the slope of the power law fixed and allowing the normalization to vary. Figure 4.7 shows the cross-correlation amplitudes as a function of stellar mass for RLAGN and the radio-quiet control sample. As can be seen, the ratio between the clustering amplitude of the RLAGN and the control galaxies depends both on stellar mass and on the scale at which the clustering is evaluated. On scales less than 1 Mpc $h^{-1}$, there is a relatively strong dependence of the ratio on stellar mass, with RLAGN in low mass galaxies clustered much more strongly than the controls, but RLAGN in high mass galaxies clustered similarly to the controls. On larger scales, there is a much weaker trend with mass.

### 4.4.3 Dependence on Radio Luminosity

We now investigate if there is any dependence of RLAGN clustering on the luminosity of the radio source. Prestage and Peacock [1988] studied the local galaxy density around radio galaxies at $z < 0.25$, finding that weak FRI sources are typically found

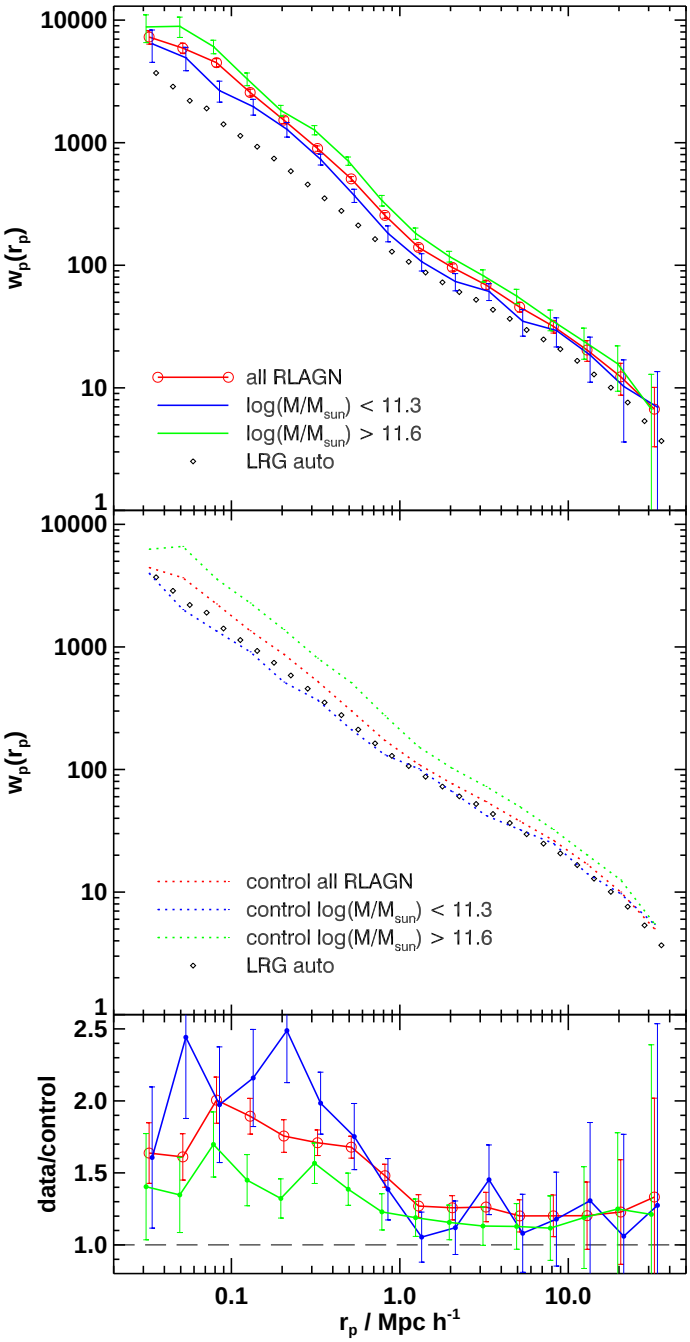


**Figure 4.5** • Top: projected cross-correlation function $w_p(r_p)$ between radio-loud AGN and MegaZ luminous red galaxies (red) in the range 0.3 to 30 Mpc $h^{-1}$. The green and blue lines indicate the cross-correlation of massive objects with $\log(M/M_\odot) > 11.6$, and of less massive systems with $\log(M/M_\odot) < 11.3$. The LRG-LRG auto-correlation function is shown for reference (diamond symbols). Middle: cross-correlation of control samples of radio-quiet LRGs that have the same distribution of redshift and stellar mass as the radio-loud systems. Bottom: ratio of $w_p(r_p)$ between RLAGN and their corresponding control samples. Note the curves are slightly shifted along the x-axis to improve the visibility.

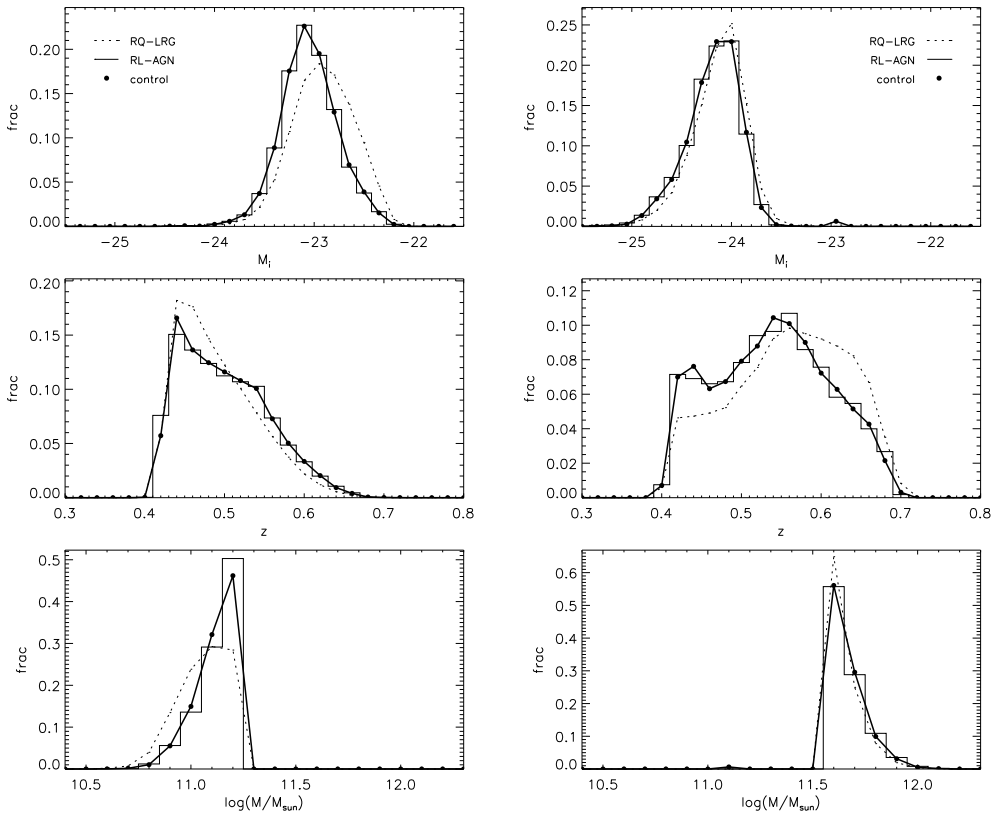


**Figure 4.6** • Normalized distributions of $i$-band absolute magnitude, redshift and stellar mass of radio-quiet LRG (dotted), radio-loud AGN (histogram), and control radio-quiet LRG (large dots) selected to have similar distributions as of RLAGN. Left panels are for objects with $\log(M/M_{\odot}) < 11.3$ and right panels for $\log(M/M_{\odot}) > 11.6$.

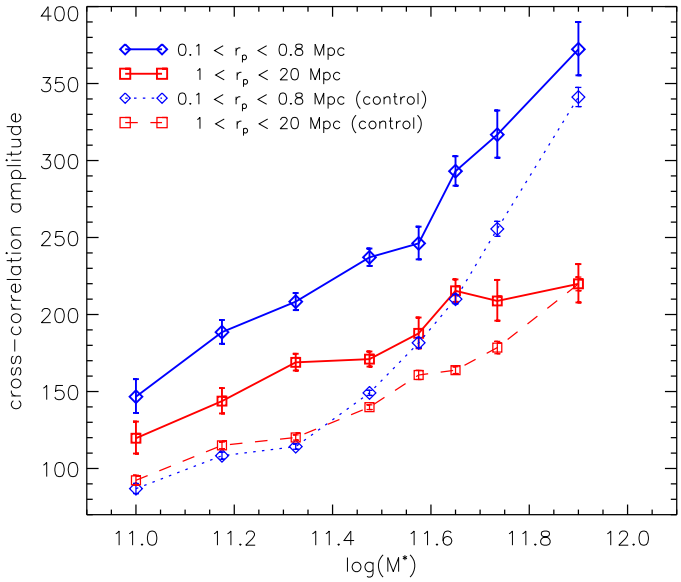


**Figure 4.7** • The dependence of the cross-correlation amplitude of RLAGN and control galaxies on stellar mass. The amplitude is computed by fitting a power law with fixed exponent (see text for details). Results are shown for RLAGN (solid lines) and their corresponding control radio-quiet LRG (dotted, dashed lines). Fits are calculated at two different spatial scales, $0.1 < r_p < 0.8$ Mpc $h^{-1}$ (blue) and $1 < r_p < 20$ Mpc $h^{-1}$ (red).

in denser regions compared to the more luminous FRII sources. Yates et al. [1989] (and later Hill and Lilly 1991) extended such studies to higher redshifts, concluding that powerful radio galaxies at $z \sim 0.5$ are typically found in environments three times richer than their counterparts at $z \sim 0.2$, but also that the most luminous objects ($P_{178MHz} \sim 10^{27.1}$ W Hz$^{-1}$ sr$^{-1}$) occupy richer environments than the weaker objects ($P_{178MHz} \sim 10^{26.1}$ W Hz$^{-1}$ sr$^{-1}$). However, given the limitations of the samples available, they were unable to determine if such clustering trends were primarily dependent on redshift or on radio luminosity, or on a combination of both. Best [2004] studied the density of galaxies around nearby radio-loud AGN. He found a positive correlation between local density and radio luminosity for RLAGN without emission lines, but found that RLAGN with emission-lines in their optical spectra tended to avoid regions of high density.

In this work, we split our RLAGN sample into a low-luminosity subsample with $\log(P_{1.4GHz}[\text{W Hz}^{-1}]) < 24.6$, and a high-luminosity subsample $\log(P_{1.4GHz}[\text{W Hz}^{-1}]) > 25.7$. These cuts allow us to sample the faint and bright end of the radio luminosity distribution. We again build control samples in the same way as before and we present the cross-correlation results in Figure 4.8. The top panel of Figure 4.8 shows that low luminosity RLAGN are more clustered than high luminosity systems at all scales. When compared to control samples, this "boost" in clustering is only visible at scales larger than ∼1 Mpc $h^{-1}$.

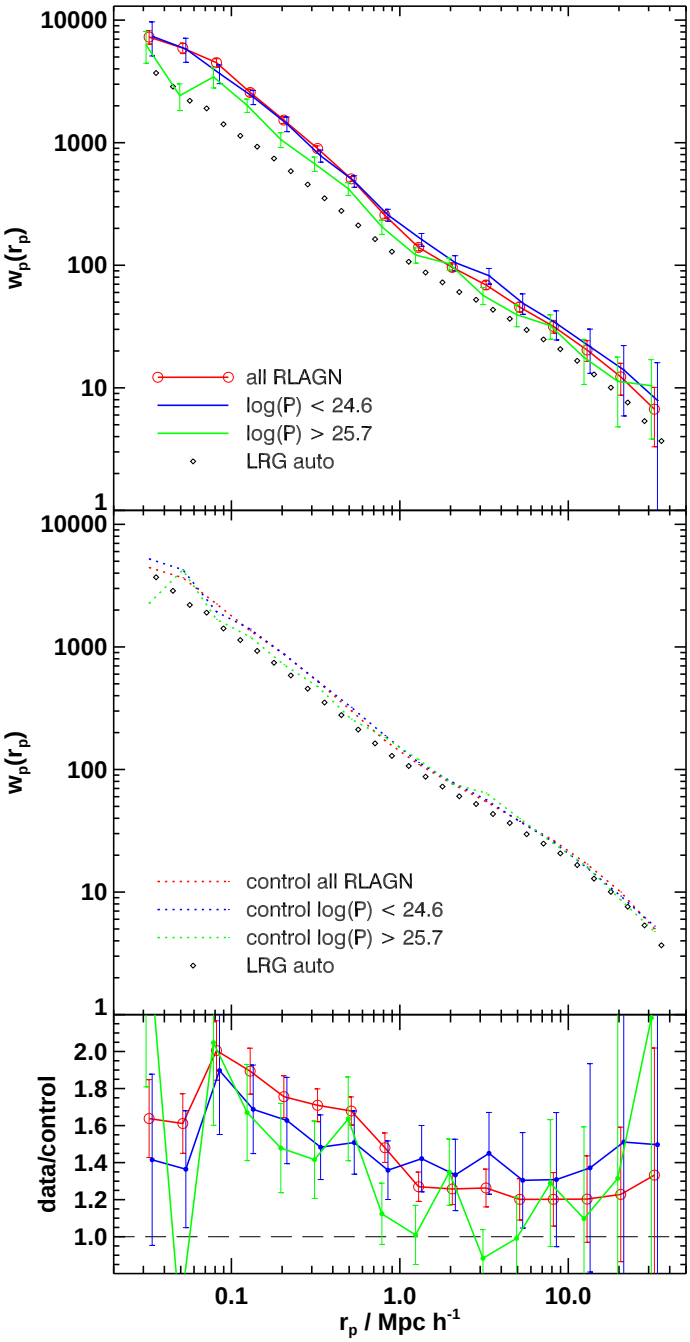


**Figure 4.8** • Top: projected cross-correlation function $w_p(r_p)$ between radio-loud AGN and MegaZ luminous red galaxies (red) in the range 0.3 to 30 Mpc $h^{-1}$. Green and blue lines indicate the cross-correlation of luminous objects with $\log(P_{1.4GHz}[W\ Hz^{-1}]) > 25.7$, and of less powerful AGN with $\log(P_{1.4GHz}[W\ Hz^{-1}]) < 24.6$. The LRG-LRG auto-correlation is shown for reference (diamond symbols). Middle: cross-correlation of control samples of radio-quiet LRGs that have the same distribution of redshift and stellar mass as the radio-loud systems. Bottom: ratio of $w_p(r_p)$ between RLAGN and their corresponding control samples. Note the curves are slightly shifted along the x-axis to improve the visibility.

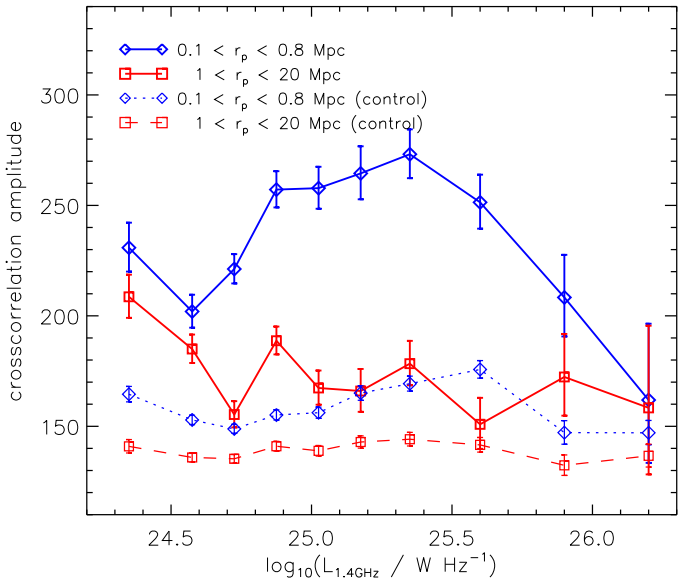


**Figure 4.9** • The dependence of the cross-correlation amplitude on radio luminosity. Results are shown for both, RLAGN (solid lines) and their corresponding control radio-quiet LRGs (dotted, dashed lines). Fits are calculated for two different ranges in scale: $0.1 < r_p < 0.8$ Mpc $h^{-1}$ (blue) and $1 < r_p < 20$ Mpc $h^{-1}$ (red).

To quantify the variation of clustering with radio luminosity in more detail, we once again proceed by fitting a power law to the cross-correlation functions for RLAGN subsamples split by radio luminosity. We fit separate power laws on scales below and above 1 Mpc $h^{-1}$. The variation in the clustering amplitude with luminosity is plotted Figure 4.9. Apart from the high clustering amplitude of RLAGN when compared to control systems, two interesting features can be observed. First, the clustering amplitude of radio galaxies on large scales is only very weakly anti-correlated with radio power. On small scales, the clustering *increases* with radio luminosity, peaks at $\log(\mathrm{P_{1.4GHz}}[\mathrm{W\ Hz^{-1}}])\sim 25.3$, and then decreases for most luminous radio sources.

We can qualitatively interpret this behavior of the clustering in terms of ability of radio jets to do work against the pressure of the surrounding material. Barthel and Arnaud [1996] argue that the confining effect of a dense intracluster medium reduces the adiabatic loses of radio lobes, leading to higher levels of synchrotron emission. Thus, a dense environment may provide a more effective 'working surface' for the lobes, giving rise to the positive correlation between small-scale clustering amplitude and radio luminosity observed in Figure 4.9 for sources with $\log(\mathrm{P_{1.4GHz}}[\mathrm{W\ Hz^{-1}}])< 25.3$. Alternatively, higher radio luminosities in denser environments may be a result of increased jet powers resulting from the higher cooling rates in these denser regions. Why does the clustering amplitude drop for radio sources with luminosities higher than this value? As we will argue in the next sec-

tion, a radio luminosity of $\log(P_{1.4GHz}[W\ Hz^{-1}])\sim 25.3$ may mark the beginning of a transition to a population of AGN that are more similar to the quasars, which as we will show, are significantly less clustered that the RLAGN.

### 4.4.4 Quasar clustering and AGN Unification

In this section, we compare the clustering of radio galaxies and quasars at z∼0.5. Our goal is to develop a better understanding of the relationship between these two types of active galaxy.

AGN unification models provide an appealing way to account for the diversity of the observed AGN population. The basic hypothesis is that the observed characteristics of AGN depend mainly on their orientation relative to the line-of-sight. Comprehensive reviews of unification models can be found in Barthel 1989, Antonucci 1993 or Urry and Padovani 1995.

Here, we attempt to test one fundamental requirement of the unification scheme of radio-loud objects, namely that the environment of radio galaxies and radio quasars should be statistically identical. We note that previous work has already suggested that low excitation radio galaxies (which include most FRI sources, but also a significant fraction low luminosity FRII radio galaxies) do not participate in the same unification framework as quasars or broad line radio galaxies (e.g. Hardcastle 2004; Hardcastle et al. 2007). We will therefore confine our attention to the most luminous radio-loud galaxies and radio-loud quasars in our sample, i.e. both with luminosities in excess of $10^{25}$ W Hz$^{-1}$.

Up to now, observational evidence has not yielded conclusive evidence as to whether powerful RLAGN and RLQSOs cluster in the same way. The first problem is that the available samples have been small. In the local universe, powerful radio galaxies with $\log(P_{1.4GHz}[W\ Hz^{-1}])\sim 26$ have typical comoving densities of $10^{-8}$ Mpc$^{-3}$ dex$^{-1}$ at z∼0.1, so large volumes are required to detect a significant number of sources. Smith and Heckman [1989] studied the environments ∼30 low redshift radio quasars and powerful radio galaxies, concluding that both populations were clustered in much the same way as radio-quiet QSOs. At higher redshifts ($0.3 < z < 0.5$), Yates et al. [1989] also found that the environments of radio galaxies and radio-loud quasars were similar, with higher luminosity systems slightly more clustered. Barr et al. [2003] found that luminous radio-loud quasars exist in a variety of environments including rich clusters, compact groups and in low-density environments.

In this work we have calculated the cross-correlation function between radio-quiet and radio-loud quasars, and the same reference sample of LRGs used in Section 4.4.1. The resulting $w_p(r_p)$ are plotted in Figure 4.10. As can be seen, *there is no significant difference in clustering strength between radio-loud and radio-quiet quasars*. It is interesting that the clustering strength of RLAGN seems to be larger

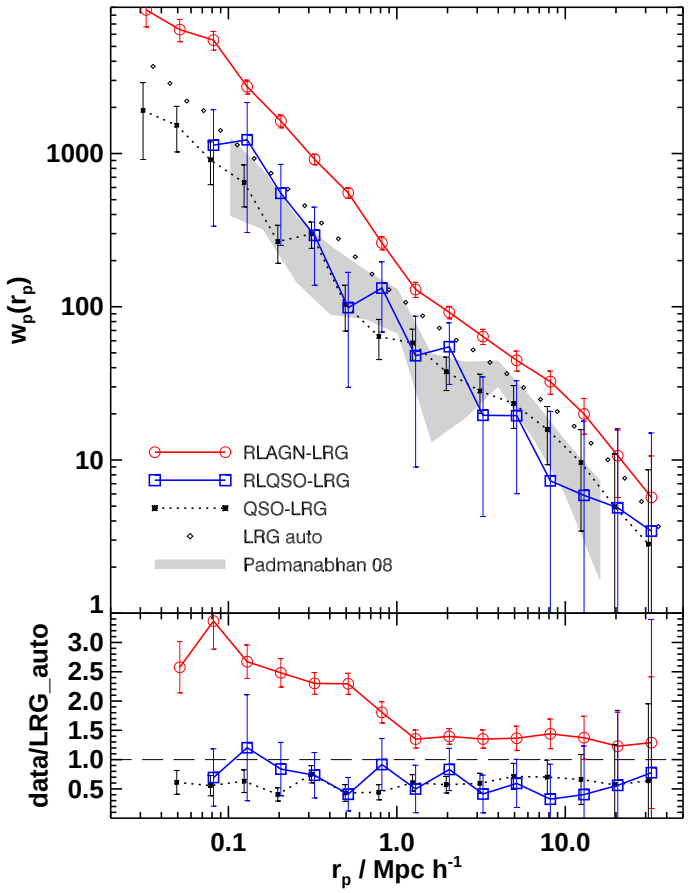


**Figure 4.10** • Projected cross-correlation function $w_p(r_p)$ between quasars and LRGs (dotted, black), and between radio-loud quasars and LRGs (blue). For comparison, we plot the cross-correlation of radio-loud AGN and LRGs (red), as well as the LRG-LRG auto-correlation (small diamonds). The grey shaded area indicates the QSO-LRG cross-correlation derived by Padmanabhan et al. [2009]. The bottom panel shows the ratio of $w_p(r_p)$ respect to the LRG auto-correlation. The analysis is restricted to sources with integrated luminosities above $10^{25}$ W Hz$^{-1}$.

than that of radio-loud quasars on all scales, and particularly at $r_p$ <1 Mpc $h^{-1}$. The mean relative bias of radio-loud quasars respect to the LRG population remains roughly constant at ∼0.7, while the bias of RLAGN varies strongly from ∼2.5 to ∼1.5 below 1 Mpc $h^{-1}$, and then stays relatively constant at larger scales.

We note that our quasar/LRG cross-correlation function agrees extremely well with that derived by Padmanabhan et al. [2009]. Shen et al. [2009] analyzed the clustering of radio-loud and radio-quiet quasars in SDSS DR5 at $0.4 < z < 2.5$ and found that radio quasars cluster more strongly than radio-quiet quasars with the same black hole masses. As we will show in Section 4.4.5, matching the radio-quiet and radio-loud quasar sample in black hole mass does not alter our conclusion. We speculate that disagreement with Shen et al. [2009] may arise because we consider a much narrower range in redshift. We note that Wold et al. [2000] also found little difference between the environments of radio-loud and radio-quiet quasars over roughly the same redshift range as that probed in this study.

We conclude, therefore, that powerful radio galaxies appear to be hosted by very massive halos, more massive than their quasar counterparts. In principle, this suggests that the unification scheme for the two classes of AGN is not as straightforward as first thought, and additional parameters other than orientation are required to explain the difference between RLAGN and RLQSOs.

### 4.4.5 Black Hole Mass

One such parameter could be the mass of the black hole. Some observational evidence supports the idea that radio jet power might be closely related to the mass of the black hole and its accretion rate. Links between radio luminosity and black hole mass have been found in radio galaxies (Franceschini et al. 1998), and in quasars (Lacy et al. 2001; Boroson 2002). However, other authors have argued against such strong correlations (Ho 2002; Snellen et al. 2003; Metcalf and Magliocchetti 2006).

To control for the effect of black hole mass, we constructed a sample of RLAGN with a similar distribution in $M_{bh}/P_{1.4GHz}$ as that of radio-loud quasars. The parameter $M_{bh}/P_{1.4GHz}$ can be considered as a kind of inverse Eddington ratio that measures how much radio emission per unit black hole mass is produced by the jet. Figure 4.11 shows the resulting cross-correlations. A slight decrease in $w_p(r_p)$ is observable at scales above 1 Mpc $h^{-1}$ for the RLQSO sample, but the effect is of low significance. Figure 4.12 shows the distribution in $M_{bh}/P_{1.4GHz}$ of the RLAGN and RLQSO samples before and after the matching procedure.

We find that the difference in clustering does not change for the samples that are matched in $M_{bh}/P_{1.4GHz}$, meaning that black hole mass has a negligible influence in driving the observed differences between the clustering of radio quasars and radio galaxies. From Figure 4.2 it can be seen that some radio-loud quasars are hosted by black holes more massive than $10^{9.3}$ $M_\odot$, which are not present in the RLAGN

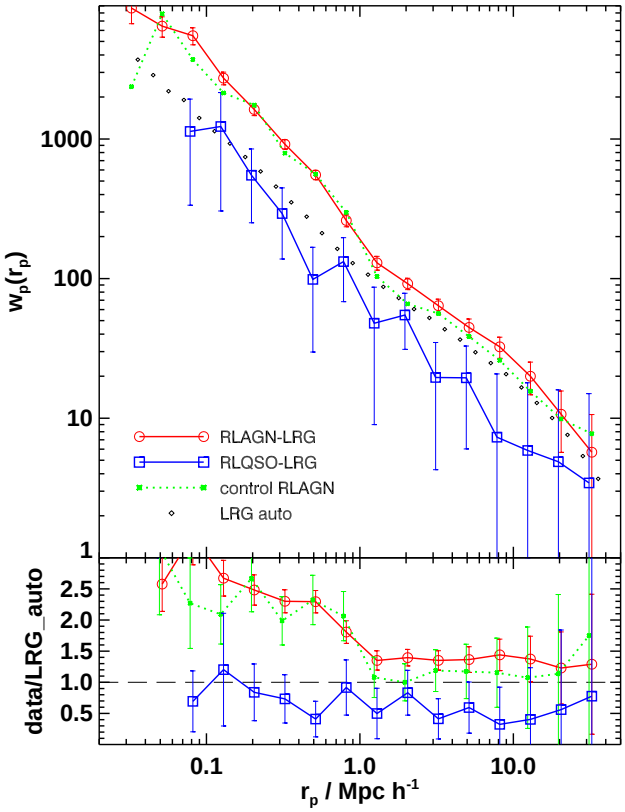


**Figure 4.11** • Projected cross-correlation function $w_p(r_p)$ between radio-loud quasars and LRGs (blue). Also shown is the cross-correlation of a control sample of radio-loud AGN (green) selected to have a similar distribution of $M_{bh}/P_{1.4GHz}$ as the radio-loud quasars. For comparison we plot the cross-correlation of RLAGN and LRG (red), and the LRG-LRG auto-correlation (small diamonds). The bottom panel shows the ratio of $w_p(r_p)$ to the LRG auto-correlation. The analysis is restricted to sources with integrated luminosities above $10^{25}$ W Hz$^{-1}$.

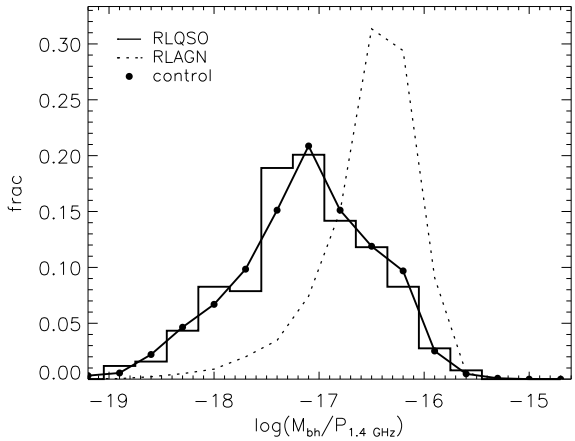


**Figure 4.12** • Normalized distributions of $M_{bh}/P_{1.4GHz}$ for radio-loud AGN (dotted), radio-loud QSOs (histogram), and control radio AGN (large dots) selected to have a similar distribution in $M_{bh}/P_{1.4GHz}$ as the radio-loud quasars.

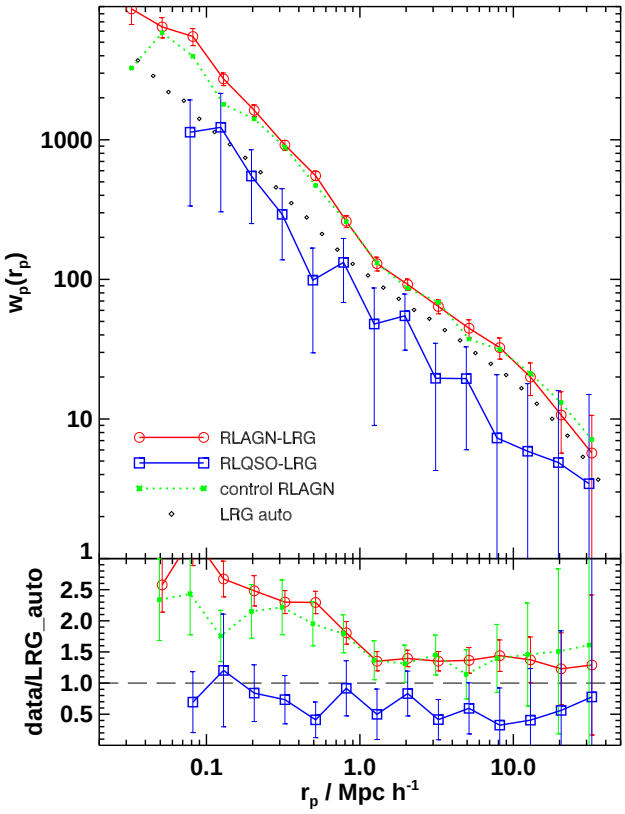


**Figure 4.13** • Projected cross-correlation function $w_p(r_p)$ between radio quasars and LRG (blue). Also shown is the cross-correlation of a control sample of radio-loud LRG (green) selected to have a similar distribution of $\log(P_{1.4GHz})$ as in radio quasars. For comparison we plot again cross-correlation of RLAGN and LRG (red), and the LRG-LRG auto-correlation (small diamonds). The bottom panel shows the ratio of $w_p(r_p)$ respect to the LRG auto-correlation. The analysis is restricted to sources with integrated luminosities (after adding all associated components) above $10^{25}$ W Hz$^{-1}$.

population (we suspect that errors in the virial black hole mass estimates are to blame). We have repeated the cross-correlation analysis of radio quasars with black hole masses in the range $10^8$ M$_\odot$ $< M_{bh} <$ $10^9$ M$_\odot$ and find that this makes no difference to our results.

### 4.4.6 Radio Luminosity

It is also interesting to investigate whether clustering differences between radio-loud AGN and quasars depend on radio luminosity. To test this, we build control samples using the same methodology as before, but this time matching in $\log(P_{1.4GHz})$[1]. Figures 4.13 and 4.14 show the corresponding cross-correlation functions and radio luminosity distributions of the matched samples. The clustering of RLAGN remains essentially unchanged.

[1]We note that a fraction of the RLQSOs will be core-dominated, so that a fraction of the luminosity of some sources will be due to relativistic beaming. This would affect the matching in radio luminosity between beamed and non-beamed objects. However, because of the weak dependence of clustering amplitude on radio

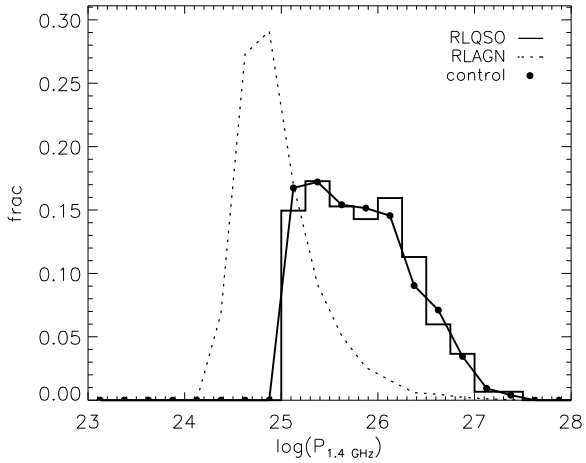


**Figure 4.14** • Normalized distributions of $\log(P_{1.4\mathrm{GHz}})$ for radio-loud AGN (dotted), radio-loud QSO (histogram), and control radio AGN (large dots) selected to have a similar distribution as of radio-loud quasars.

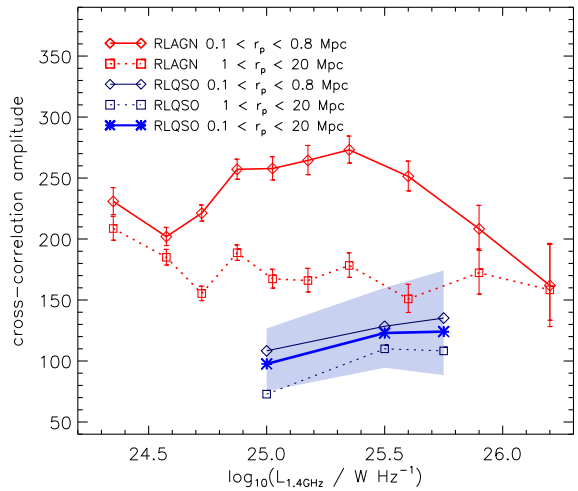


**Figure 4.15** • Change of the cross-correlation amplitude for RLAGN (red) and RLQSO (blue), obtained by fitting a power law with varying amplitude and fixed exponent. Radio quasars are splitted in bins of increasing radio luminosity [$\log(P_{1.4\mathrm{GHz}})$>25.0,>25.5,>25.75]. Fits are calculated at two different spatial scales, $0.1 < r_p < 0.8$ Mpc $h^{-1}$ (solid) and $1 < r_p < 20$ Mpc $h^{-1}$ (dotted). A single fit over the range $0.1 - 20$ Mpc $h^{-1}$ is indicated by the thick blue line, enclosed by the shaded error region.

We now calculate cross-correlation functions for radio-loud quasars of increasing radio luminosities [$\log(P_{1.4GHz})$>25.0,>25.5,>25.75]. We do find an increase in clustering strength as function of radio power on all scales in the range $0.1 < r_p < 20$ Mpc $h^{-1}$. This is plotted in Figure 4.15, where we compare the cross-correlation amplitude of radio-loud AGN and QSO. The amplitude is calculated using a single power-law fit over the entire range, since the correlation function of quasars does not exhibit a clear break at a scale of ∼1 Mpc $h^{-1}$, as is the case for radio galaxies. We find that RLAGN are more strongly clustered than RLQSO at all radio luminosities that we are able to probe. However, the clustering amplitude of RLQSOs increases as a function of radio luminosity, while that of RLAGNs decreases at the very highest radio luminosities. Extrapolation of our results suggests that both kinds of AGN might have similar clustering at radio luminosities in excess of $10^{26}$ W Hz$^{-1}$. This would imply that the unified model for radio-loud quasars and radio galaxies can only be valid at these very high radio luminosities. This is consistent with the dependence of the relative numbers of the two AGN types as a function of radio power (Figure 4.2).

## 4.5 Summary

In this work, we have successfully applied cross-correlation techniques to characterize the environments of $\sim 14,000$ radio-loud AGN with $P_{1.4GHz} > 10^{24}$ W Hz$^{-1}$, selected from $\sim 1.2$ million LRG at $0.4 < z < 0.8$. We have also compared the clustering of RLAGN with that of radio-loud quasars over the same redshift interval. By using control samples of radio-quiet objects matched in redshift, stellar mass and optical luminosity (or radio luminosity, when appropriate) we have isolated the effect such parameters have in influencing the clustering signal. The main results of this paper can be summarized as follows:

- Radio AGN at $0.4 < z < 0.8$ are substantially more clustered than their parent luminous red galaxy population. Radio-loud AGN are also more strongly clustered than radio-quiet galaxies of the same stellar mass and redshift. The clustering differences are largest on scales less than 1 Mpc $h^{-1}$.
- Radio-loud AGN hosted by more massive galaxies are more strongly clustered than those hosted by less massive galaxies. However, the clustering *difference* between RLAGN and control samples of radio-quiet galaxies is most pronounced for RLAGN in low mass hosts.
- We study the dependence of the clustering amplitude on the luminosity of the radio source. For $r_p > 1$ Mpc $h^{-1}$ there is a weak, but significant anti-correlation with radio power. For $r_p < 1$ Mpc $h^{-1}$ the dependence of clustering

luminosity for the quasars, this effect does not influence our conclusions

amplitude on luminosity is more complex: the cross-correlation amplitude increases with luminosity up to $\sim 10^{25.3}$ W Hz$^{-1}$, and then decreases for the most luminous radio sources in our sample.

- We have compared the environments of radio-loud AGN and radio-loud QSOs. RLAGN are clustered more strongly than RLQSOs on all scales, indicate that they populate dark matter halos of different mass. These results hold even when the RLAGN and RLQSO samples are matched in radio luminosity and black hole mass.
- There are indications that the very most luminous RLAGN and RLQSOs in our sample (P$> 10^{26}$ W Hz$^{-1}$) do have similar clustering amplitudes. Only at these very high radio powers are the space-densities of radio-loud quasars and radio galaxies similar. This implies that unification of the two AGN populations can only be valid above P$\sim 10^{26}$ W Hz$^{-1}$.

One major limitation of this study with regard to constraining AGN unification scenarios, is that it is based purely on photometric data from the SDSS, so we are unable to split our RLAGN sample into high-excitation and low-excitation sources. It is quite possible that the presence or absence of emission lines will provide the best way to define a population of radio galaxies that are clearly unified with the quasars. In this case, we would expect to find that the high-excitation radio galaxy population would cluster in a similar way to the quasars.

In addition, we note that because the parent sample of our RLAGN catalogue consists of luminous *red* galaxies, it is also likely that we completely miss some number of RLAGN with bluer colors and stronger emission lines. The analysis of the RLAGN luminosity function presented in Donoso et al. [2009] indicates that the missing sources cannot constitute more than $\sim$20% of the total RLAGN population, so will not dominate the clustering signal of the radio AGN population as a whole. Nevertheless the quasar analogues among the radio galaxy population may still be under-represented in our analysis.

Fortunately, upcoming large spectroscopic surveys such as BOSS will target nearly complete samples of more than a million massive galaxies at $0.4 < z < 0.8$ and will provide optical spectra for tens of thousands of radio galaxies. We will then be able to quantify the fraction of RLAGN of given radio luminosity that have emission lines and how the clustering depends on emission line strength.

The most definitive result to emerge from our analysis is clear proof that the environment of a galaxy on the scale of the dark matter halo in which it resides (i.e. on scales of $\sim$1 Mpc $h^{-1}$ and below), does play a key role in determining not only the probability that a galaxy a is radio-loud AGN, but also the total luminosity of the radio jet. Combining our results with those of Best et al. [2005a], we conclude that both black hole mass and environment must determine the radio-loud character of an active galaxy.

Our previous work also demonstrated that strong evolution of the radio AGN population only occurs above a characteristic radio luminosity of $\sim 10^{25}$ W Hz$^{-1}$ (Donoso et al. 2009). It is very intriguing that the results in this paper indicate that this luminosity marks the break point in clustering trends, and that the radio luminosity where denser environment ceases to have a boosting influence also is of order $10^{25}$ W Hz$^{-1}$.

Finally, the strong evolution of the radio source population at radio luminosities above $\sim 10^{25}$ W Hz$^{-1}$ combined with the strong clustering of this population, must imply that the heating rate of the gas in groups and clusters of galaxies is higher at redshifts $\sim 0.5$ than it is at the present day. We intend to quantify this in more detail in upcoming work.

# 5

# Modeling the Radio-loud Galaxy Population

In this chapter I will describe the implementation of a simple prescription for the distribution of the radio-loud galaxy population in dark matter haloes at $z = 0.5$, by using a large-scale N-body simulation coupled with a semianalytic model of galaxy formation that incorporates feedback from radio AGN as wel as improved tracking of the formation history of galaxies in haloes.

Then I will describe the derivation of the time-averaged heating output of radio sources hosted by galaxies as a function of stellar mass and redshift. I will also show how the models can be used to calculate the heating effect of radio sources in halos of different mass, and at two different cosmic epochs.

## 5.1 Introduction

### 5.1.1 AGN Feedback in SAMs

As explained in the introduction to this thesis, recent models of galaxy formation built on top of large cosmological dark matter simulations have implemented a variety of feedback processes and are now able to explain successfully many observed properties of galaxies in the nearby Universe and at higher redshifts.

In particular, the model from De Lucia and Blaizot 2007 includes prescriptions for star formation, supernova feedback, galaxy mergers, metal enrichment, and also an improved scheme to track the formation history of central galaxies in haloes. In this model, black holes grow through direct merging, accretion of cold gas driven by mergers (quasar mode), and through the accretion of hot gas when massive black holes are located in halos with an quasi-static atmosphere of hot gas (radio mode). As explained in chapter 1, radio mode feedback becomes more important at low

redshifts and is responsible shutting off the gas supply in cooling flows. The model largely follows the prescriptions given in Croton et al. 2006, with slightly modified treatments of galaxy mergers, dust attenuation and the initial mass function.

In these SAMs, radio activity is the result of continual hot gas accretion onto a central supermassive black hole once a static hot halo has formed around the host galaxy. The mechanical heating generated by this black hole accretion is $L_{bh} = \eta \dot{M}_{bh} c^2$, where $c$ is the speed of light, $\eta = 0.1$ is the efficiency for the mass-energy conversion near the black hole event horizon, and $\dot{M}_{bh}$ is the black hole accretion rate. The accreation rate is assumed to be proportional to the black hole and hot gas mass, multiplied by an efficiency factor and divided by the Hubble time. As noted before, these relations are calibrated in order to reproduce the observed luminosity function of galaxies.

### 5.1.2 Halo Occupation Distribution Models of Galaxy Clustering

Although semi-analytic models are successful at allowing the models to reproduce key observational data, we would like to test the AGN feedback prescription embedded in the models in a more direct way, rather than relying on "indirect" evidence, like the good match to luminosity functions. Progress on this can be achieved by constructing halo occupation distributions (HODs) for radio galaxies. A HOD describes the relation between galaxies and dark matter, at the level of individual dark matter haloes. The properties of galaxies located in center of dark matter haloes are expected to differ from those of satellite galaxies. This is because processes such as gas accretion and merging affect primarily the central galaxies. HOD models specify how galaxies populate their host haloes and how they are distributed among central or satellite locations. Once the HOD is specified, it is then simple to predict how galaxies are clustered. In fact, the general procedure that is usually adopted is to "tune" the HOD until the observed clustering and luminosity/mass function of galaxies are reproduced.

In our case, a HOD for massive galaxies and radio-loud AGN that can account for their observed clustering properties is important, because this allows us to constrain the mass of the haloes in which these objects are located. In addition, it makes it possible to estimate how much energy is being dumped on average into these halos at different redshifts, providing further input to refine the radio-mode feedback implementation in the semi-analytic models.

In this chapter, we will attempt to use the output of semianalytic models and a simple model to populate dark matter haloes with radio sources, in order to create "mock" catalogs of radio AGN that can reproduce the observed mass function and clustering of RLAGN. While models constructed in this way have been shown to adequately match observations of optical and radio AGNs at low redshift, it is of interest to extend them to higher redshifts. Coupling the model information with the bivariate radio luminosity-mass functions derived before, we will estimate the

total heating effect that radio sources have in haloes of different mass, in galaxies of different stellar mass, and as function of cosmic epoch between $z = 0$ and $z = 0.5$.

### 5.1.3 The heating power of RLAGN in the local universe

It is important to quantify the heating power of RLAGN, because typical lifetimes of radio-loud AGN are in the order of $10^7$-$10^8$ yr, which is very short compared to most processes in galaxy formation. We have shown in chapter 3 that the fraction of galaxies that host RLAGN is a strong function of stellar mass; it reaches 20-30% for the most massive systems at both z=0.14 and z=0.55. This means that in order to observe such high fractions in our samples, radio-loud activity must be constantly re-triggered.

In section 3.5 we have seen for a galaxy of a certain stellar mass, the bivariate radio luminosity-mass function gives the probability that it hosts a radio AGN of a certain power. Probabilistically, it can be interpreted as the fraction of time that a galaxy of a given mass spends as a radio AGN of a given radio luminosity. In principle, this could be used to derive the total heating power of radio sources as function of their stellar mass.

However, the total energetic output of radio jets is 2-3 orders of magnitude larger than the observed radio luminosity, so that in order to estimate true heating output or RLAGN, a conversion between radio and mechanical luminosities of radio sources is needed. Using observational estimates of the mechanical output of radio cavities and bubbles in the hot X-ray emitting gas of cluster and groups of galaxies, Best et al. 2006 derived a conversion relation, allowing them to calculate the time-averaged energy output associated with recurrent radio source activity as function of the mass of the central black hole. Moreover, by comparing the heating effect of RLAGN with radiative cooling rates derived from X-ray observations, Best et al. 2006 found a remarkable agreement between these heating and cooling rates across a wide range of host galaxy masses. This means that, averaged over time, the energy produced by RLAGN can balance the radiative energy losses from the hot halo of its host galaxy. In this way, radio source activity can suppress the cooling of the gas and therefore control the rate of growth of the elliptical host galaxy.

## 5.2 The Millennium Simulation

The semianalytic model for the formation and evolution of galaxies that we use (De Lucia and Blaizot 2007) is implemented on top of the Millennium Run, which is a large dark matter cosmological simulation with $2160^3$ ($\sim 10^{10}$) particles in a periodic box of size 500 Mpc $h^{-1}$. The particle mass is $8.6{\times}10^8$ $M_\odot$ $h^{-1}$, so that low mass haloes that host faint galaxies are typically resolved with at least 100 particles. The simulation volume is large enough to include interesting objects of low space

density, such as quasars or large galaxy clusters.

The initial conditions of the simulation were created using a Gaussian random field with a $\lambda$CDM linear power spectrum produced by the CMBFAST code (Seljak and Zaldarriaga 1996). This random field was used to displace particles from a homogeneous distribution set at z=127. The simulation was then evolved to z=0 using a special version of the GADGET-2 code (Springel 2005). A full description of the Millennium Run is given in Springel et al. [2005].

Large cosmological simulations such like the Millennium exhibit a rich substructure of gravitationally bound dark matter subhaloes orbiting within larger virialized haloes. As structures merge hierarchically in CDM universes, there can be several progenitors and usually one descendant for any given halo. To track the formation history of tens of millions of haloes and subhaloes, hierarchical merging trees of each z=0 halo are constructed based on the haloes and subhaloes identified by a FOF[1] algorithm at different redshifts. As merger trees encode the full formation history of each halo, they are the backbone of semianalytic models that (implemented in post-processing) simulate a wide range of baryonic processes relevant to the formation and evolution of galaxies and black holes.

## 5.3 Modeling of Radio-loud AGN

### 5.3.1 The basic model at $z \sim 0$

Mandelbaum et al. [2009] utilized a halo occupation model to interpret the clustering of radio-loud AGN in the local universe, using the same sample of observed radio-loud AGN selected from SDSS DR4 used in this work. They introduced a simple model in which the probability of a galaxy of given stellar mass to be an RLAGN is enhanced if it is the central galaxy of its own halo. The clustering analysis relies on the assumption that the AGN sample derives from a parent population which matches the statistical properties of galaxies as a function of stellar mass (i.e. the stellar mass function and the clustering). Then, a halo model parameter such as $f_{cen}$, which is the fraction of RLAGN that are hosted by central galaxies, can be used as a way of matching the observed AGN clustering, as it modifies the probability that each galaxy in the parent population to be a radio-loud AGN.

Motivated by the recent semianalyic models of Croton et al. [2006] and Bower et al. [2006], Mandelbaum et al. [2009] found that a two parameter model was able to reproduce the observed clustering signal. These parameters are the fraction of central galaxies $f_{cen}$, and the minimum halo mass $M_h^{min}$, the later of which constrains radio AGN to occur only in haloes more massive than $M_h^{min}$. This basically means that

[1] Friends-Of-Friends (FOF) technique basically links particles providing their separation is smaller than a fraction $f$ of the mean interparticle separation. A fraction $f = 0.2$ roughly combines particles in groups with overdensity of 200, which corresponds approximately to a virialized group.

the probability of a galaxy to be radio-loud depends on its location as central or satellite galaxy, but also on the mass of its hosting dark matter halo. While such a simple on/off dependence on halo mass is almost certainly an oversimplification of reality, it is a reasonable first order approximation that can be used to reproduce the observations from the models. Moreover, the semi-analytic models mentioned above suggest that feedback from radio AGN becomes important in haloes of masses above a few times $10^{11} - 10^{12}$ $M_\odot$, in which gas is cooling quasi-statically. Pasquali et al. [2009] also found, based on the analysis of SDSS DR4 groups of galaxies, that radio-loud AGN activity is predominant in haloes of masses $\sim 10^{13}$ $M_\odot$ $h^{-1}$.

In their best-fitting model of Mandelbaum et al. [2009], 74% ($f_{cen}$=0.74) of radio AGN are located at the centres of their own dark matter haloes, which are hosted in haloes above $10^{12.75}$ $M_\odot$ ($M_h^{min} = 10^{12.75}$ $M_\odot$). However, the exact values of the parameters are uncertain as there is a strong degeneracy between $f_{cen}$ and $M_h^{min}$. This is evidenced as a large banana-shaped region in the two-dimensional likelihood map of these parameters, plotted in Figure 6 of Mandelbaum et al. [2009].

### 5.3.2 Extension of the model to $z \sim 0.55$.

The first step in our work is to check if this model that successfully accounts for observations of RLAGN in the local universe, can also be applied at high redshift. The test is whether the model provides a reasonable approximation to the observed clustering of radio AGN at $z = 0.55$.

For this we use the direct output of the semianalytic model of De Lucia and Blaizot [2007] and implemented the occupation model described above. In practice, we selected a single snapshot of the 500 Mpc $h^{-1}$ simulation box at $z = 0.5$. It contains around $9 \times 10^6$ galaxies, among which we selected galaxies to construct mock samples of the radio AGNs and of the parent sample (this is the equivalent of the observed MegaZ LRG sample). Then we computed the mass function and the cross-correlation function of radio AGNs and of the parent objects, and compared with their corresponding observational estimates.

We found that the mass function of galaxies above $\sim 10^{11.0}$ $M_\odot$ approximately reproduces the one derived from the observed MegaZ-LRG sample, but in order to fit observations more closely we introduce a small shift of 0.05 dex to all stellar masses. Then, by selecting galaxies above $10^{11}$ $M_\odot$, the model is able to reproduce the clustering of the observed LRG population over the range in $r_p$ from $\sim 0.01$ Mpc $h^{-1}$ to $\sim 10$ Mpc $h^{-1}$.

The next step is to select the model galaxies that will host radio-AGNs. We do this according to the location of the galaxy in the dark matter halo (central or satellite) and the mass of the halo. As RLAGN at $z = 0.5$ are hosted in massive galaxies above $\sim 10^{11}$ $M_\odot$ we have decided to keep the minimum halo mass fixed at $M_h^{min} = 10^{12.75}$ $M_\odot$ and vary $f_{cen}$ in order to fit the observed cross-correlation

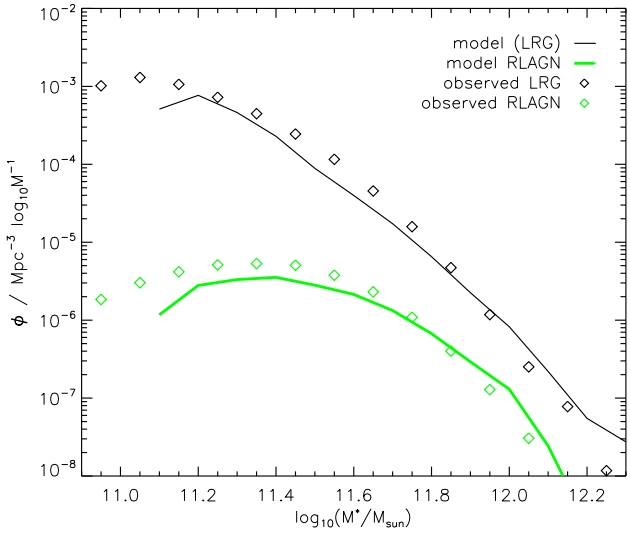


**Figure 5.1** • Mass function of luminous red galaxies and radio-loud AGN at $z = 0.5$ and the corresponding estimates derived from an occupation model based on the semianalytic model (SAM) of De Lucia and Blaizot [2007]. The model corresponds to the best-fitting model for RLAGN, with a fraction of $f_{cen} = 0.54$ for a fixed minimum dark matter haloes mass of $M_h^{min} = 10^{12.75}$. The SAM output corresponds to a snapshot at $z \sim 0.5$ of the 500 Mpc h$^{-1}$ simulation box of the Millennium Run.

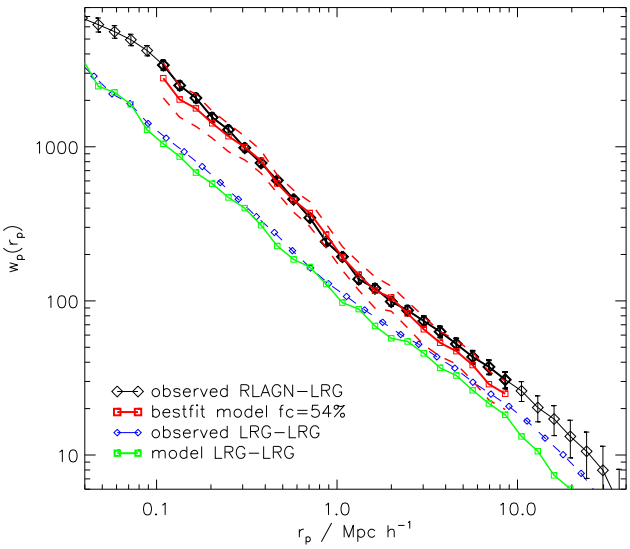


**Figure 5.2** • Projected LRG-LRG and RLAGN-LRG correlation function as derived from the MegaZ catalogue, and the corresponding estimates calculated from an occupation model based on the semianalytic model (SAM) of De Lucia and Blaizot [2007]. The model corresponds to the best-fitting model for RLAGN, with a fraction of $f_{cen} = 0.54$, for a fixed minimum dark matter haloes mass of $M_h^{min} = 10^{12.75}$.

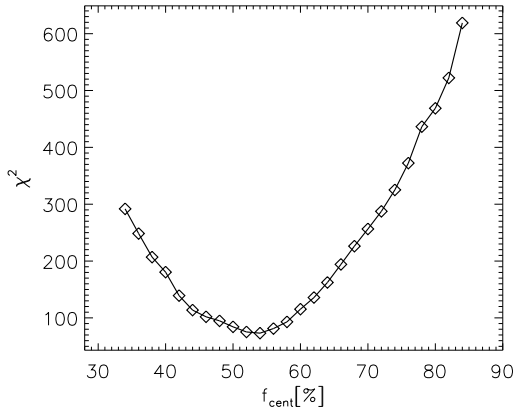


**Figure 5.3** • $\chi^2$ statistic for different values of the fraction of central galaxies that are hosting RLAGN in the occupation model. The best-fit model has a value of $f_{cen} = 0.54$, for a fixed minimum dark matter halo mass of $M_h^{min} = 10^{12.75}$.

function. We generated a series of models with $f_{cen}$ varying from 0.34 to 0.84, with a step size of 0.02. For each model we calculated the projected cross-correlation and compared with the observed $w_{rp}$ estimate over the $r_p$ interval from 0.05 to 10 Mpc $h^{-1}$. The best-fitting model was found at $f_{cen} = 54\%$ using the standard $\chi^2$ statistic. In Figures 5.1 and 5.2 we reproduce the observed and model mass functions of both RLAGNs and LRGs, as well as the corresponding estimates of $w_{rp}$ for the best-fit model. We also plot the $\chi^2$ statistic for the different values of $f_{cen}$ in Figure 5.3. It is worth noting that there is a good agreement between observations and the predictions of this simple model, especially if we consider that the comparison is between the direct semianalytic output in a real-space simulation box, and observations of galaxies in redshift-space.

The final step is to assign radio luminosities to the semianalytic catalog of radio-AGNs. We use the stellar mass to connect the distribution of radio luminosities in the observed and model catalogs. In practice, we divide observed RLAGN in stellar mass bins of size $\delta m = 0.1$ (in log) and derive the distribution of radio luminosities in each bin. Then, we assign radio luminosities to model RLAGNs in each stellar mass bin according to the corresponding distribution of radio powers. In this way, the model can reproduce the observed radio luminosity vs stellar mass plane, as can be appreciated in Figure 5.4.

## 5.4 Mechanical Luminosities of Radio-loud AGN

Having shown that this simple occupation model for RLAGN works successfully at $z = 0.5$, we now focus on how to estimate the heating power that these systems dump into the environment.

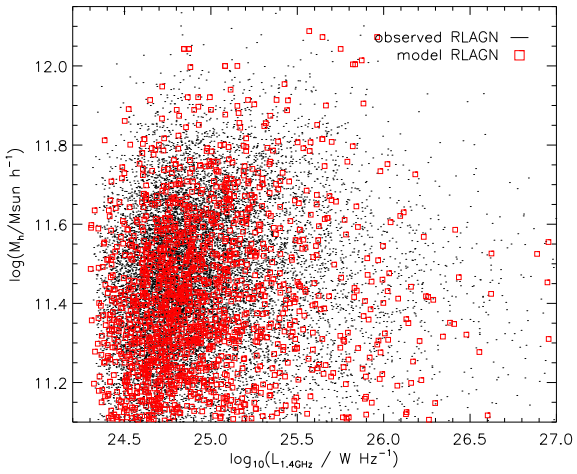


**Figure 5.4** • Stellar mass versus radio luminosity for observed RLAGN at $z = 0.5$, and radio AGN selected according to our best-fit occupation model.

Estimates of the total kinetic energy outputof a radio jet are typically a factor of $10^2$-$10^3$ higher than the radio luminosity of a radio source (Bicknell 1995). This means that monochromatic radio luminosity is not a good indicator of the mechanical energy output of a radio source. Hence, in order to determine the time averaged heating output of radio-loud AGN, it is necessary to convert between radio luminosity and mechanical energy output.

While in principle such conversion might vary as the radio source ages (i.e. for fixed jet kinetic power, the radio luminosity changes as the source ages, see Kaiser et al. 1997), it is reasonable to assume that at the population level is is possible to derive an age-averaged statistical relation between radio and mechanical luminosity. Bîrzan et al. [2004] studied the radio cavities and bubbles produced in groups and clusters that host radio galaxies, and derived the (pV) energy associated with the cavities, as well as their radio luminosities and ages. Best et al. [2006] combined this data to determine the conversion from radio to mechanical luminosities, given by

$$\frac{L_{mech}}{10^{36}\mathrm{W}} = 3.0 \pm 0.2 \left( \frac{L_{1.4\mathrm{GHz}}}{10^{25}\mathrm{W\ Hz^{-1}}} \right)^{0.4\pm0.13} \tag{5.1}$$

Bîrzan et al. [2004] showed that the mechanical luminosity of the system is also correlated with its X-ray luminosity. This suggests that more parameters than just the radio luminosity are required to fully characterize the heating. Nevertheless, to a first order of magnitude a good approximation over five decades in radio power is given by equation 5.1, which is plotted as the solid line in Figure 5.5.

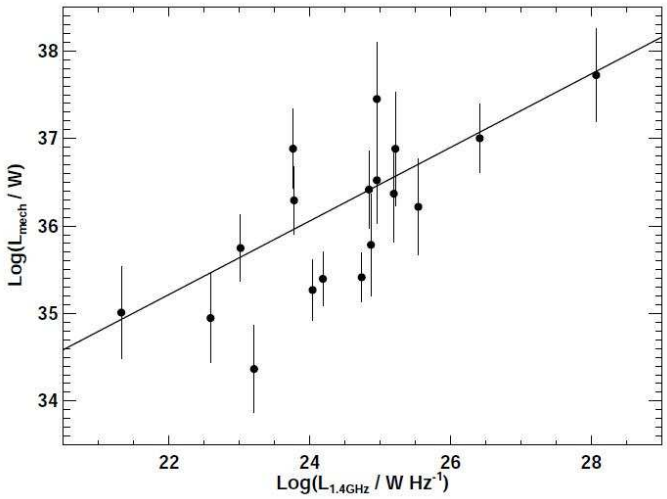


**Figure 5.5** • Mechanical luminosity vs radio monochromatic radio luminosity estimated by Bîrzan et al. [2004] from cavities and bubbles in clusters and groups of galaxies hosting radio sources. The solid line corresponds to the best-fit power-law expression derived by Best et al. [2006] and given by equation 5.1. While there is no single scaling factor between mechanical and radio luminosities, it provides a reasonable fit to the data over five decades in radio power.

## 5.5 The heating effect of Radio-loud AGN

We applied the method described above to our samples of RLAGN to derive the heating power as function of stellar mass by combining equation 5.1 with our estimates of the bivariate radio luminosity - mass function derived in chapter 3. This was done by integrating the curves in Figure 3.7 multiplied with the mechanical luminosities calculated from the corresponding radio luminosities.

The high-redshift RLAGNs selected from the MegaZ catalogue have radio powers starting at $\sim 10^{24.4}$ W Hz$^{-1}$, while low redshift radio AGNs extend much further down in luminosity, to $\sim 10^{22}$ W Hz$^{-1}$. As these faint sources are not present in the high-redshift sample, we integrate the radio luminosity distributions above $\sim 10^{24.4}$ W Hz$^{-1}$ in both cases. The resulting heating rate is shown in Figure 5.6. As expected, the time-averaged energy output of radio sources is larger for more massive systems, given that the fraction of radio sources in massive objects is comparatively high (around 20-30%). For high-redshift RLAGNs, the energy associated with radio source activity is a factor of $20-25$ larger in galaxies of $M_* \sim 10^{12}$ M$_\odot$ compared to systems of $M_* \sim 10^{11}$ M$_\odot$. At low redshifts, the RLAGN heating output is slightly smaller over the whole mass range, and the difference with high redshift sources is progressively larger in low mass galaxies. Again, this is consistent with the trends observed in the evolution of the fraction of RLAGN in Figures 3.5 and 3.7. If we integrate the heating rates over the stellar mass range, the total heating output at $z = 0.5$ is a factor of $\sim 2.5$ larger than at $z = 0.14$. Most of this extra heating power is provided by massive radio galaxies of $M_* \sim 10^{12}$ M$_\odot$.

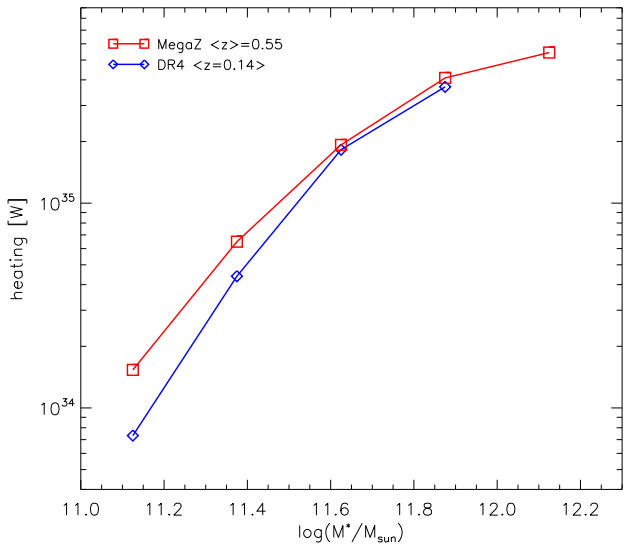


**Figure 5.6** • Time-averaged heating rate associated with radio-loud AGN activity as function of galaxy stellar mass, derived by combining the bivariate-radio luminosity mass function (Figure 3.7) with a conversion relation between radio power and mechanical luminosity (equation 5.1). The analysis is restricted to sources above $\sim 10^{24.4}$ W Hz$^{-1}$.

By using our occupation model for radio AGN we can translate the above heating relation from stellar mass to halo mass. We go through the same procedure applied to model RLAGNs at $z = 0.5$, but this time we do the integration directly in bins of halo mass. For RLAGN at $z = 0.1$ we use a similar procedure, but using the best-fitting model for RLAGN by Mandelbaum et al. 2009. The results are shown in Figure 5.7. At high redsfhit, the heating in haloes of $\sim 10^{15}$ M$_\odot$ h$^{-1}$ is factor of 6-7 larger than in $\sim 10^{12.8}$ M$_\odot$ h$^{-1}$ haloes, broadly consistent with the trend based on stellar mass. In addition, the total heating power at high redshift is also a factor of $\sim 2.5$ larger than at low redshift, indicating that for a fixed halo mass the net heating effect due to radio galaxies was substantially larger in the past in the past than at present.

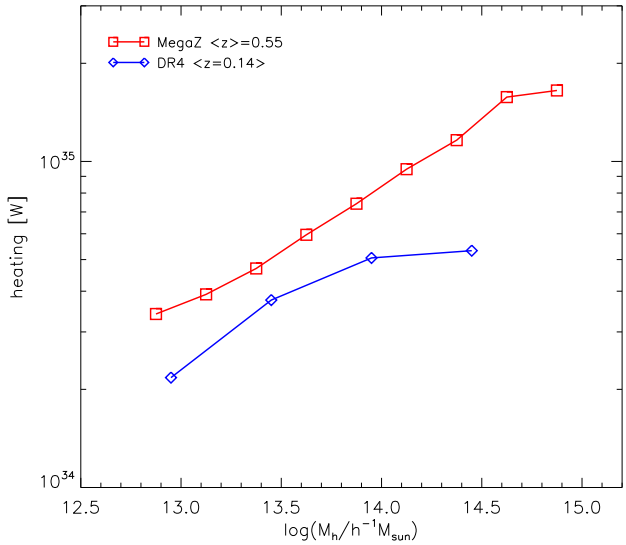


**Figure 5.7** • Time-averaged heating rate associated with radio-loud AGN activity as function of halo mass, for our best-fit occupation model of RLAGN at $z = 0.5$.

# 6

# Summary and Perspectives

We have constructed a catalogue of 14453 radio-loud AGN with 1.4 GHz fluxes above 3.5 mJy in the redshift range $0.4 < z < 0.8$, based on the cross-correlation of NVSS and FIRST radio source catalogs with the MegaZ-LRG catalogue of luminous red galaxies. The vast majority of the radio AGN are single component sources in both NVSS and FIRST. However, there is a significant fraction of objects without high S/N FIRST detections, which are required for accurate identification of the optical counterpart. We have introduced a method for analyzing the FIRST radio maps around the candidate positions of these sources. This allowed us to dig deeper into the FIRST survey and use lower S/N detections to pinpoint the location of the host galaxy.

We have presented a new determination of the luminosity function of radio-loud AGN at $z \sim 0.55$ that is in excellent agreement with other results in the literature, but with notably smaller error bars. By comparing our radio luminosity function at $z \sim 0.55$ to that derived for a large sample of nearby radio AGN from the SDSS DR4 we have quantified in detail the evolution of the radio galaxy population as well as its dependence on radio luminosity. The main result is that we find compelling evidence for strong cosmic evolution of radio sources. The comoving number density of radio AGN with luminosities less than $10^{25}$ W Hz$^{-1}$ increases by a factor of $\sim 1.5$ between $z = 0.14$ and $z = 0.55$. At higher luminosities, this factor increases sharply, reaching values $\sim 10$ at a radio luminosity of $10^{26}$W Hz$^{-1}$. We find that neither a pure luminosity evolution nor a pure density evolution scenario provides a good description of the data.

We have analyzed how the relation between radio AGN and their host galaxies evolves with redshift. The fraction of galaxies with radio luminosities above a given threshold is a steeply increasing function of stellar mass at both $z \sim 0.1$ and at $z \sim 0.55$. The fraction of radio loud AGN increases with redshift and this increase is largest at the highest radio luminosities and also for lower mass galaxies. We

have also calculated the bivariate radio luminosity-mass function at $z \sim 0.14$ and $z \sim 0.55$. Its shape does not appear to depend on mass at either redshift, but there is strong evolution in the shape at the *bright-end* of the function. The fraction of galaxies brighter than $10^{25}$ W hz$^{-1}$ declines with significantly shallower slope at higher redshifts. In other words, two main conclusions can be drawn from these analysis:

- There is a characteristic luminosity of $\sim 10^{25}$ W Hz$^{-1}$ below which the radio source population evolves very weakly with redshift. Above this characteristic luminosity, there is strong evolution, with the most powerful radio sources undergoing the largest increase in co-moving number density. These results are in broad agreement with past studies.
- The strongest evolution in the fraction of galaxies that host radio-loud AGN takes place in the lower mass galaxies in our sample.

The most plausible explanation for these different trends in evolution, is that there are two classes of radio galaxy, likely associated with the high excitation/low excitation "dichotomy") that have different fueling/triggering mechanisms. As discussed before, it has been suggested that low luminosity AGN are likely associated with massive ($\sim 10^{13}$ M$_\odot$) dark matter haloes that have quasistatic hot gas atmospheres. The abundance of such halos is predicted to remain approximately constant out to redshifts $\sim 1$, which is consistent with the weak evolution we see in this population. These "hot-halo" triggered sources at $z \sim 0.5$ would then produce radio emission that roughly compensates the radiative losses of the cooling gas.

The reason for the remarkably strong evolution in the comoving abundance of high-luminosity radio AGN is somewhat more difficult to understand. It is tempting to link this population with the strongly accreting population of luminous quasars, which are thought to be hosted in dark matter halos with masses of $\sim 10^{12} M_\odot$. However, only $\sim 10\%$ of optical quasars are radio-loud, and this raises the question as to whether there is simply a short radio-loud phase during the lifetime of every optical quasar, or whether optically luminous AGN and powerful radio galaxies are triggered by different mechanisms. If, as in quasars, these sources are not regulated by cooling from a surrounding hot gaseous halo, but by other mechanisms like interactions/mergers, then we would not expect to find them in an equilibrium state like in low excitation AGNs.

To shed further light on these matters we have analyzed the clustering properties of luminous radio galaxies and radio quasars present in our samples. To do this, we have successfully applied cross-correlation techniques to characterize the environments of radio-loud AGN with $P_{1.4GHz} > 10^{24.4}$ W Hz$^{-1}$. We have also compared the clustering of RLAGN with that of radio-loud quasars. By using control samples of radio-quiet objects matched in redshift, stellar mass and optical luminosity (or radio luminosity/black hole mass, when appropriate) we have isolated the effect such

parameters have in influencing the clustering signal. The main results regarding our clustering analysis can be summarized as follows:

- Radio AGN at $0.4 < z < 0.8$ are substantially more clustered compared to their parent luminous red galaxy population, and also compared to radio-quiet galaxies of the same stellar mass and redshift. The clustering differences are largest on scales less than 1 Mpc $h^{-1}$.
- Radio-loud AGN hosted by more massive galaxies are more strongly clustered than those hosted by less massive galaxies. However, the difference in clustering between RLAGN and control samples is most pronounced for low mass RLAGN.
- We have studied the dependence of the clustering amplitude on the luminosity of the radio source. For $r_p > 1$ Mpc $h^{-1}$ there is a weak, but significant anti-correlation with radio power. For $r_p < 1$ Mpc $h^{-1}$ the dependence of clustering amplitude on luminosity is more complex: the cross-correlation amplitude increases with luminosity up to $\sim 10^{25.3}$ W Hz$^{-1}$, and then decreases for the most luminous radio sources in our sample.
- We have compared the environments of radio-loud AGN and radio-loud QSOs. RLAGN are clustered more strongly than RLQSOs on all scales, indicate that they populate dark matter halos of different mass. These results hold even when the RLAGN and RLQSO samples are matched in radio luminosity and black hole mass.
- There are indications that the very most luminous RLAGN and RLQSOs in our sample (P$> 10^{26}$ W Hz$^{-1}$) do have similar clustering amplitudes. Only at these very high radio powers are the space-densities of radio-loud quasars and radio galaxies similar. This implies that unification of the two AGN populations can only be valid above P$\sim 10^{26}$ W Hz$^{-1}$.

The most definitive result to emerge from our analysis is clear proof that the environment of a galaxy on the scale of the dark matter halo in which it resides, does play a key role in determining not only the probability that a galaxy a is radio-loud AGN, but also the total luminosity of the radio jet. We have also demonstrated that strong evolution of the radio AGN population occurs above a characteristic radio luminosity of $\sim 10^{25}$ W Hz$^{-1}$. It is very intriguing that this luminosity marks the break point in clustering trends, and that the radio luminosity where a denser environment ceases to have a boosting influence also is of order $10^{25}$ W Hz$^{-1}$.

By using a cosmological N-body simulations coupled with semianalytic models of galaxy formation that incorporate the feedback effect from radio AGN, we have successfully applied a simple prescription (HOD) to populate dark matter haloes with powerful radio-loud AGNs at $z = 0.5$. The best-fitting model can reproduce the observed mass function and clustering of radio AGN, as well of their parent

LRG population. With just a small change to the fraction of RLAGN hosted by central galaxies, we have shown that the basic parameters of this simple model can account for observations at both, low and high redshift.

Finally, combining the model information with the bivariate radio luminosity-mass functions derived before, we have estimate the total heating effect that radio sources have in haloes of different mass, in hosts of different stellar mass, and as function of cosmic epoch between $z = 0$ and $z = 0.5$. As suggested by the strong evolution of luminous radio sources above $\sim 10^{25}$ W Hz$^{-1}$ and by the strong clustering of this population, the net heating rate due to radio AGNs in groups and clusters of galaxies is factor of $\sim 2.5$ larger at $z = 0.5$ than at the present epoch.

One limitation of this work with regard to constraining AGN unification scenarios, is that it is based purely on photometric data from the SDSS, so we are unable to split our RLAGN sample into high-excitation and low-excitation sources. It is quite possible that the presence or absence of emission lines will provide the best way to define a population of radio galaxies that are clearly unified with the quasars. In this case, we would expect to find that the high-excitation radio galaxy population would cluster in a similar way to the quasars.

Fortunately, upcoming large spectroscopic surveys such as BOSS will target nearly complete samples of more than a million massive galaxies at $0.4 < z < 0.8$ and will provide optical spectra for tens of thousands of radio galaxies. We will then be able to quantify the fraction of RLAGN of given radio luminosity that have emission lines and how the clustering depends on emission line strength.

It is worth to mention that the new generation of instruments currently under construction, will generate large radio and optical surveys with dramatic improvements in size and sensibility. The LOFAR (Low Frequency Array) is an interferometric array of 5000 radio antennas distributed across the Netherlands and other European countries. It will map the northern sky with unprecedented sensitivity at the mostly unexplored frequency range of 16-240 MHz. Once completed, LOFAR will be able to detect hundreds of thousands of of radio AGN up to $z \sim 1$ and hundreds of the most powerful sources at $z \sim 7$. Pan-STARRS (Panoramic Survey Telescope And Rapid Response System) is a new optical instrument that will conduct multi-band photometry of the entire sky in a continuous basis. It will produce large catalogs of optical counterparts for radio sources as deep as $m_R = 27.5$. Toegether, these radio and optical surveys will dramatically improve existing samples, allowing us to study the evolution of the radio galaxy population in great detail.

# Acknowledgments

This work is not only dedicated, but also the product of the joint, sometimes indirect efforts of many people, that have contributed in unimaginable ways.

First, I would like to thank my wife Silvana for standing at my side and for giving me a vital dose of hope when I most needed. I have reached this point not only thanks to her, but also *because* of her. She is my reason to go on.

I would also like to thank Guinevere and Simon for guiding my firsts humble steps in researching the cosmos. I shall never forget their advises, their teaching lessons, discussions, and their tremendous ability to stimulate and grow new ideas. Guinevere, these were rich times that I enjoyed very much, and for that I will be forever grateful. My special gratitude to Philip Best from whom I learned the magic of the radio universe. As a renowed argentine writer said once *"let others be proud of the pages they have written. I am proud of the pages I have read"*.

I also want to thank the students and postdocs with whom I had stimulating scientific discussions. There is a permanent road between Cheng's desk and my place here on top of MPA reception. Thank you very much Cheng. I want to thank Francesco Shankar, Roderick Overzier, Vivienne Wild, Anja von der Linden and Dimitri Gadotti.

My gratitude to all of you.

# Curriculum Vitae

## Personal Information

| | |
|---|---|
| First & Last Name: | **Emilio Donoso** |
| Date of birth: | 14$^{\text{th}}$ July, 1977 |
| Place of birth: | San Juan, Argentina |
| Citizenship: | Argentinean |

## Contact Information


| | |
|---|---|
| Address 1: | *Max-Planck-Institut für Astrophysik* |
| | Karl-Schwarzschild-Straße, 1 |
| | D-85748 Garching b. München - Germany |
| Address 2: | *California Institute of Technology* |
| | 1200 East California Boulevard |
| | Pasadena, 91125, United States of America |
| E-mail: | edonoso@mpa-garching.mpg.de |
| | emiliodon@gmail.com |


## Education

09.2006-today **PhD in Astrophysics**

*Max-Planck-Institut für Astrophysik*

To the moment, I am completing my PhD degree in astrophysics. I work for the Cosmology Group, studying the properties and evolution of radio galaxies across cosmic time. Expected graduation: Feb. 2010.

03.1999-08.2006 **Licenciatura in Astronomy (B.Sc. + M.Sc. equivalent)**

*Universidad Nacional de San Juan, Argentina*

My thesis was an statistical study of the alignments between luminous red galaxies and the surrounding large scale structure of the universe. Graduated with best score (9.1/10).

03.1996-12.1998 **Undergraduate studies in Computer Science**

*Universidad Nacional de Buenos Aires, Argentina*

03.1991-12.1995 **Secondary School**

*Colegio Central Universitario, Argentina*

## Academic Positions

04.2003-07.2006 **Research Assistant in Solar Physics**

*Observatorio Astronómico Félix Aguilar, Argentina*

Developement of software for the automated detection of structures in the solar surface (i.e. sunspots, filaments, prominences).

04.2005-07.2006 **Teaching Assistant in Analytic Geometry**

*Universidad Nacional de San Juan, Argentina*

## Refereed Publications

**Donoso E.**, Li Cheng, Best P.N.B., Kauffmann G., Heckman T.

Clustering of Radio Galaxies and Quasars

Monthly Not. of the Royal Astr. Society, 2009, submitted

**Donoso E.**, Best P.N.B., Kauffmann G.

Evolution of the Radio Loud Galaxy Population

Monthly Not. of the Royal Astr. Society, Volume 392, Issue 2, pp.617-629, 2009

**Donoso E.**, O'Mill A., Lambas D.G.

Alignment between luminous red galaxies and surrounding structures at $z \sim 0.5$

Monthly Not. of the Royal Astr. Society, Volume 369, Issue 1, pp.479-484, 2006

## Non-refereed Publications

**Donoso E.**, Ghivarelli S.

Solar Submillimetric Observations

Monograph, 2nd School of Solar Physics, Argentina, 2001

## Additional Courses/Schools

06.08.2007-10.08.2007 **Summer School on Multiwavelength Analysis of Galaxy Populations (MAGPOP)**

Seeon Castel, Bavaria, Germany.

06.12.2004-10.12.2004 **2nd Chilean School of Advanced Astrophysics**

Pontificia Universidad Católica de Chile, Santiago, Chile

28.07.2003-01.08.2003 **5$^{\text{th}}$ J.J. Giambiagi Winter School on Precision Cosmology**

Universidad de Buenos Aires, Argentina

15.06.2003-11.07.2003 **9$^{\text{th}}$ Vatican Observatory School on Galaxy Evolution (VOSS)**

Vatican Observatory, Rome, Italy

12.08.2002-30.08.2002 **26$^{\text{th}}$ International School for Young Astronomers, IAU-UNESCO**

El Leoncito, Argentina

14.10.2001-22.10.2001 **2$^{\text{nd}}$ School of Solar Physics**

Max-Planck Institut für Aeronomie, Max-Planck Institut für Extraterrestrische Physik, Instituto de Astronomía y Física del Espacio. El Leoncito, Argentina

# Bibliography


R. Antonucci. Unified models for active galactic nuclei and quasars. *ARA&A*, 31:473–521, 1993. doi: 10.1146/annurev.aa.31.090193.002353.

C. Auriemma, G. C. Perola, R. D. Ekers, R. Fanti, C. Lari, W. J. Jaffe, and M. H. Ulrich. A Determination of the Local Radio Luminosity Function of Elliptical Galaxies. *A&A*, 57:41–+, May 1977.

I. K. Baldry, K. Glazebrook, J. Brinkmann, Ž. Ivezić, R. H. Lupton, R. C. Nichol, and A. S. Szalay. Quantifying the Bimodal Color-Magnitude Distribution of Galaxies. *ApJ*, 600:681–694, Jan. 2004. doi: 10.1086/380092.

J. A. Baldwin, M. M. Phillips, and R. Terlevich. Classification parameters for the emission-line spectra of extragalactic objects. *Publ. Astr. Soc. Pac.*, 93:5–19, Feb. 1981. doi: 10.1086/130766.

J. M. Barr, M. N. Bremer, J. C. Baker, and M. D. Lehnert. The cluster environments of radio-loud quasars at 0.6 ¡ z ¡ 1.1. *MNRAS*, 346:229–250, Nov. 2003. doi: 10.1046/j.1365-2966.2003.07089.x.

P. D. Barthel. Is every quasar beamed? *ApJ*, 336:606–611, Jan. 1989. doi: 10.1086/167038.

P. D. Barthel and K. A. Arnaud. Anomalous radio-loudness of Cygnus A and other powerful radio galaxies. *MNRAS*, 283:L45–L49, Nov. 1996.

S. A. Baum, E. L. Zirbel, and C. P. O'Dea. Toward Understanding the Fanaroff-Riley Dichotomy in Radio Source Morphology and Power. *ApJ*, 451:88–+, Sept. 1995. doi: 10.1086/176202.

R. H. Becker, R. L. White, and D. J. Helfand. The FIRST Survey: Faint Images of the Radio Sky at Twenty Centimeters. *ApJ*, 450:559–+, Sept. 1995. doi: 10.1086/176166.

E. F. Bell and R. S. de Jong. Stellar Mass-to-Light Ratios and the Tully-Fisher Relation. *ApJ*, 550: 212–229, Mar. 2001. doi: 10.1086/319728.

E. F. Bell, D. H. McIntosh, N. Katz, and M. D. Weinberg. The Optical and Near-Infrared Properties of Galaxies. I. Luminosity and Stellar Mass Functions. *ApJS*, 149:289–312, Dec. 2003. doi: 10.1086/378847.

A. J. Benson, R. G. Bower, C. S. Frenk, C. G. Lacey, C. M. Baugh, and S. Cole. What Shapes the Luminosity Function of Galaxies? *ApJ*, 599:38–49, Dec. 2003. doi: 10.1086/379160.

P. N. Best. The environmental dependence of radio-loud AGN activity and star formation in the 2dFGRS. *MNRAS*, 351:70–82, June 2004. doi: 10.1111/j.1365-2966.2004.07752.x.

P. N. Best, G. Kauffmann, T. M. Heckman, J. Brinchmann, S. Charlot, Ž. Ivezić, and S. D. M. White. The host galaxies of radio-loud active galactic nuclei: mass dependences, gas cooling and active galactic nuclei feedback. *MNRAS*, 362:25–40, Sept. 2005a. doi: 10.1111/j.1365-2966.2005.09192.x.

P. N. Best, G. Kauffmann, T. M. Heckman, and Ž. Ivezić. A sample of radio-loud active galactic nuclei in the Sloan Digital Sky Survey. *MNRAS*, 362:9–24, Sept. 2005b. doi: 10.1111/j.1365-2966.2005.09283.x.

P. N. Best, C. R. Kaiser, T. M. Heckman, and G. Kauffmann. AGN-controlled cooling in elliptical galaxies. *MNRAS*, 368:L67–L71, May 2006. doi: 10.1111/j.1745-3933.2006.00159.x.

P. N. Best, A. von der Linden, G. Kauffmann, T. M. Heckman, and C. R. Kaiser. On the prevalence of radio-loud active galactic nuclei in brightest cluster galaxies: implications for AGN heating of cooling flows. *MNRAS*, 379:894–908, Aug. 2007. doi: 10.1111/j.1365-2966.2007.11937.x.

G. V. Bicknell. Relativistic Jets and the Fanaroff-Riley Classification of Radio Galaxies. *ApJS*, 101:29–+, Nov. 1995. doi: 10.1086/192232.

L. Bîrzan, D. A. Rafferty, B. R. McNamara, M. W. Wise, and P. E. J. Nulsen. A Systematic Study of Radio-induced X-Ray Cavities in Clusters, Groups, and Galaxies. *ApJ*, 607:800–809, June 2004. doi: 10.1086/383519.

R. D. Blandford and M. J. Rees. Extended and compact extragalactic radio sources - Interpretation and theory. *Physica Scripta*, 17:265–274, Mar. 1978. doi: 10.1088/0031-8949/17/3/020.

M. R. Blanton and S. Roweis. K-Corrections and Filter Transformations in the Ultraviolet, Optical, and Near-Infrared. *AJ*, 133:734–754, Feb. 2007. doi: 10.1086/510127.

H. Boehringer, W. Voges, A. C. Fabian, A. C. Edge, and D. M. Neumann. A ROSAT HRI study of the interaction of the X-ray-emitting gas and radio lobes of NGC 1275. *MNRAS*, 264:L25–L28, Oct. 1993.

T. A. Boroson. Black Hole Mass and Eddington Ratio as Drivers for the Observable Properties of Radio-loud and Radio-quiet QSOs. *ApJ*, 565:78–85, Jan. 2002. doi: 10.1086/324486.

R. G. Bower, A. J. Benson, R. Malbon, J. C. Helly, C. S. Frenk, C. M. Baugh, S. Cole, and C. G. Lacey. Breaking the hierarchy of galaxy formation. *MNRAS*, 370:645–655, Aug. 2006. doi: 10.1111/j.1365-2966.2006.10519.x.

A. H. Bridle and R. A. Perley. Extragalactic Radio Jets. *ARA&A*, 22:319–358, 1984. doi: 10.1146/annurev.aa.22.090184.001535.

A. H. Bridle, D. H. Hough, C. J. Lonsdale, J. O. Burns, and R. A. Laing. Deep VLA imaging of twelve extended 3CR quasars. *AJ*, 108:766–820, Sept. 1994. doi: 10.1086/117112.

M. J. I. Brown, R. L. Webster, and B. J. Boyle. The Evolution of Radio Galaxies at Intermediate Redshift. *AJ*, 121:2381–2391, May 2001. doi: 10.1086/320410.

M. J. I. Brown, A. Dey, B. T. Jannuzi, K. Brand, A. J. Benson, M. Brodwin, D. J. Croton, and P. R. Eisenhardt. The Evolving Luminosity Function of Red Galaxies. *ApJ*, 654:858–877, Jan. 2007. doi: 10.1086/509652.

I. W. A. Browne. Is it possible to turn an elliptical radio galaxy into a BL Lac object? *MNRAS*, 204:23P–27P, July 1983.

G. Bruzual and S. Charlot. Stellar population synthesis at the resolution of 2003. *MNRAS*, 344:1000–1028, Oct. 2003. doi: 10.1046/j.1365-8711.2003.06897.x.

T. Budavári, L. Dobos, A. S. Szalay, G. Greene, J. Gray, and A. H. Rots. Footprint Services for Everyone. In R. A. Shaw, F. Hill, and D. J. Bell, editors, *Astronomical Data Analysis Software and Systems XVI*, volume 376 of *Astronomical Society of the Pacific Conference Series*, pages 559–+, Oct. 2007.

R. Cannon, M. Drinkwater, A. Edge, D. Eisenstein, R. Nichol, P. Outram, K. Pimbblet, R. de Propris, I. Roseboom, D. Wake, P. Allen, J. Bland-Hawthorn, T. Bridges, D. Carson, K. Chiu, M. Colless, W. Couch, S. Croom, S. Driver, S. Fine, P. Hewett, J. Loveday, N. Ross, E. M. Sadler, T. Shanks, R. Sharp, J. A. Smith, C. Stoughton, P. Weilbacher, R. J. Brunner, A. Meiksin, and D. P. Schneider. The 2dF-SDSS LRG and QSO (2SLAQ) Luminous Red Galaxy Survey. *MNRAS*, 372:425–442, Oct. 2006. doi: 10.1111/j.1365-2966.2006.10875.x.

L. Clewley and M. J. Jarvis. The cosmic evolution of low-luminosity radio sources from the Sloan Digital Sky Survey Data Release 1. *MNRAS*, 352:909–914, Aug. 2004. doi: 10.1111/j.1365-2966.2004.07981.x.

A. L. Coil, J. F. Hennawi, J. A. Newman, M. C. Cooper, and M. Davis. The DEEP2 Galaxy Redshift Survey: Clustering of Quasars and Galaxies at z = 1. *ApJ*, 654:115–124, Jan. 2007. doi: 10.1086/509099.

S. Cole, C. G. Lacey, C. M. Baugh, and C. S. Frenk. Hierarchical galaxy formation. *MNRAS*, 319: 168–204, Nov. 2000. doi: 10.1046/j.1365-8711.2000.03879.x.

S. Cole, W. J. Percival, J. A. Peacock, P. Norberg, C. M. Baugh, C. S. Frenk, I. Baldry, J. Bland-Hawthorn, T. Bridges, R. Cannon, M. Colless, C. Collins, W. Couch, N. J. G. Cross, G. Dalton, V. R. Eke, R. De Propris, S. P. Driver, G. Efstathiou, R. S. Ellis, K. Glazebrook, C. Jackson, A. Jenkins, O. Lahav, I. Lewis, S. Lumsden, S. Maddox, D. Madgwick, B. A. Peterson, W. Sutherland, and K. Taylor. The 2dF Galaxy Redshift Survey: power-spectrum analysis of the final data set and cosmological implications. *MNRAS*, 362:505–534, Sept. 2005. doi: 10.1111/j.1365-2966.2005.09318.x.

M. Colless, G. Dalton, S. Maddox, W. Sutherland, P. Norberg, S. Cole, J. Bland-Hawthorn, T. Bridges, R. Cannon, C. Collins, W. Couch, N. Cross, K. Deeley, R. De Propris, S. P. Driver, G. Efstathiou, R. S. Ellis, C. S. Frenk, K. Glazebrook, C. Jackson, O. Lahav, I. Lewis, S. Lumsden, D. Madgwick, J. A. Peacock, B. A. Peterson, I. Price, M. Seaborne, and K. Taylor. The 2dF Galaxy Redshift Survey: spectra and redshifts. *MNRAS*, 328:1039–1063, Dec. 2001. doi: 10.1046/j.1365-8711.2001.04902.x.

A. Collister, O. Lahav, C. Blake, R. Cannon, S. Croom, M. Drinkwater, A. Edge, D. Eisenstein, J. Loveday, R. Nichol, K. Pimbblet, R. de Propris, I. Roseboom, N. Ross, D. P. Schneider, T. Shanks, and D. Wake. MegaZ-LRG: a photometric redshift catalogue of one million SDSS luminous red galaxies. *MNRAS*, 375:68–76, Feb. 2007. doi: 10.1111/j.1365-2966.2006.11305.x.

A. A. Collister and O. Lahav. ANNz: Estimating Photometric Redshifts Using Artificial Neural Networks. *Publ. Astr. Soc. Pac.*, 116:345–351, Apr. 2004. doi: 10.1086/383254.

J. J. Condon. Radio emission from normal galaxies. *ARA&A*, 30:575–611, 1992. doi: 10.1146/annurev.aa.30.090192.003043.

J. J. Condon, W. D. Cotton, E. W. Greisen, Q. F. Yin, R. A. Perley, G. B. Taylor, and J. J. Broderick. The NRAO VLA Sky Survey. *AJ*, 115:1693–1716, May 1998. doi: 10.1086/300337.

J. J. Condon, W. D. Cotton, and J. J. Broderick. Radio Sources and Star Formation in the Local Universe. *AJ*, 124:675–689, Aug. 2002. doi: 10.1086/341650.

R. J. Cool, D. J. Eisenstein, X. Fan, M. Fukugita, L. Jiang, C. Maraston, A. Meiksin, D. P. Schneider, and D. A. Wake. Luminosity Function Constraints on the Evolution of Massive Red Galaxies since z ˜ 0.9. *ApJ*, 682:919–936, Aug. 2008. doi: 10.1086/589642.

S. M. Croom, B. J. Boyle, T. Shanks, R. J. Smith, L. Miller, P. J. Outram, N. S. Loaring, F. Hoyle, and J. da Ângela. The 2dF QSO Redshift Survey - XIV. Structure and evolution from the two-point correlation function. *MNRAS*, 356:415–438, Jan. 2005. doi: 10.1111/j.1365-2966.2004.08379.x.

D. J. Croton, V. Springel, S. D. M. White, G. De Lucia, C. S. Frenk, L. Gao, A. Jenkins, G. Kauffmann, J. F. Navarro, and N. Yoshida. The many lives of active galactic nuclei: cooling flows, black holes and the luminosities and colours of galaxies. *MNRAS*, 365:11–28, Jan. 2006. doi: 10.1111/j.1365-2966.2005.09675.x.

M. Davis and P. J. E. Peebles. A survey of galaxy redshifts. V - The two-point position and velocity correlations. *ApJ*, 267:465–482, Apr. 1983. doi: 10.1086/160884.

G. De Lucia and J. Blaizot. The hierarchical formation of the brightest cluster galaxies. *MNRAS*, 375:2–14, Feb. 2007. doi: 10.1111/j.1365-2966.2006.11287.x.

D. S. De Young. On the relation between Fanaroff-Riley types I and II radio galaxies. *ApJL*, 405:L13–L16, Mar. 1993. doi: 10.1086/186754.

A. Dekel and J. Silk. The origin of dwarf galaxies, cold dark matter, and biased galaxy formation. *ApJ*, 303:39–55, Apr. 1986. doi: 10.1086/164050.

E. Donoso, P. N. Best, and G. Kauffmann. Evolution of the radio-loud galaxy population. *MNRAS*, 392:617–629, Jan. 2009. doi: 10.1111/j.1365-2966.2008.14068.x.

J. S. Dunlop and J. A. Peacock. The Redshift Cut-Off in the Luminosity Function of Radio Galaxies and Quasars. *MNRAS*, 247:19–+, Nov. 1990.

G. Efstathiou. Suppressing the formation of dwarf galaxies via photoionization. *MNRAS*, 256:43P–47P, May 1992.

D. J. Eisenstein, J. Annis, J. E. Gunn, A. S. Szalay, A. J. Connolly, R. C. Nichol, N. A. Bahcall, M. Bernardi, S. Burles, F. J. Castander, M. Fukugita, D. W. Hogg, Ž. Ivezić, G. R. Knapp, R. H. Lupton, V. Narayanan, M. Postman, D. E. Reichart, M. Richmond, D. P. Schneider, D. J. Schlegel, M. A. Strauss, M. SubbaRao, D. L. Tucker, D. Vanden Berk, M. S. Vogeley, D. H. Weinberg, and B. Yanny. Spectroscopic Target Selection for the Sloan Digital Sky Survey: The Luminous Red Galaxy Sample. *AJ*, 122:2267–2280, Nov. 2001. doi: 10.1086/323717.

A. C. Fabian, J. S. Sanders, S. W. Allen, C. S. Crawford, K. Iwasawa, R. M. Johnstone, R. W. Schmidt, and G. B. Taylor. A deep Chandra observation of the Perseus cluster: shocks and ripples. *MNRAS*, 344:L43–L47, Sept. 2003. doi: 10.1046/j.1365-8711.2003.06902.x.

B. L. Fanaroff and J. M. Riley. The morphology of extragalactic radio sources of high and low luminosity. *MNRAS*, 167:31P–36P, May 1974.

L. Ferrarese and D. Merritt. A Fundamental Relation between Supermassive Black Holes and Their Host Galaxies. *ApJL*, 539:L9–L12, Aug. 2000. doi: 10.1086/312838.

A. Franceschini, S. Vercellone, and A. C. Fabian. Supermassive Black Holes in Early-Type Galaxies: Relationship with Radio Emission and Constraints on the Black Hole Mass Function. *MNRAS*, 297:817–824, July 1998. doi: 10.1046/j.1365-8711.1998.01534.x.

J. A. Frieman, B. Bassett, A. Becker, C. Choi, D. Cinabro, F. DeJongh, D. L. Depoy, B. Dilday, M. Doi, P. M. Garnavich, C. J. Hogan, J. Holtzman, M. Im, S. Jha, R. Kessler, K. Konishi, H. Lampeitl, J. Marriner, J. L. Marshall, D. McGinnis, G. Miknaitis, R. C. Nichol, J. L. Prieto, A. G. Riess, M. W. Richmond, R. Romani, M. Sako, D. P. Schneider, M. Smith, N. Takanashi, K. Tokita, K. van der Heyden, N. Yasuda, C. Zheng, J. Adelman-McCarthy, J. Annis, R. J. Assef, J. Barentine, R. Bender, R. D. Blandford, W. N. Boroski, M. Bremer, H. Brewington, C. A. Collins, A. Crotts, J. Dembicky, J. Eastman, A. Edge, E. Edmondson, E. Elson, M. E. Eyler, A. V. Filippenko, R. J. Foley, S. Frank, A. Goobar, T. Gueth, J. E. Gunn, M. Harvanek, U. Hopp, Y. Ihara, Ž. Ivezić, S. Kahn, J. Kaplan, S. Kent, W. Ketzeback, S. J. Kleinman, W. Kollatschny, R. G. Kron, J. Krzesiński, D. Lamenti, G. Leloudas, H. Lin, D. C. Long, J. Lucey, R. H. Lupton, E. Malanushenko, V. Malanushenko, R. J. McMillan, J. Mendez, C. W. Morgan, T. Morokuma, A. Nitta, L. Ostman, K. Pan, C. M. Rockosi, A. K. Romer, P. Ruiz-Lapuente, G. Saurage, K. Schlesinger, S. A. Snedden, J. Sollerman, C. Stoughton, M. Stritzinger, M. Subba Rao, D. Tucker, P. Vaisanen, L. C. Watson, S. Watters, J. C. Wheeler, B. Yanny, and D. York. The Sloan Digital Sky Survey-II Supernova Survey: Technical Summary. *AJ*, 135: 338–347, Jan. 2008. doi: 10.1088/0004-6256/135/1/338.

M. Fukugita, T. Ichikawa, J. E. Gunn, M. Doi, K. Shimasaku, and D. P. Schneider. The Sloan Digital Sky Survey Photometric System. *AJ*, 111:1748–+, Apr. 1996. doi: 10.1086/117915.

K. Gebhardt, R. Bender, G. Bower, A. Dressler, S. M. Faber, A. V. Filippenko, R. Green, C. Grillmair, L. C. Ho, J. Kormendy, T. R. Lauer, J. Magorrian, J. Pinkney, D. Richstone, and S. Tremaine. A Relationship between Nuclear Black Hole Mass and Galaxy Velocity Dispersion. *ApJL*, 539:L13–L16, Aug. 2000. doi: 10.1086/312840.

R. Genzel, A. Eckart, T. Ott, and F. Eisenhauer. On the nature of the dark mass in the centre of the Milky Way. *MNRAS*, 291:219–234, Oct. 1997.

J. E. Gunn, M. Carr, C. Rockosi, M. Sekiguchi, K. Berry, B. Elms, E. de Haas, Ž. Ivezić, G. Knapp, R. Lupton, G. Pauls, R. Simcoe, R. Hirsch, D. Sanford, S. Wang, D. York, F. Harris, J. Annis, L. Bartozek, W. Boroski, J. Bakken, M. Haldeman, S. Kent, S. Holm, D. Holmgren, D. Petravick, A. Prosapio, R. Rechenmacher, M. Doi, M. Fukugita, K. Shimasaku, N. Okada, C. Hull, W. Siegmund, E. Mannery, M. Blouke, D. Heidtman, D. Schneider, R. Lucinio, and J. Brinkman. The Sloan Digital Sky Survey Photometric Camera. *AJ*, 116:3040–3081, Dec. 1998. doi: 10.1086/300645.

A. J. S. Hamilton. Toward Better Ways to Measure the Galaxy Correlation Function. *ApJ*, 417: 19–+, Nov. 1993. doi: 10.1086/173288.

M. J. Hardcastle. Bgg revisited: The environments of low-excitation radio galaxies and unified models. *A&A*, 414:927–929, Feb. 2004. doi: 10.1051/0004-6361:20035605.

M. J. Hardcastle, D. A. Evans, and J. H. Croston. The X-ray nuclei of intermediate-redshift radio sources. *MNRAS*, 370:1893–1904, Aug. 2006. doi: 10.1111/j.1365-2966.2006.10615.x.

M. J. Hardcastle, D. A. Evans, and J. H. Croston. Hot and cold gas accretion and feedback in radio-loud active galaxies. *MNRAS*, 376:1849–1856, Apr. 2007. doi: 10.1111/j.1365-2966.2007.11572.x.

N. Häring and H.-W. Rix. On the Black Hole Mass-Bulge Mass Relation. *ApJL*, 604:L89–L92, Apr. 2004. doi: 10.1086/383567.

T. M. Heckman, G. Kauffmann, J. Brinchmann, S. Charlot, C. Tremonti, and S. D. M. White. Present-Day Growth of Black Holes and Bulges: The Sloan Digital Sky Survey Perspective. *ApJ*, 613:109–118, Sept. 2004. doi: 10.1086/422872.

I. Heywood, K. M. Blundell, and S. Rawlings. The prevalence of Fanaroff-Riley type I radio quasars. *MNRAS*, 381:1093–1102, Nov. 2007. doi: 10.1111/j.1365-2966.2007.12278.x.

R. C. Hickox, C. Jones, W. R. Forman, S. S. Murray, C. S. Kochanek, D. Eisenstein, B. T. Jannuzi, A. Dey, M. J. I. Brown, D. Stern, P. R. Eisenhardt, V. Gorjian, M. Brodwin, R. Narayan, R. J. Cool, A. Kenter, N. Caldwell, and M. E. Anderson. Host Galaxies, Clustering, Eddington Ratios, and Evolution of Radio, X-Ray, and Infrared-Selected AGNs. *ApJ*, 696:891–919, May 2009. doi: 10.1088/0004-637X/696/1/891.

G. J. Hill and S. J. Lilly. A change in the cluster environments of radio galaxies with cosmic epoch. *ApJ*, 367:1–18, Jan. 1991. doi: 10.1086/169597.

R. G. Hine and M. S. Longair. Optical spectra of 3CR radio galaxies. *MNRAS*, 188:111–130, July 1979.

L. C. Ho. On the Relationship between Radio Emission and Black Hole Mass in Galactic Nuclei. *ApJ*, 564:120–132, Jan. 2002. doi: 10.1086/324399.

Ž. Ivezić, R. H. Lupton, M. Jurić, S. Tabachnik, T. Quinn, J. E. Gunn, G. R. Knapp, C. M. Rockosi, and J. Brinkmann. Color Confirmation of Asteroid Families. *AJ*, 124:2943–2948, Nov. 2002. doi: 10.1086/344077.

C. A. Jackson and J. V. Wall. Extragalactic radio-source evolution under the dual-population unification scheme. *MNRAS*, 304:160–174, Mar. 1999. doi: 10.1046/j.1365-8711.1999.02310.x.

M. J. Jarvis, S. Rawlings, S. Eales, K. M. Blundell, A. J. Bunker, S. Croft, R. J. McLure, and C. J. Willott. A sample of 6C radio sources designed to find objects at redshift z¿4 - III. Imaging and the radio galaxy K-z relation. *MNRAS*, 326:1585–1600, Oct. 2001. doi: 10.1111/j.1365-2966.2001.04730.x.

C. R. Kaiser, J. Dennett-Thorpe, and P. Alexander. Evolutionary tracks of FRII sources through the P-D diagram. *MNRAS*, 292:723–+, Dec. 1997.

G. Kauffmann, J. M. Colberg, A. Diaferio, and S. D. M. White. Clustering of galaxies in a hierarchical universe - I. Methods and results at z=0. *MNRAS*, 303:188–206, Feb. 1999. doi: 10.1046/j.1365-8711.1999.02202.x.

G. Kauffmann, T. M. Heckman, C. Tremonti, J. Brinchmann, S. Charlot, S. D. M. White, S. E. Ridgway, J. Brinkmann, M. Fukugita, P. B. Hall, Ž. Ivezić, G. T. Richards, and D. P. Schneider. The host galaxies of active galactic nuclei. *MNRAS*, 346:1055–1077, Dec. 2003a. doi: 10.1111/j.1365-2966.2003.07154.x.

G. Kauffmann, T. M. Heckman, S. D. M. White, S. Charlot, C. Tremonti, J. Brinchmann, G. Bruzual, E. W. Peng, M. Seibert, M. Bernardi, M. Blanton, J. Brinkmann, F. Castander, I. Csábai, M. Fukugita, Z. Ivezic, J. A. Munn, R. C. Nichol, N. Padmanabhan, A. R. Thakar, D. H. Weinberg, and D. York. Stellar masses and star formation histories for $10^5$ galaxies from the Sloan Digital Sky Survey. *MNRAS*, 341:33–53, May 2003b. doi: 10.1046/j.1365-8711.2003.06291.x.

G. Kauffmann, T. M. Heckman, and P. N. Best. Radio jets in galaxies with actively accreting black holes: new insights from the SDSS. *MNRAS*, 384:953–971, Mar. 2008. doi: 10.1111/j.1365-2966.2007.12752.x.

K. I. Kellermann, R. Sramek, M. Schmidt, D. B. Shaffer, and R. Green. VLA observations of objects in the Palomar Bright Quasar Survey. *AJ*, 98:1195–1207, Oct. 1989. doi: 10.1086/115207.

M. J. Kukula, J. S. Dunlop, D. H. Hughes, and S. Rawlings. The radio properties of radio-quiet quasars. *MNRAS*, 297:366–382, June 1998. doi: 10.1046/j.1365-8711.1998.01481.x.

M. Lacy, S. A. Laurent-Muehleisen, S. E. Ridgway, R. H. Becker, and R. L. White. The Radio Luminosity-Black Hole Mass Correlation for Quasars from the FIRST Bright Quasar Survey and a "Unification Scheme" for Radio-loud and Radio-quiet Quasars. *ApJL*, 551:L17–L21, Apr. 2001. doi: 10.1086/319836.

A. Lawrence. The relative frequency of broad-lined and narrow-lined active galactic nuclei - Implications for unified schemes. *MNRAS*, 252:586–592, Oct. 1991.

M. J. Ledlow and F. N. Owen. 20 CM VLA Survey of Abell Clusters of Galaxies. VI. Radio/Optical Luminosity Functions. *AJ*, 112:9–+, July 1996. doi: 10.1086/117985.

C. Li, G. Kauffmann, Y. P. Jing, S. D. M. White, G. Börner, and F. Z. Cheng. The dependence of clustering on galaxy properties. *MNRAS*, 368:21–36, May 2006a. doi: 10.1111/j.1365-2966.2006.10066.x.

C. Li, G. Kauffmann, L. Wang, S. D. M. White, T. M. Heckman, and Y. P. Jing. The clustering of narrow-line AGN in the local Universe. *MNRAS*, 373:457–468, Dec. 2006b. doi: 10.1111/j.1365-2966.2006.11079.x.

C. Li, G. Kauffmann, T. M. Heckman, Y. P. Jing, and S. D. M. White. Interaction-induced star formation in a complete sample of $10^5$ nearby star-forming galaxies. *MNRAS*, 385:1903–1914, Apr. 2008. doi: 10.1111/j.1365-2966.2008.13000.x.

S. J. Lilly and M. S. Longair. Stellar populations in distant radio galaxies. *MNRAS*, 211:833–855, Dec. 1984.

M. S. Longair. On the interpretation of radio source counts. *MNRAS*, 133:421–+, 1966.

R. Lupton, J. E. Gunn, Z. Ivezić, G. R. Knapp, and S. Kent. The SDSS Imaging Pipelines. In F. R. Harnden, Jr., F. A. Primini, and H. E. Payne, editors, *Astronomical Data Analysis Software and Systems X*, volume 238 of *Astronomical Society of the Pacific Conference Series*, pages 269–+, 2001.

D. Lynden-Bell. Galactic Nuclei as Collapsed Old Quasars. *Nature*, 223:690–694, Aug. 1969. doi: 10.1038/223690a0.

J. Machalski and J. J. Condon. Radio Emission from Galaxies in the Las Campanas Redshift Survey. *ApJS*, 123:41–78, July 1999. doi: 10.1086/313228.

M. Magliocchetti, S. J. Maddox, O. Lahav, and J. V. Wall. Variance and skewness in the FIRST survey. *MNRAS*, 300:257–268, Oct. 1998. doi: 10.1046/j.1365-8711.1998.01904.x.

R. Mandelbaum, C. Li, G. Kauffmann, and S. D. M. White. Halo masses for optically selected and for radio-loud AGN from clustering and galaxy-galaxy lensing. *MNRAS*, 393:377–392, Feb. 2009. doi: 10.1111/j.1365-2966.2008.14235.x.

R. G. McMahon, R. L. White, D. J. Helfand, and R. H. Becker. Optical Counterparts for 70,000 Radio Sources: APM Identifications for the FIRST Radio Survey. *ApJS*, 143:1–23, Nov. 2002. doi: 10.1086/342623.

B. R. McNamara, M. Wise, P. E. J. Nulsen, L. P. David, C. L. Sarazin, M. Bautz, M. Markevitch, A. Vikhlinin, W. R. Forman, C. Jones, and D. E. Harris. Chandra X-Ray Observations of the Hydra A Cluster: An Interaction between the Radio Source and the X-Ray-emitting Gas. *ApJL*, 534:L135–L138, May 2000. doi: 10.1086/312662.

R. B. Metcalf and M. Magliocchetti. The role of black hole mass in quasar radio activity. *MNRAS*, 365:101–109, Jan. 2006. doi: 10.1111/j.1365-2966.2005.09649.x.

G. K. Miley, R. A. Overzier, A. W. Zirm, H. C. Ford, J. Kurk, L. Pentericci, J. P. Blakeslee, M. Franx, G. D. Illingworth, M. Postman, P. Rosati, H. J. A. Röttgering, B. P. Venemans, and E. Helder. The Spiderweb Galaxy: A Forming Massive Cluster Galaxy at z 2. *ApJL*, 650: L29–L32, Oct. 2006. doi: 10.1086/508534.

H. J. Mo and S. D. M. White. The abundance and clustering of dark haloes in the standard ΛCDM cosmogony. *MNRAS*, 336:112–118, Oct. 2002. doi: 10.1046/j.1365-8711.2002.05723.x.

K. Nandra, I. M. George, R. F. Mushotzky, T. J. Turner, and T. Yaqoob. ASCA Observations of Seyfert 1 Galaxies. II. Relativistic Iron K alpha Emission. *ApJ*, 477:602–+, Mar. 1997. doi: 10.1086/303721.

M. Obrić, Ž. Ivezić, P. N. Best, R. H. Lupton, C. Tremonti, J. Brinchmann, M. A. Agüeros, G. R. Knapp, J. E. Gunn, C. M. Rockosi, D. Schlegel, D. Finkbeiner, M. Gaćeša, V. Smolčić, S. F. Anderson, W. Voges, M. Jurić, R. J. Siverd, W. Steinhardt, A. S. Jagoda, M. R. Blanton, and D. P. Schneider. Panchromatic properties of 99000 galaxies detected by SDSS, and (some by) ROSAT, GALEX, 2MASS, IRAS, GB6, FIRST, NVSS and WENSS surveys. *MNRAS*, 370: 1677–1698, Aug. 2006. doi: 10.1111/j.1365-2966.2006.10675.x.

J. B. Oke and J. E. Gunn. Secondary standard stars for absolute spectrophotometry. *ApJ*, 266: 713–717, Mar. 1983. doi: 10.1086/160817.

D. E. Osterbrock. Observational Model of the Ionized Gas in Seyfert and Radio-Galaxy Nuclei. *Proceedings of the National Academy of Science*, 75:540–544, Feb. 1978. doi: 10.1073/pnas.75.2.540.

N. Padmanabhan, D. J. Schlegel, D. P. Finkbeiner, J. C. Barentine, M. R. Blanton, H. J. Brewington, J. E. Gunn, M. Harvanek, D. W. Hogg, Ž. Ivezić, D. Johnston, S. M. Kent, S. J. Kleinman, G. R. Knapp, J. Krzesinski, D. Long, E. H. Neilsen, Jr., A. Nitta, C. Loomis, R. H. Lupton, S. Roweis, S. A. Snedden, M. A. Strauss, and D. L. Tucker. An Improved Photometric Calibration of the Sloan Digital Sky Survey Imaging Data. *ApJ*, 674:1217–1233, Feb. 2008. doi: 10.1086/524677.

N. Padmanabhan, M. White, P. Norberg, and C. Porciani. The real-space clustering of luminous red galaxies around z ¡ 0.6 quasars in the Sloan Digital Sky Survey. *MNRAS*, 397:1862–1875, Aug. 2009. doi: 10.1111/j.1365-2966.2008.14071.x.

A. Pasquali, F. C. van den Bosch, H. J. Mo, X. Yang, and R. Somerville. The rise and fall of galaxy activity in dark matter haloes. *MNRAS*, 394:38–50, Mar. 2009. doi: 10.1111/j.1365-2966.2008.14233.x.

P. J. E. Peebles. *The large-scale structure of the universe*. 1980.

L. Pentericci, J. D. Kurk, H. J. A. Röttgering, G. K. Miley, W. van Breugel, C. L. Carilli, H. Ford, T. Heckman, P. McCarthy, and A. Moorwood. A search for clusters at high redshift. II. A proto cluster around a radio galaxy at z=2.16. *A&A*, 361:L25–L28, Sept. 2000.

R. M. Prestage and J. A. Peacock. The cluster environments of powerful radio galaxies. *MNRAS*, 230:131–160, Jan. 1988.

G. T. Richards, X. Fan, H. J. Newberg, M. A. Strauss, D. E. Vanden Berk, D. P. Schneider, B. Yanny, A. Boucher, S. Burles, J. A. Frieman, J. E. Gunn, P. B. Hall, Ž. Ivezić, S. Kent, J. Loveday, R. H. Lupton, C. M. Rockosi, D. J. Schlegel, C. Stoughton, M. SubbaRao, and D. G. York. Spectroscopic Target Selection in the Sloan Digital Sky Survey: The Quasar Sample. *AJ*, 123:2945–2975, June 2002. doi: 10.1086/340187.

A. G. Riess, L.-G. Strolger, J. Tonry, S. Casertano, H. C. Ferguson, B. Mobasher, P. Challis, A. V. Filippenko, S. Jha, W. Li, R. Chornock, R. P. Kirshner, B. Leibundgut, M. Dickinson, M. Livio, M. Giavalisco, C. C. Steidel, T. Benítez, and Z. Tsvetanov. Type Ia Supernova Discoveries at z¿1 from the Hubble Space Telescope: Evidence for Past Deceleration and Constraints on Dark Energy Evolution. *ApJ*, 607:665–687, June 2004. doi: 10.1086/383612.

A. G. Riess, L. Macri, S. Casertano, M. Sosey, H. Lampeitl, H. C. Ferguson, A. V. Filippenko, S. W. Jha, W. Li, R. Chornock, and D. Sarkar. A Redetermination of the Hubble Constant with the Hubble Space Telescope from a Differential Distance Ladder. *ApJ*, 699:539–563, July 2009. doi: 10.1088/0004-637X/699/1/539.

N. P. Ross, J. da Ângela, T. Shanks, D. A. Wake, R. D. Cannon, A. C. Edge, R. C. Nichol, P. J. Outram, M. Colless, W. J. Couch, S. M. Croom, R. de Propris, M. J. Drinkwater, D. J. Eisenstein, J. Loveday, K. A. Pimbblet, I. G. Roseboom, D. P. Schneider, R. G. Sharp, and P. M. Weilbacher. The 2dF-SDSS LRG and QSO Survey: the LRG 2-point correlation function and redshift-space distortions. *MNRAS*, 381:573–588, Oct. 2007. doi: 10.1111/j.1365-2966.2007.12289.x.

E. M. Sadler, C. R. Jenkins, and C. G. Kotanyi. Low-luminosity radio sources in early-type galaxies. *MNRAS*, 240:591–635, Oct. 1989.

E. M. Sadler, C. A. Jackson, R. D. Cannon, V. J. McIntyre, T. Murphy, J. Bland-Hawthorn, T. Bridges, S. Cole, M. Colless, C. Collins, W. Couch, G. Dalton, R. De Propris, S. P. Driver, G. Efstathiou, R. S. Ellis, C. S. Frenk, K. Glazebrook, O. Lahav, I. Lewis, S. Lumsden, S. Maddox, D. Madgwick, P. Norberg, J. A. Peacock, B. A. Peterson, W. Sutherland, and K. Taylor. Radio sources in the 2dF Galaxy Redshift Survey - II. Local radio luminosity functions for AGN and star-forming galaxies at 1.4 GHz. *MNRAS*, 329:227–245, Jan. 2002. doi: 10.1046/j.1365-8711.2002.04998.x.

E. M. Sadler, R. D. Cannon, T. Mauch, P. J. Hancock, D. A. Wake, N. Ross, S. M. Croom, M. J. Drinkwater, A. C. Edge, D. Eisenstein, A. M. Hopkins, H. M. Johnston, R. Nichol, K. A. Pimbblet, R. de Propris, I. G. Roseboom, D. P. Schneider, and T. Shanks. Radio galaxies in the 2SLAQ Luminous Red Galaxy Survey - I. The evolution of low-power radio galaxies to z ˜ 0.7. *MNRAS*, 381:211–227, Oct. 2007. doi: 10.1111/j.1365-2966.2007.12231.x.

D. J. Schlegel, D. P. Finkbeiner, and M. Davis. Maps of Dust Infrared Emission for Use in Estimation of Reddening and Cosmic Microwave Background Radiation Foregrounds. *ApJ*, 500:525–+, June 1998. doi: 10.1086/305772.

M. Schmidt. Space Distribution and Luminosity Functions of Quasi-Stellar Radio Sources. *ApJ*, 151:393–+, Feb. 1968. doi: 10.1086/149446.

D. P. Schneider, P. B. Hall, G. T. Richards, M. A. Strauss, D. E. Vanden Berk, S. F. Anderson, W. N. Brandt, X. Fan, S. Jester, J. Gray, J. E. Gunn, M. U. SubbaRao, A. R. Thakar, C. Stoughton, A. S. Szalay, B. Yanny, D. G. York, N. A. Bahcall, J. Barentine, M. R. Blanton, H. Brewington, J. Brinkmann, R. J. Brunner, F. J. Castander, I. Csabai, J. A. Frieman, M. Fukugita, M. Harvanek, D. W. Hogg, Ž. Ivezić, S. M. Kent, S. J. Kleinman, G. R. Knapp, R. G. Kron, J. Krzesiński, D. C. Long, R. H. Lupton, A. Nitta, J. R. Pier, D. H. Saxe, Y. Shen,

S. A. Snedden, D. H. Weinberg, and J. Wu. The Sloan Digital Sky Survey Quasar Catalog. IV. Fifth Data Release. *AJ*, 134:102–117, July 2007. doi: 10.1086/518474.

U. Seljak and M. Zaldarriaga. A Line-of-Sight Integration Approach to Cosmic Microwave Background Anisotropies. *ApJ*, 469:437–+, Oct. 1996. doi: 10.1086/177793.

Y. Shen, M. A. Strauss, M. Oguri, J. F. Hennawi, X. Fan, G. T. Richards, P. B. Hall, J. E. Gunn, D. P. Schneider, A. S. Szalay, A. R. Thakar, D. E. Vanden Berk, S. F. Anderson, N. A. Bahcall, A. J. Connolly, and G. R. Knapp. Clustering of High-Redshift (z¿=2.9) Quasars from the Sloan Digital Sky Survey. *AJ*, 133:2222–2241, May 2007. doi: 10.1086/513517.

Y. Shen, J. E. Greene, M. A. Strauss, G. T. Richards, and D. P. Schneider. Biases in Virial Black Hole Masses: An SDSS Perspective. *ApJ*, 680:169–190, June 2008. doi: 10.1086/587475.

Y. Shen, M. A. Strauss, N. P. Ross, P. B. Hall, Y.-T. Lin, G. T. Richards, D. P. Schneider, D. H. Weinberg, A. J. Connolly, X. Fan, J. F. Hennawi, F. Shankar, D. E. Vanden Berk, N. A. Bahcall, and R. J. Brunner. Quasar Clustering from SDSS DR5: Dependences on Physical Properties. *ApJ*, 697:1656–1673, June 2009. doi: 10.1088/0004-637X/697/2/1656.

R. K. Sheth and G. Tormen. Large-scale bias and the peak background split. *MNRAS*, 308:119–126, Sept. 1999. doi: 10.1046/j.1365-8711.1999.02692.x.

C. Simpson. A new look at the isotropy of narrow-line emission in extragalactic radio sources. *MNRAS*, 297:L39–L43, June 1998. doi: 10.1046/j.1365-8711.1998.01678.x.

E. P. Smith and T. M. Heckman. Multicolor surface photometry of powerful radio galaxies. II - Morphology and stellar content. *ApJ*, 341:658–678, June 1989. doi: 10.1086/167524.

I. A. G. Snellen, M. D. Lehnert, M. N. Bremer, and R. T. Schilizzi. Fundamental galaxy parameters for radio-loud active galactic nuclei and the black hole-radio power connection. *MNRAS*, 342: 889–900, July 2003. doi: 10.1046/j.1365-8711.2003.06629.x.

D. N. Spergel, R. Bean, O. Doré, M. R. Nolta, C. L. Bennett, J. Dunkley, G. Hinshaw, N. Jarosik, E. Komatsu, L. Page, H. V. Peiris, L. Verde, M. Halpern, R. S. Hill, A. Kogut, M. Limon, S. S. Meyer, N. Odegard, G. S. Tucker, J. L. Weiland, E. Wollack, and E. L. Wright. Three-Year Wilkinson Microwave Anisotropy Probe (WMAP) Observations: Implications for Cosmology. *ApJS*, 170:377–408, June 2007. doi: 10.1086/513700.

V. Springel. The cosmological simulation code GADGET-2. *MNRAS*, 364:1105–1134, Dec. 2005. doi: 10.1111/j.1365-2966.2005.09655.x.

V. Springel, S. D. M. White, A. Jenkins, C. S. Frenk, N. Yoshida, L. Gao, J. Navarro, R. Thacker, D. Croton, J. Helly, J. A. Peacock, S. Cole, P. Thomas, H. Couchman, A. Evrard, J. Colberg, and F. Pearce. Simulations of the formation, evolution and clustering of galaxies and quasars. *Nature*, 435:629–636, June 2005. doi: 10.1038/nature03597.

C. Stoughton, R. H. Lupton, M. Bernardi, M. R. Blanton, S. Burles, F. J. Castander, A. J. Connolly, D. J. Eisenstein, J. A. Frieman, G. S. Hennessy, R. B. Hindsley, Ž. Ivezić, S. Kent, P. Z. Kunszt, B. C. Lee, A. Meiksin, J. A. Munn, H. J. Newberg, R. C. Nichol, T. Nicinski, J. R. Pier, G. T. Richards, M. W. Richmond, D. J. Schlegel, J. A. Smith, M. A. Strauss, M. SubbaRao, A. S. Szalay, A. R. Thakar, D. L. Tucker, D. E. Vanden Berk, B. Yanny, J. K. Adelman, J. E. Anderson, Jr., S. F. Anderson, J. Annis, N. A. Bahcall, J. A. Bakken, M. Bartelmann, S. Bastian, A. Bauer, E. Berman, H. Böhringer, W. N. Boroski, S. Bracker, C. Briegel, J. W. Briggs, J. Brinkmann, R. Brunner, L. Carey, M. A. Carr, B. Chen, D. Christian, P. L. Colestock, J. H.

Crocker, I. Csabai, P. C. Czarapata, J. Dalcanton, A. F. Davidsen, J. E. Davis, W. Dehnen, S. Dodelson, M. Doi, T. Dombeck, M. Donahue, N. Ellman, B. R. Elms, M. L. Evans, L. Eyer, X. Fan, G. R. Federwitz, S. Friedman, M. Fukugita, R. Gal, B. Gillespie, K. Glazebrook, J. Gray, E. K. Grebel, B. Greenawalt, G. Greene, J. E. Gunn, E. de Haas, Z. Haiman, M. Haldeman, P. B. Hall, M. Hamabe, B. Hansen, F. H. Harris, H. Harris, M. Harvanek, S. L. Hawley, J. J. E. Hayes, T. M. Heckman, A. Helmi, A. Henden, C. J. Hogan, D. W. Hogg, D. J. Holmgren, J. Holtzman, C.-H. Huang, C. Hull, S.-I. Ichikawa, T. Ichikawa, D. E. Johnston, G. Kauffmann, R. S. J. Kim, T. Kimball, E. Kinney, M. Klaene, S. J. Kleinman, A. Klypin, G. R. Knapp, J. Korienek, J. Krolik, R. G. Kron, J. Krzesiński, D. Q. Lamb, R. F. Leger, S. Limmongkol, C. Lindenmeyer, D. C. Long, C. Loomis, J. Loveday, B. MacKinnon, E. J. Mannery, P. M. Mantsch, B. Margon, P. McGehee, T. A. McKay, B. McLean, K. Menou, A. Merelli, H. J. Mo, D. G. Monet, O. Nakamura, V. K. Narayanan, T. Nash, E. H. Neilsen, Jr., P. R. Newman, A. Nitta, M. Odenkirchen, N. Okada, S. Okamura, J. P. Ostriker, R. Owen, A. G. Pauls, J. Peoples, R. S. Peterson, D. Petravick, A. Pope, R. Pordes, M. Postman, A. Prosapio, T. R. Quinn, R. Rechenmacher, C. H. Rivetta, H.-W. Rix, C. M. Rockosi, R. Rosner, K. Ruthmansdorfer, D. Sandford, D. P. Schneider, R. Scranton, M. Sekiguchi, G. Sergey, R. Sheth, K. Shimasaku, S. Smee, S. A. Snedden, A. Stebbins, C. Stubbs, I. Szapudi, P. Szkody, G. P. Szokoly, S. Tabachnik, Z. Tsvetanov, A. Uomoto, M. S. Vogeley, W. Voges, P. Waddell, R. Walterbos, S.-i. Wang, M. Watanabe, D. H. Weinberg, R. L. White, S. D. M. White, B. Wilhite, D. Wolfe, N. Yasuda, D. G. York, I. Zehavi, and W. Zheng. Sloan Digital Sky Survey: Early Data Release. *AJ*, 123:485–548, Jan. 2002. doi: 10.1086/324741.

G. M. Szabó, Ž. Ivezić, M. Jurić, and R. Lupton. The properties of Jovian Trojan asteroids listed in SDSS Moving Object Catalogue 3. *MNRAS*, 377:1393–1406, June 2007. doi: 10.1111/j.1365-2966.2007.11687.x.

G. Tabor and J. Binney. Elliptical Galaxy Cooling Flows Without Mass Drop-Out. *MNRAS*, 263:323–+, July 1993.

C. Tasse, P. N. Best, H. Röttgering, and D. Le Borgne. Radio-loud AGN in the XMM-LSS field. II. A dichotomy in environment and accretion mode? *A&A*, 490:893–904, Nov. 2008. doi: 10.1051/0004-6361:20079299.

R. Terlevich, G. Tenorio-Tagle, J. Franco, and J. Melnick. The starburst model for active galactic nuclei - The broad-line region as supernova remnants evolving in a high-density medium. *MNRAS*, 255:713–728, Apr. 1992.

The SDSS-II SEGUE Collaboration: Brian Yanny, C. Rockosi, H. J. Newberg, and G. R. Knapp. SEGUE: A Spectroscopic Survey of 240,000 stars with g=14-20. *ArXiv e-prints*, Feb. 2009.

C. M. Urry and P. Padovani. Unified Schemes for Radio-Loud Active Galactic Nuclei. *Publ. Astr. Soc. Pac.*, 107:803–+, Sept. 1995. doi: 10.1086/133630.

D. A. Wake, R. C. Nichol, D. J. Eisenstein, J. Loveday, A. C. Edge, R. Cannon, I. Smail, D. P. Schneider, R. Scranton, D. Carson, N. P. Ross, R. J. Brunner, M. Colless, W. J. Couch, S. M. Croom, S. P. Driver, J. da Ângela, S. Jester, R. de Propris, M. J. Drinkwater, J. Bland-Hawthorn, K. A. Pimbblet, I. G. Roseboom, T. Shanks, R. G. Sharp, and J. Brinkmann. The 2df SDSS LRG and QSO survey: evolution of the luminosity function of luminous red galaxies to z = 0.6. *MNRAS*, 372:537–550, Oct. 2006. doi: 10.1111/j.1365-2966.2006.10831.x.

S. D. M. White and C. S. Frenk. Galaxy formation through hierarchical clustering. *ApJ*, 379:52–79, Sept. 1991. doi: 10.1086/170483.

M. Wold, M. Lacy, P. B. Lilje, and S. Serjeant. Clustering of galaxies around radio quasars at 0.5 ¡ z ¡ 0.8. *MNRAS*, 316:267–282, Aug. 2000. doi: 10.1046/j.1365-8711.2000.03473.x.

M. G. Yates, L. Miller, and J. A. Peacock. The cluster environments of powerful, high-redshift radio galaxies. *MNRAS*, 240:129–166, Sept. 1989.

D. G. York, J. Adelman, J. E. Anderson, Jr., S. F. Anderson, J. Annis, N. A. Bahcall, J. A. Bakken, R. Barkhouser, S. Bastian, E. Berman, W. N. Boroski, S. Bracker, C. Briegel, J. W. Briggs, J. Brinkmann, R. Brunner, S. Burles, L. Carey, M. A. Carr, F. J. Castander, B. Chen, P. L. Colestock, A. J. Connolly, J. H. Crocker, I. Csabai, P. C. Czarapata, J. E. Davis, M. Doi, T. Dombeck, D. Eisenstein, N. Ellman, B. R. Elms, M. L. Evans, X. Fan, G. R. Federwitz, L. Fiscelli, S. Friedman, J. A. Frieman, M. Fukugita, B. Gillespie, J. E. Gunn, V. K. Gurbani, E. de Haas, M. Haldeman, F. H. Harris, J. Hayes, T. M. Heckman, G. S. Hennessy, R. B. Hindsley, S. Holm, D. J. Holmgren, C.-h. Huang, C. Hull, D. Husby, S.-I. Ichikawa, T. Ichikawa, Ž. Ivezić, S. Kent, R. S. J. Kim, E. Kinney, M. Klaene, A. N. Kleinman, S. Kleinman, G. R. Knapp, J. Korienek, R. G. Kron, P. Z. Kunszt, D. Q. Lamb, B. Lee, R. F. Leger, S. Limmongkol, C. Lindenmeyer, D. C. Long, C. Loomis, J. Loveday, R. Lucinio, R. H. Lupton, B. MacKinnon, E. J. Mannery, P. M. Mantsch, B. Margon, P. McGehee, T. A. McKay, A. Meiksin, A. Merelli, D. G. Monet, J. A. Munn, V. K. Narayanan, T. Nash, E. Neilsen, R. Neswold, H. J. Newberg, R. C. Nichol, T. Nicinski, M. Nonino, N. Okada, S. Okamura, J. P. Ostriker, R. Owen, A. G. Pauls, J. Peoples, R. L. Peterson, D. Petravick, J. R. Pier, A. Pope, R. Pordes, A. Prosapio, R. Rechenmacher, T. R. Quinn, G. T. Richards, M. W. Richmond, C. H. Rivetta, C. M. Rockosi, K. Ruthmansdorfer, D. Sandford, D. J. Schlegel, D. P. Schneider, M. Sekiguchi, G. Sergey, K. Shimasaku, W. A. Siegmund, S. Smee, J. A. Smith, S. Snedden, R. Stone, C. Stoughton, M. A. Strauss, C. Stubbs, M. SubbaRao, A. S. Szalay, I. Szapudi, G. P. Szokoly, A. R. Thakar, C. Tremonti, D. L. Tucker, A. Uomoto, D. Vanden Berk, M. S. Vogeley, P. Waddell, S.-i. Wang, M. Watanabe, D. H. Weinberg, B. Yanny, and N. Yasuda. The Sloan Digital Sky Survey: Technical Summary. *AJ*, 120:1579–1587, Sept. 2000. doi: 10.1086/301513.